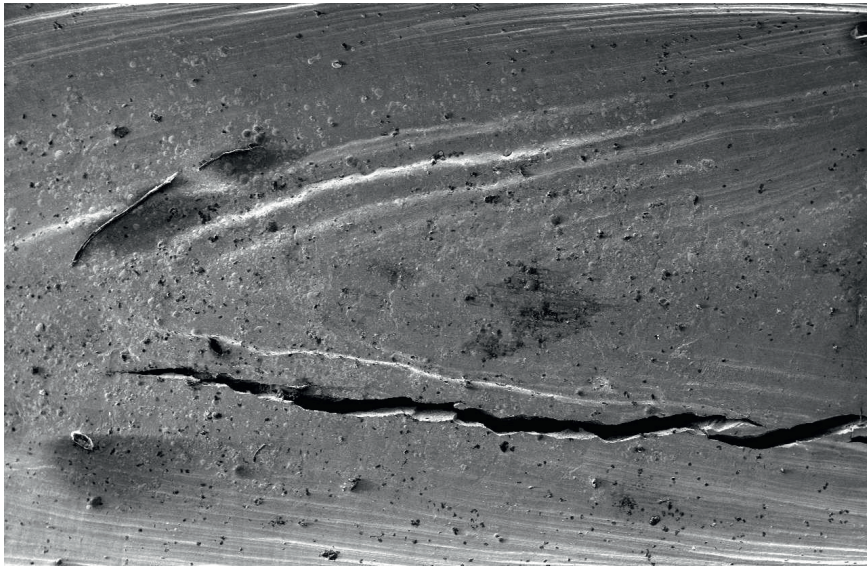


# A Study of the Fatigue Behaviour of Laser and Hybrid Laser Welds



Md. Minhaj Alam





Licentiate Thesis

**A study of the fatigue behaviour  
of laser and hybrid laser welds**

**Md. Minhaj Alam**

Luleå University of Technology  
Department of Applied Physics and Mechanical Engineering  
Division of Manufacturing Systems Engineering  
971 87 Luleå,  
Sweden

Luleå, November 2009

Printed by Universitetstryckeriet, Luleå 2009

ISSN: 1402-1757

ISBN 978-91-7439-059-9

Luleå 2009

[www.ltu.se](http://www.ltu.se)

**The process of scientific discovery is, in effect,  
a continual flight from wonder**



## Abstract

This licentiate thesis focuses on the fatigue cracking behaviour of laser and hybrid laser-MAG welded structures. Beside the welding process and the resulting weld, several topics related to fatigue of welded structures are treated such as; macro and micro surface geometry, weld defects and their influence on fatigue performance of welded structures, fatigue analysis by the nominal and effective notch stress method, fatigue life prediction using LEFM (Linear Elastic Fracture Mechanics), fatigue testing, metallurgical analysis, elastic and elastic-plastic finite element analysis. The main objective is to gain understanding of the impact of weld defects and weld shape details on the fatigue behaviour of laser and hybrid laser welded joints.

The first paper is a literature survey which compiled useful information regarding fracture and fatigue analysis of various welded joints.

In the second paper fatigue testing by bending of laser hybrid welded eccentric fillet joints was carried out. The weld surface geometry was measured and studied in order to understand the crack initiation mechanisms. The crack initiation location and the crack propagation path were studied and compared to Finite Element stress analysis, taking into account the surface macro- and micro-geometry. Based on the nominal stress approach, SN-curves were designed for laser hybrid welded eccentric fillet joints. The competing criteria of throat depth and stress raising by the weld toe radii and by the surface ripples are explained, showing that surface ripples can be critical.

The third paper is the continuation of the second paper, but studying the fatigue crack propagation of laser hybrid welded eccentric fillet joints. Microscopic analysis was carried out to identify internal weld defects. Nominal and effective notch stress analysis was carried out to compare standardized values. LEFM analysis was conducted for this joint geometry for four point bending load in order to study the effect of LOF on fatigue life. In good agreement between simulation and metallurgy, cracking starts and propagates from the lower toe, but for certain geometries alternatively from the weld bead or upper toe, even in case of Lack of Fusion, as was well be explained. Improved understanding of the crack propagation for these geometrical conditions was obtained and in turn illustrated. Lack of fusion surprisingly was not critical and only slightly lowered the fatigue life.

Two dimensional linear elastic finite element analyses is carried out in the fourth paper on laser welding of a beamer in order to study the impact of geometrical aspects of the joint design and of the weld root on the fatigue performance. Critical geometrical aspects were classified and then studied by FE-analysis with respect to their impact on the fatigue behaviour. Stress comparison of full 15 mm and partial 6 mm weld penetration of the beam was done by varying the toe and root geometry to identify the critical details. Generalization of the knowledge by new methods was an important aspect, particularly to apply the findings for other joints. Together the papers provide better understanding of fatigue behaviour for complex geometries and are therefore suitable guidelines for improved weld design.





## Preface

When you start to read this thesis, you start to read my work at the Division of Manufacturing Systems Engineering at Luleå University of Technology since September 2007. But this is not completely true that it is only my work. Towards the PhD journey, I have arrived upto mid of my destination with the help from many people who really deserve gratitude from me.

First of all, I would like to thank to ALMIGHTY ALLAH for making me capable to live like a normal people, gave me knowledge to work and shows the way of true path.

I would like to give heartiest thank to my supervisor Professor Alexander Kaplan for appoint me, even though he did not know me before. You also deserve thank for your continuous support and creating new ideas for my work. I believe it would not be possible to finish this thesis within time without your assist even in the mid night or in the early morning by web meeting. It is highly appreciable. When I ran out of ideas, your support was vital. I do not know if you ever doubted my capacity; if so, you hide it well.

Special thanks to Dr. Zuheir Barsoum for his courage and help at the beginning of my PhD when I was struggling to find out the way. Special thanks also go to Prof. Hans Åke Häggblad and Dr. Pär Jonsén for being my co-author and spending lot of time with me by giving valuable advice. I am sincerely grateful and show my gratitude for the funding provided by VINNOVA – The Swedish Innovation Agency (projects LOST, no. 2006-00563 and HYBRIGHT, no. 2005-02895) and by the K&A Wallenberg Foundation (Fibre Laser, project no. KAW 2007-0119). Thanks also go to my colleagues at the Division of Manufacturing Systems Engineering at LTU for all their countless support. I did not feel insecure as newcomer in this university for their endless help and courage. Dr. Peter Norman deserves thanks as being my mentor and helps me to cope up with the university environment. I would also like to give thanks to Tore Silver and Greger Wiklund for all the helps in the laser lab and with my unlimited questions. It might irritate them. Sorry for that.

Most significantly, I am expressing my deep and warmest appreciation to my family. My dear parents, who give me proper guidance, educate me, encourage me for higher studies, and give me freedom to choose my career with unconditional love. Thank you for helping and thanks for being with me. Also thanks to my only younger sister, Manni for his affection. Specially thanks to my mother in law for keeping patience and faith on me. Lajori, my daughter missing her much while writing this paper. I like to send my love to her. Last but not least, I would like to express my deepest gratitude to my beloved wife, Sharna, for her continuous tolerance, unconditional support, encouragement and giving me a lovely kid this year. I honestly say “Sorry” to you both for not giving company at this time due to this thesis work.

Md. Minhaj Alam  
November, 2009



## List of publications

The thesis is composed of the following publications

### Paper I

M. M. Alam, P. Jonsén, A. F. H. Kaplan, Fatigue behaviour study of laser hybrid welded eccentric fillet joints – Part II: State-of-the-art of fracture mechanics and fatigue analysis of welded joints, in Proceedings of NOLAMP 12 Conference, Copenhagen, Denmark (2009).

### Paper II

M. M. Alam, Z. Barsoum, P. Jonsén, H. A. Häggblad, A. F. H. Kaplan, The influence of surface geometry and topography on the fatigue cracking behaviour of laser hybrid welded eccentric fillet joints, Applied Surface Science, 2009. (In press available online)

### Paper III

M. M. Alam, Z. Barsoum, P. Jonsén, H. A. Häggblad, A. F. H. Kaplan, Fatigue cracking behaviour for laser hybrid welded eccentric fillet joints including lack of fusion, Engineering Fracture Mechanics, 2009. (Submitted)

### Paper IV

M. M. Alam, J. Karlsson, A. F. H. Kaplan, Generalising fatigue stress analysis of different laser weld geometries, Mechanics of Materials, 2009 (Submitted)



**Table of contents**

Abstract.....	i
Preface.....	iii
List of publications .....	v
INTRODUCTION	
1. Organisation of the thesis .....	1
2. Motivation of the research .....	3
3. Methodological approach .....	4
4. Laser and hybrid laser welding .....	5
4.1. Laser welding .....	5
4.2 Hybrid laser welding .....	10
5. Fatigue cracking.....	13
5.1 Fundamental knowledge of fatigue analysis .....	15
5.2 Fatigue mechanism.....	16
5.3 Fatigue assessment methods .....	16
6. Summary of the papers .....	20
7. General conclusions of the thesis.....	23
8. Future outlook.....	24
9. References.....	25
ANNEX	
Paper I: State-of-the-Art of Fracture and Fatigue.....	27
Paper II: Influence of Surface Geometry and Topography .....	63
Paper III: Fatigue Cracking including Lack of Fusion .....	85
Paper IV: Stress Analysis of Laser Weld Geometries .....	111



# INTRODUCTION

## 1. Organisation of the thesis

The present Licentiate thesis is composed of an introduction, one State-of-the-Art review manuscript, Paper I, and three scientific publication manuscripts, Papers II,III,IV.

### Organisation of the Introduction

- In the introduction *the links (“red wire”) between the three research publications II-IV* are explained through their common as well as complimentary research aspects in terms of:
  - Organisation of the thesis [Section 1]
  - Motivation of the research [Section 2]
  - Methodological approach [Section 3]
  - General conclusions of the thesis [Section 7]
  - Future outlook [Section 8]
- The *two main subjects* of the thesis (i.e. laser welding and stress analysis of welds) are briefly described, including the state-of-the-art [Section 4, 5; Paper I]
- The four papers and their results are *summarised* [Section 6,7]

### Context of the Papers

Annex:

Paper I: Fatigue behaviour study of laser hybrid welded eccentric fillet joints – Part II: State-of-the-art of fracture mechanics and fatigue analysis of welded joints

Paper II: The influence of surface geometry and topography on the fatigue cracking behaviour of laser hybrid welded eccentric fillet joints

Paper III: Fatigue cracking behaviour for laser hybrid welded eccentric fillet joints including lack of fusion

Paper IV: Generalising fatigue stress analysis of different laser weld geometries

The thematic focus of the four papers is illustrated in Fig. 1, particularly the methods applied and the aspects studied. As the research of Papers II-IV focuses on fatigue analysis of laser welds (thus not the welding process itself), Paper I provides a review of the State-of-the-Art of fracture mechanics and fatigue analysis of welded joints in general. In Paper II the fatigue behaviour of a certain hybrid laser welded joint is studied, both experimentally and by Finite Element Analysis (FEA) with respect to maximum stress and crack initiation locations, particularly in dependence of weld shape and surface ripples. In Paper III, as a continuation of Paper II, the fatigue crack propagation is studied (including the influence of Lack of Fusion), again both

experimentally and by FEA. Paper IV presents FEA research results of stress raisers for different laser welded joints, particularly of different root geometries, also in comparison to the weld geometries applied in Paper II and III. All three papers aim also at generalisation and illustration of the knowledge revealed.

	Paper I	Paper II	Paper III	Paper IV
Welded joint	■			
Laser welded joint				■
Hybrid laser welded joint		■	■	■
State-of-the-Art	■	■	■	
Welding process		■		■
Weld shape measurement		■		■
Metallurgy, fractography		■	■	■
Fatigue testing, evaluation	■	■	■	
Stress FEA	■	■	■	■
Cracking FEA	■		■	
Joint geometry		■	■	■
Weld shape		■	■	■
Weld roughness		■		
Welding defects (LoF)			■	
Illustrative description		■	■	■
Flow chart documentation				■

**Fig. 1** Differences in the thematic focus of the four papers composing the core of the thesis (■: core subject, ■: partially involved)

While the author of the thesis coordinated the corresponding research and carried out many of the results by himself, the research was conducted in close cooperation with the academic and industrial partners of the VINNOVA-projects HYBRIGHT (Paper II, III) and LOST (Paper IV). In particular, Dr. Zuheir Barsoum (KTH) and Dr. Pär Jonsén (LTU) contributed significantly with FEA for Papers II and III. Moreover, Dr. Pär Jonsén and Prof. Hans-Åke Häggblad (LTU) carried out the fatigue testing and were involved in its analysis for Papers II, III. Jan Karlsson (LTU) carried out the experimental laser welding study in Paper IV. The above researchers plus the main PhD-supervisor, Prof. Alexander Kaplan, were a close team of the research, with intense valuable discussion, where the border of contribution is often difficult to draw. The author of the thesis is grateful for this fruitful close cooperation.

The four papers are accompanied by the below cited three conference manuscripts, containing additional findings and more detailed descriptions of the methods applied



and presenting the results in a more focused rather than interdisciplinary manner for the respective research community (laser processing, fatigue analysis).

#### Additional publications of relevance

M. M. Alam, Z. Barsoum, P. Jonsén, H. A. Häggblad, A. F. H. Kaplan, The effects of surface topography and lack of fusion on the fatigue strength of laser hybrid welds, in Proceedings of ICALEO 28 Conference, Orlando, Florida, USA, (2009) 38-46

M. M. Alam, Z. Barsoum, P. Jonsén, H. A. Häggblad, A. F. H. Kaplan, Geometrical aspects of the fatigue behaviour of laser hybrid fillet welds, in Proceedings of Fatigue Design Conference, Senlis, Paris, France, 2009.

M. M. Alam, Z. Barsoum, P. Jonsén, H. A. Häggblad, A. F. H. Kaplan, Fatigue behavior study of laser hybrid welded eccentric fillet joints, in Proceedings of NOLAMP 12 Conference, Copenhagen, Denmark (2009).

## **2. Motivation of the research**

Various welding processes are used in industry today - the main factors for their distinctions are the source of the energy used for welding and the strength of the welded joint. Traditional welding processes, e.g. arc welding of various kind, are already well adapted by the manufacturer and got the trust on the mechanical strength of the joint. New welding technology, e.g. laser or hybrid laser welding, is still struggling to gain faith from the manufacturers although research has often demonstrated higher mechanical strength of laser or hybrid laser welded joints than conventional arc welded joints [1-3]. What makes the situation more complicated is the fact that laser welding often becomes most advantageous when changing the joint and product design or even the material (e.g. to high strength steel). The corresponding standards are unsatisfactory. Thus the original motivation behind this thesis comes directly from the manufacturer requirement to study the fatigue behaviour of laser and hybrid laser welded joints. In particular, closer cooperation between research groups on the welding process and on stress analysis of the resulting weld was a desired goal.

Papers II and III (accompanied by a literature review in Paper I) result from the research project HYBRIGHT with the aim of studying the fracture mechanics of various hybrid laser welded industrial cases. Of particular interest was fatigue cracking and the judgement of geometrical aspects like joint design, weld shaping, roughness and welding defects. The motivation was improved understanding of the fatigue behaviour in order to optimise hybrid laser welds and in turn to build confidence in industry on this technique. In particular, the research aims at supporting the development of improved standards.

Paper IV addresses different joints for laser welding of a beamer in frame of the technology platform project LOST that addresses welding for lightweight structures in

a larger context. Similar as for the other project, improved understanding of laser welded joints is desired for judging different design options and welding techniques, also hybrid laser welding.

Beside knowledge through case studies, aim of the research is the generalisation of stress analysis knowledge for transferring it to different applications and for creating standards. Therefore, particular focus was put on discussing, illustrating and formulating the results from a generalising point of view.

Eventually, the motivation is improved understanding, confidence and use of laser and hybrid laser welding as advanced welding techniques.

### **3. Methodological approach**

For achieving improved understanding of the fatigue behaviour of laser (Paper IV) and laser hybrid (Papers II, III) welded joints, experimental and analytical work has been carried out by different suitable methods. The research methodology applied for this thesis is as follows:

After preparation and welding of specific joint cases with suitable parameters, the identification of the geometry of welded samples but also of hypothetical geometries of relevance is an essential starting point. In particular, aspects like ripple roughness or lack of fusion were measured. The definition and identification of suitable properties describing the critical surface conditions, like toe radii or throat depth, is a valuable tool.

As a next step, for each weld geometry FEA simulation of the stress field is conducted, in particular yielding the location and value of maximum stress (for a defined load condition) as the most likely crack initiation location. For the sake of simplicity so far only the elastic regime was studied, valid beyond  $10^5$  cycles and stress analysis was reduced to the cross section, thus to two dimensions. Fatigue testing of the welded samples and subsequent fractography enables analysis and comparison of the crack initiation locations and provides the characteristics of the weld through lifetime cycles and standardised SN-curves.

Starting from the maximum stress locations, FEA simulation of the crack propagation is conducted to develop an understanding, both, of the speed and direction of cracking, particularly of its interaction with defects like lack of fusion or complex joint geometries.

One particular challenge is the interpretation of the results, as the contributing mechanisms are difficult to separate. Sensitivity studies for changing a particular dimension partially helped to overcome this dilemma. Also the definition of indicators based on surface properties (e.g. the inverse of the throat depth or of the toe radius) enabled accompanying analytical evaluation. The extension of the field study to

similar weld shapes also makes the different contributions and the identification of the most critical geometrical aspects clearer.

From the findings recommendations for the weld geometry (joint type, top and root shape, roughness, defects, etc.) and in turn for the joint design, joint preparation, welding technique and welding parameters are given.

Key methods applied and developed for improved transfer of knowledge are the attempt to generalise the findings, to clearly isolate different mechanisms, to illustrate the findings (particularly the stress flow depending on the geometry), to illustrate the trends (e.g. between similar joint and root geometries) and to state clear formulations and guideline of the findings, inserted in a flow chart (e.g. BFC), suitable to be extended. These approaches hopefully encourage the academic and industrial research community for improved common development and transfer of results, leading to a more powerful use of the findings.

## **4. Laser and hybrid laser welding**

Welding is defined by the American Welding Society (AWS) as a localized coalescence of metals or non-metals produced by either heating of the materials to a suitable temperature with or without the application of pressure, or by the application of pressure alone, with or without the use of filler metal. Welding is a key technology in industrial manufacturing in order to maintain the mechanical strength of a product by the joint, which is a complex criterion with respect to its definition and control. Laser welding and its variant hybrid laser welding are advanced welding techniques that offer several advantages but still often are a niche technology. Beside other reasons, limited understanding of the fatigue behaviour of the welds leads to lack of design standards and lack of confidence.

### **4.1. Laser welding**

The theoretical fundamental principles of stimulated emission and the quantum-mechanical fundamental principles of the laser were postulated by A. Einstein and others in the beginning of last century. However, it took more than 40 years until the development of the first (ruby) laser took place in the Hughes Research Laboratories. The following years were characterized by a rapid development of laser technology. Already in 1970, and especially with the availability of high-power lasers in the beginning of the Eighties, CO<sub>2</sub>- and solid-state lasers were used in material processing. Nowadays, the power of these lasers is often in the range of 5-10 kW (up to 50 kW in some cases) for the CO<sub>2</sub> lasers, 0.3-4 kW for Nd: YAG lasers and up to 30 kW for fiber laser. Table 1 provides an overview of the characteristics of some of the commercially available high power cw laser sources. There are many manufacturing methods possible when using a laser beam as an optical energy source (cutting, micromachining, surface treatment, rapid prototyping) but the main focus will be laser welding in this thesis.

Table 1: Laser source comparison

	<b>CO<sub>2</sub></b>	<b>Lamp-pumped Nd:YAG</b>	<b>Diode-pumped Nd:YAG</b>	<b>Yb-fibre (multi-mode)</b>	<b>Thin disc Yb-YAG</b>
Lasing medium	Gas mixture	Crystalline rod	Crystalline rod	Doped fibre	Crystalline disk
Wavelength, micron	10.6	1.06	1.06	1.07	1.03
Beam transmission	Mirror, lens	Fibre, lens	Fibre, lens	Fibre, lens	Fibre, lens
Typical delivery fibre Ø, micron	-	600	400	100-200	150-200
Output powers, kW	Up to 15kW	Up to 4kW	Up to 6kW	Up to 30kW	Up to 10kW
Typical beam quality, mm.mrad	3.7	25	12	12	7
Maintenance interval, khrs	2	0.8-1	2-5	100	2-5
Power efficiency, %	5-8	3-5	10-20	20-30	10-20
Approximate cost per kW, k\$	60	130-150	150-180	130-150	130-150
Footprint of laser source	large	medium	medium	small	medium
Laser mobility	low	low	low	high	low

Laser welding is a widely known technique, sometimes massively used (70% of the welds of the VW Golf VI body-in-white are laser welded and 50-75% of large passenger ships at Meyer Shipyard, Germany are hybrid laser welded) but often a high performance niche technology. The laser is focused onto the workpiece creating a concentrated heat source in order to melt and fuse material together [4], see Fig. 2. The main characteristic advantage of laser welding is the capability of distribution of the energy (via the drilled vapour capillary, the so-called keyhole) deep into the material to generate a narrow, deep weld [5, 6]. The energy required for melting the surface is about  $10^6$  W/cm<sup>2</sup>, which is one of the highest among the different welding processes available. Due to excellent focusing capabilities, high power lasers suitable for welding have nowadays reached cw-power densities of the order of  $10^7$ - $10^8$  W/cm<sup>2</sup>. This high energy concentration produces a weld with a high depth to width ratio with minimal thermal distortion.

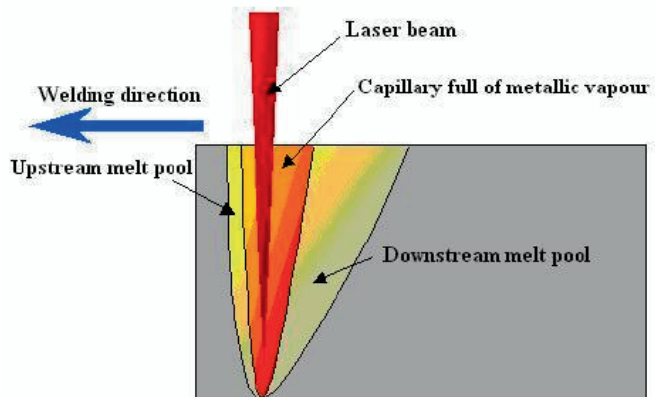


**Fig. 2** Schematic view from the side of the laser welding process

In laser welding we distinguish between two main processes: heat conduction welding and deep penetration welding, see Fig. 3. In heat conduction welding, the materials to be joined are melted by absorption of the laser beam at the material surface from where the heat flows into depth – the solidified melt joins the materials. Welding penetration depths in this context are typically below 2 mm. Deep penetration welding starts at energy densities of approx.  $10^6 \text{ W/cm}^2$  where evaporation is reached and a vapour capillary is created inside the material. The resulting vapour pressure inside the material keeps the capillary open, being of similar diameter as the laser beam. The beam is moved through the material by the motion system, following the contour to be welded. The hydrostatic pressure, the surface tension of the melt, and the vapor pressure inside the capillary, particularly the ablation pressure locally generated by the laser beam, reach equilibrium, preventing the keyhole from collapsing. Multiple reflections inside the keyhole guide the incident laser beam deep into the material and enhance its absorption. Today, given sufficient laser power, weld depths of up to 25 mm (steel) can be achieved.

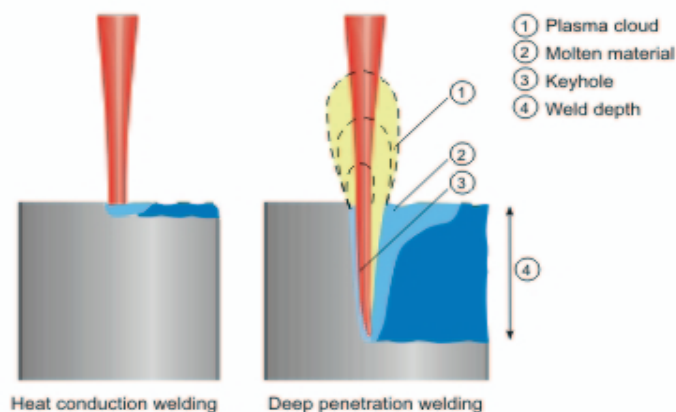


**Fig. 3** Schematic diagram of heat conduction and deep penetration laser welding (ref. [www.rofin.com](http://www.rofin.com))

Since lasers are capable of producing thin, deep welds, it seems natural to select butt joint configurations for laser welding, see Figure 4. Where butt joints are practical, they allow the greatest speed and the lowest heat input since all the metal in the weld is being used to hold the assembly together. A lap joint, Figure 5, can often be used to increase the reliability of the welding process. Lap welds melt a lot of metal to produce a small connection, but they have a much larger tolerance on position than butt welds. Since laser welding is inherently fast and has a low heat input, a lap weld is often the most practical choice.



**Fig. 4** Cross- section of laser welded butt joint, 16 mm stainless steel (ref. LTU)

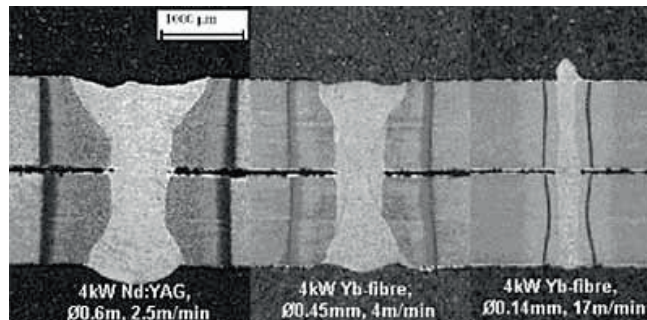


**Fig. 5** Cross- sections of laser welded lap joint configuration (ref. [www.twi.co.uk](http://www.twi.co.uk))

The laser welding process is quite fast, which is of interest when looking at productivity. But this deep and narrow shape of the weld, which has many advantages, is also one of the main drawbacks to the process because it requires careful and accurate machining and positioning of the workpieces.

Compared to conventional welding methods, laser welding offers diverse advantages:

- No tool wear, contact-free processing
- Diverse materials and different thicknesses are weldable
- Easy conversion to automatic operation
- High flexibility in terms of process and geometry
- High welding speed
- High weld seam quality, resulting in little need for reworking steps
- Low thermal material influence, low distortion
- Adjustable energy supply in relation to the material
- Highest reliability at maximum flexibility
- Safe operation by proven beam guiding systems
- Adjustment to customized requirements and local conditions by modular design of the machine
- Simultaneous operation at different machines or different welding spots by beam deflectors or splitters
- Availability of further options like quality monitoring or documentation of the process data
- Single sided access (compared to resistance spot welding)

But laser welding has also some drawbacks which are:

- High cost of equipment and maintenance
- Poor gap bridging ability, which leads to high requirements on joint preparation
- Limited welding positions
- Poor electrical efficiency (5-10 % for CO<sub>2</sub> lasers, 1-3 % for Nd:YAG lasers)
- Occasional metallurgical problems due to the high cooling rates

Laser welding is used in many sectors. Some examples are listed below; see also Fig. 6:

- Tailored blanks for the automotive industry
- Thick section welding, e.g. passenger ship panels
- Thin section welding, e.g. housings or high strength lightweight car components
- Airframe Al- and Ti-structures
- Microelectronics applications, e.g. connections
- Medical devices, e.g. pacemakers

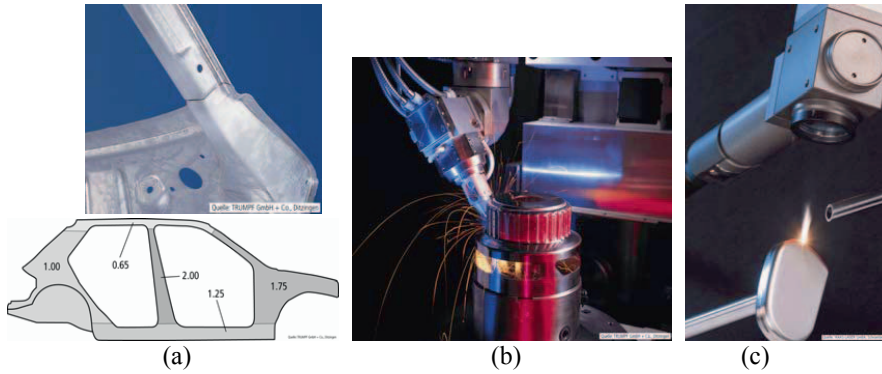


**Fig. 6** Examples of laser welding applications: (a) tailored blanks of different sheet thickness (mm) for a car side frame, (b) low distortion gear wheels, (c) sealed pacemakers (ref all: Trumpf GmbH&Co, Ditzingen, Germany)

## 4.2 Hybrid laser welding

The combination of laser beam welding (LBW) and conventional gas metal arc welding (GMAW) processes is called hybrid laser welding [7] or arc-augmented laser welding [8–10]. The principle is illustrated in Fig. 7.

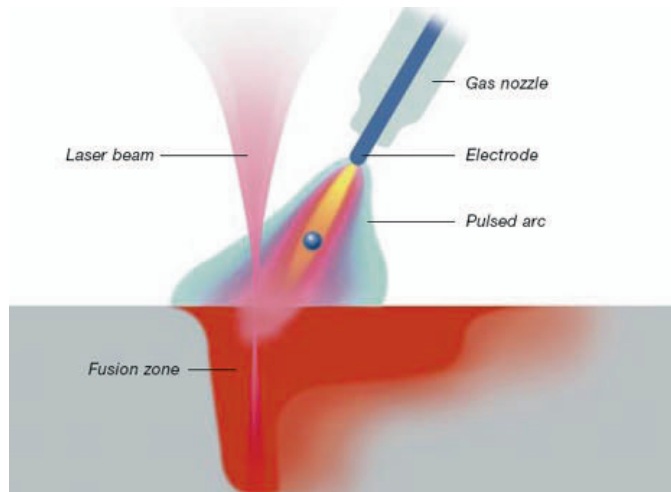


**Fig. 7** Schematic of the hybrid laser/arc welding process (ref. [www.fronius.com](http://www.fronius.com))

The potential for this combination is to combine the advantages of each process, i.e. to increase the weld bead penetration and welding speed (laser) and to add material for bridging gaps and shaping the top (MIG/MAG wire), which is difficult to realize with either laser or arc process by its own. Combining the two processes results in a new one with its inherent features and characteristics, hence widening the areas of its application and increasing its capabilities, once the mutual interaction between the two



energy sources is optimized (the larger number of parameters make it basically more difficult to control). The arc welding process, characterized by relatively lower power density and a wider process zone, creates a wide bead, thus enhancing the joint's gap bridging ability and enlarging the manufacturing tolerances for joint preparation. Simultaneously, the laser beam process, characterized by higher localized power density, leads to a deeper penetration. Thus in hybrid GMA-laser beam welding, a wide and deep bead is achieved at higher welding speeds when compared with the GMAW process by its own [11], see Fig. 8. This accordingly leads to less heat input per unit length, less thermal distortion, and therefore, less residual stresses, narrower heat-affected zone (HAZ), and more important, increased productivity.

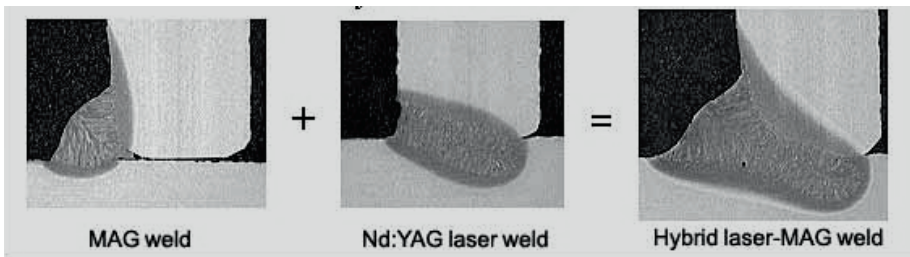


**Fig. 8** Principle of hybrid welding by combining an electric arc (MAG) and a laser (ref. [www.twi.co.uk](http://www.twi.co.uk))

Thus hybrid welding minimizes the drawbacks of both the single laser and the MIG process to obtain an optimized welding technique. Though hybrid laser welding has reduced the drawbacks of arc and laser welding, to make use of the advantages it has many parameters which have to be correctly adjusted to obtain the desired weld quality [12-13]. Those parameters are summarized briefly below.

#### Secondary energy source (Laser with TIG/plasma/MIG-MAG)

The laser combined with the TIG-process is mainly suitable for thin gauge. To choose a laser with plasma arc has a certain advantage which is the pilot arc. The pilot arc is a low current (5 A) constant arc that is emitted through the nozzle. It usually gives a stable process. Laser with MIG/MAG is usually applied to fill up a gap between two parts and is the most common method.

#### Laser power

An increase in laser power will generally increase the weld penetration. In the case of hybrid laser-arc welding (as opposed to the autonomous laser process) this phenomenon is accentuated because the reflectivity of the workpiece is reduced when the metal is heated by the arc.

#### Welding speed

The weld penetration increases when the welding speed is decreased because the heat input per unit length of weld is higher. Also the gap filling capability by the filler wire is improved at lower welding speeds (at constant filler wire feeding). The ratio

between welding speed and filler wire feeding is important for the stability of the keyhole and thus for the stability of the process itself.

#### Focal point position

The maximum weld penetration for the hybrid laser-arc process is generally obtained when the laser beam is focused below the top sheet surface (2 to 4 mm). Investigations have also shown that no change in focal point position is needed when Nd:YAG/TIG hybrid welding compared to pure laser welding takes place.

#### Angle of electrode

In conventional welding, the torch angle from horizontal orientation is usually around 50°. The penetration depth does not increase at angles closer to vertical.

#### Shielding gas

The predominant constituent of the shield gas is generally an inert gas such as helium or argon. A shielding gas providing a higher ionisation potential is required since the plasma can deflect or absorb a portion of the laser energy when CO<sub>2</sub> lasers are employed. Helium is therefore often preferred to argon for laser welding, but its low density and higher price is a disadvantage, thus it is often combined with argon which is heavier without substantial alteration of the weld penetration depth. The addition of reactive gases such as oxygen and carbon dioxide has been shown to have an influence on the weld pool wetting characteristics and bead smoothness.

#### Edge Preparation

The preparation of edges is different in laser welding and conventional welding due to the different type of energy distribution. Because of the restricted width of the laser beam, perpendicular edges are needed in autogenous laser welding. Therefore, laser cut edges are preferred to shear cut edges. In MIG/MAG welding, a V-shape or other angled cut is normally made prior to welding; however, the preferred angle is often smaller than for arc-welding.

#### Relative distance between laser and MIG

The relative distance between the laser beam and the MIG torch is one of the most important parameters to control in hybrid welding. It will be dependent on the energy supplied from each source. A short distance, typically 2 mm between the laser spot and the filler wire tip has been shown to be favourable for a steady keyhole and for maximum penetration. Whether the laser or the arc is leading is also an often discussed item. For the leading arc the wire drops can enter and fill the gap easier while for the leading laser often a more stable process was reported.

#### Joint gap

For laser welding gaps up to 0.2 mm can be managed. Gaps larger than this will lead to weld defects such as an incomplete weld bead and undercut. The hybrid laser-arc process allows us to join work pieces with gaps of 1 mm without any problem and even wider gaps, if the wire feeding is set high enough. This process is therefore more tolerant to inaccurate joint preparation and joint fit-up as well as thermal distortion of

the work piece during the welding process. It is also more tolerant to a beam to gap misalignment.

#### Advantages of hybrid laser welding

- Lower capital cost, reduction of 30-40% compared to laser alone due to reduction in laser power requirement for same speed
- Higher welding speeds
- Reduction of edge preparation accuracy needed
- Control of seam width and top weld shape
- Control of metallurgical variables through the addition of filler wire
- Less material hardening
- Improved process reliability
- Higher electrical efficiency, up to 50% reduction in power consumption.

#### Disadvantages of hybrid laser welding

- More parameters to be controlled/optimized
- Process more difficult to control systematically
- The advantage of the “laser finger” makes sense only for thickness larger 3 mm
- Welding standards and experience widely missing yet

#### Industrial Applications

- Shipbuilding, e.g. Odense Shipyard, Meyer Shipyard
- Automotive, e.g. VW, Audi
- Aerospace
- Railway
- Pipelines and offshore installations
- Heavy industry, power generation

## **5. Fatigue cracking**

Welding strongly affects material by the process of heating and cooling, as well as by the addition of filler material, resulting in inhomogeneous material zones. Moreover, the shape of the weld depends on the melt flow and its resolidification. As a consequence, fatigue failures appear in welded structures mostly at the welds rather than in the base metal, see Fig. 9. For this reason, fatigue analyses are of high practical interest for all cyclic loaded welded structures, such as ships, offshore structures, cranes, bridges vehicles, railways, etc.

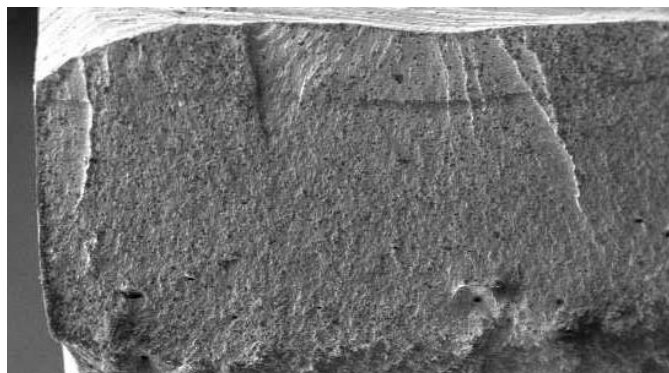


**Fig. 9** Fatigue failure in welded joint – fracture surface

For several years there has been a trend towards fatigue life improvement by using advanced welding techniques like laser welding or hybrid laser welding. Until now, all toughness improvements of the fatigue strength of welds were carried out by post-weld treatments such as TIG (Tungsten Inert Gas) dressing; hammer peening, grinding, UIT (Ultrasonic Impact Treatment) and post-weld heat treatment [14–16]. However, these methods often require well-skilled workers or special equipments, and most of these methods are time-consuming processes which inevitably make construction costs higher. Kirkhope et al. [17–18] also discusses methods of improving the fatigue life of welded steel structures by operations such as grinding, peening, water-jet eroding and remelting. They stated that the use of special welding techniques applied as part of the welding process in lieu of post-weld operations are attractive because the associated costs are lower and the quality control is simpler. Nowadays the improvement of weld surface geometry is being achieved with advanced welding technology, particularly laser and hybrid laser welding. Therefore, studies of geometrical aspects on the fatigue behavior of hybrid laser welded joints are necessary.

The fatigue failure of welded elements without crack-like defects comprises two phases: fatigue crack initiation and fatigue crack propagation [19]. To estimate fatigue crack initiation life, the weld toe stress concentration factor (SCF) is usually needed. To predict the crack propagation life, stress intensity factors (SIF) are used when a linear elastic fracture mechanics approach is employed [20]. Estimation of the fatigue life usually assumes the weld toe geometry by a weld angle, and a circular arc which defines the weld toe radius. This local geometry affects the local stress concentration and, together with defects of different types, fatigue cracks form during cyclic loading and lead to a large scatter in fatigue life data. Also there is another important weld surface geometry - weld surface waviness or ripples from where cracks may initiate. Chapetti and Otegui [21] investigated the effect of toe irregularity for fatigue resistance of welds and concluded that the period of toe waves, as well as local toe geometry, strongly influences the fatigue crack initiation and propagation life.

## 5.1 Fundamental knowledge of fatigue analysis

Fatigue is the progressive and localized structural damage that occurs when a material is subjected to cyclic loading. The maximum stress values are less than the ultimate tensile stress limit, and may be below the yield stress limit of the material. Failure of a material due to fatigue may be viewed on a microscopic level in three steps

(a) Crack Initiation - The initial crack occurs in this stage. The crack may be caused by surface scratches caused by handling, or tooling of the material; threads (as in a screw or bolt); slip bands or dislocations intersecting the surface as a result of previous cyclic loading or work hardening.

(b) Crack Propagation - The crack continues to grow during this stage as a result of continuously applied stresses.

(c) Failure - Failure occurs when the material that has not been affected by the crack cannot withstand the applied stress. This stage happens very quickly.

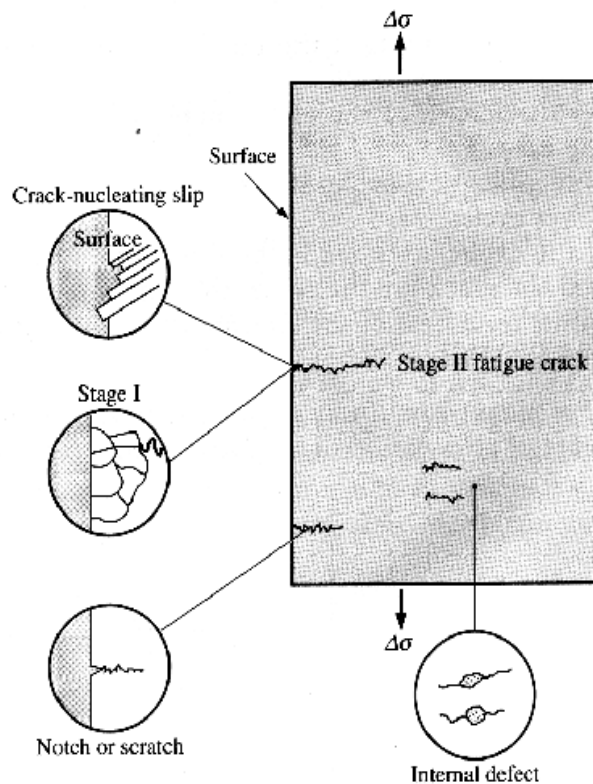


**Fig. 10** Crack Propagation due to fatigue [22]

Figure 10 illustrates the various ways in which cracks are initiated and the stages that occur after they start. This is extremely important since these cracks will ultimately lead to failure of the material if not detected and recognized. The material shown is pulled in tension with a cyclic stress in the horizontal (y-) direction. Cracks can be initiated by several different causes. There are several methods for fatigue assessment which are frequently used in fatigue life prediction or fatigue crack propagation of welded structures and components.

## 5.2 Fatigue mechanism

Fatigue is a mechanism of failure which involves the formation and growth of cracks under the action of repeated stresses. Ultimately, a crack may propagate to such an extent that total fracture of the member may occur. It is known that the local weld geometry, toe angle, toe radius, undercuts and cracks strongly influence the fatigue strength. The local geometry affects the local stress concentration and together with defects of different types fatigue cracks may form during cyclic loading and lead to large scatter in fatigue life. At present, there are two primary approaches used for predicting fatigue life, namely, the fracture mechanics approach and the S-N curve approach. The relationship between these approaches is depicted in Fig. 11.

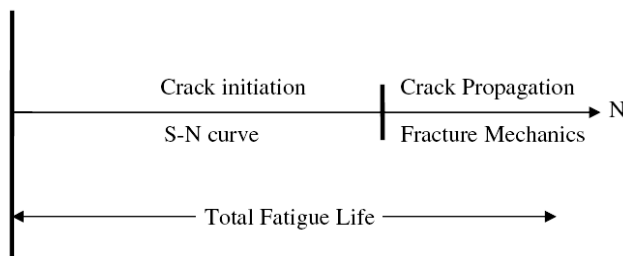


**Fig. 11** Relationship between the characteristics S-N curve and fracture mechanics approaches

## 5.3 Fatigue assessment methods

### Nominal Stress

Nominal stress is the oldest and most popular method used in fatigue analysis. The idea is to calculate a stress component, the nominal stress, which would cause the same damage on the particular welded joint as it would cause on a reference joint. These reference joints are tabled in design codes. Two main difficulties arise; first, how to choose the associated reference joints, and second, how to calculate the nominal stress. Nominal stress can, in simple cases, be calculated analytically using elementary theories of structural mechanics, based on linear-elastic behavior or by FE modeling. In general the following simple formula can be used

$$\sigma_{nom} = \frac{F}{al_w} \quad (1)$$

where,  $a$  is weld throat thickness,  $l_w$  is weld length and  $F$  is force

### Geometric Stress

The geometric stress Fig. 12 incorporates all the stress raising effects on a structural detail, with the exception of stress concentration originating from the weld itself. In fatigue calculation, the geometric stress must be determined in the critical direction and location on the welded joint. The approach is not appropriate for joints where the crack would develop from the root of the weld or from an internal defect. Geometric stress is calculated by taking the stress provided by the finite element analysis or calculated from the deformation measured by gauges at specified distances from the bead toe, as shown in Fig. 12(b). The geometric stress at the bead toe is extrapolated from the values obtained at the measuring points using a two- or three-point formula, in accordance with the following equations (t-sheet thickness)

$$\sigma_{HS} = 1.67\sigma_{0.4t} - 0.67\sigma_{1.0t} \quad (2)$$

$$\sigma_{HS} = 2.52\sigma_{0.4t} - 2.24\sigma_{0.9t} + 0.72\sigma_{1.4t} \quad (3)$$

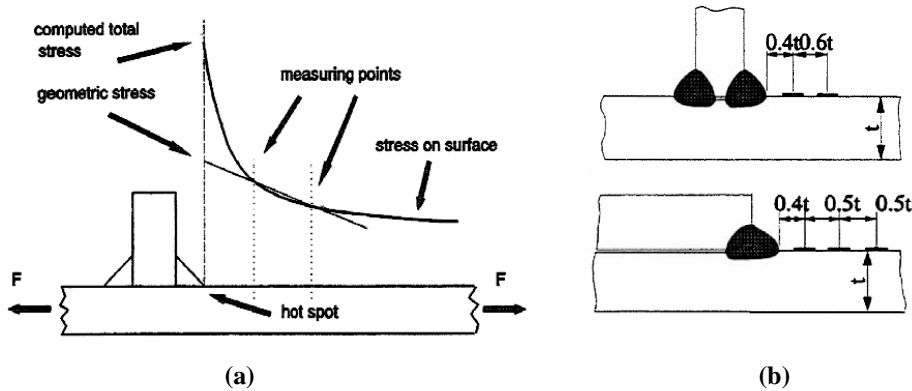


**Fig. 12** Definition of geometric stress (a) and extrapolation points (b) [23]

### Effective Notch Stress Method

The effective notch stress is the maximum stress measured at the notch, corresponding to a radius of 1 mm, as shown in Fig. 13, assuming linear elastic behaviour in the material. One essential benefit of this method is that the notch stress is independent of the geometry, so that a common fatigue strength curve can be used.

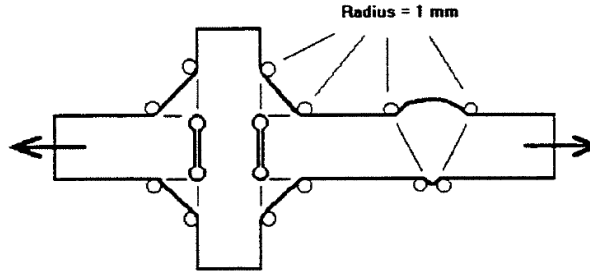


**Fig. 13** Principle of applying 1 mm notch radius at the bead toe and root [23]

### Linear Elastic Fracture Mechanics (LEFM)

The basic procedure of fracture mechanics used for fatigue crack propagation is based on the following two equations;

Fatigue crack growth,  $da/dN$  (in m/cycle):

$$\frac{da}{dN} = C(\Delta K)^m \quad (4)$$

Stress intensity factor range,  $\Delta K$  (in  $\text{MPa m}^{-0.5}$ ):

$$\Delta K = F(a)\Delta\sigma\sqrt{\pi a} \quad (5)$$

( $a$  = initial crack size in the direction of the crack growth,  $C$ ,  $m$  = material constant,  $\Delta\sigma$  = applied nominal stress,  $F(a)$  = correction factor for the stress intensity factor)

In the literature some engineering values for initial crack sizes in welds in steel can be found. Radaj [24] suggests the value  $a = 0.1\text{--}0.5$  mm for a line crack and for a semi elliptical crack he gives  $a/c = 0.1\text{--}0.5$  for the depth/width ratio. In a literature survey by Samuelsson [25] the following typical flaw sizes were found for use in conjunction with welds. At the surface, welding causes defects with depths from 0.01 to 0.05 mm.

When the applied stress range,  $\Delta\sigma$ , is constant during crack propagation, the fatigue crack growth equation can be written as follows

$$dN = \frac{da}{C[F(a)\Delta\sigma\sqrt{\pi a}]^m} \quad (6)$$

Then, the fatigue crack propagation life,  $N_p$ , from an initial crack size  $a_i$  to a final crack size  $a_f$  can be computed as follows:



$$N_p = \int_{N_i}^{N_f} dN = \int_{a_i}^{a_f} \frac{da}{C[F(a)\Delta\sigma\sqrt{\pi a}]^m} \quad (7)$$

The stress intensity factor range,  $\Delta K$ , for a crack initiating at the weld toe may be conveniently expresses as follows:

$$\Delta K = F_S \cdot F_E \cdot F_G \cdot F_T \cdot \sigma \sqrt{\pi a} \quad (8)$$

where,  $F_S$  = correction factor for free surface,  $F_E$  = correction factor for crack shape,  $F_G$  = geometry correction factor accounting for the effect of stress concentration due to geometrical discontinuity,  $F_T$  = correction factor for finite thickness or finite width.

The conventional approach in LEFM uses only one crack tip driving force, namely  $\Delta K$ . The crack growth rate in Region II in Fig.14 is then calculated using the power law Eq. (4). For describing crack growth in all Regions I, II and III, there are numerous equations. For fatigue calculations of welded joints, which are assumed to have an initial defect, only the crack growth in Region II is usually considered. As a lower limit for crack growth, in constant amplitude loading, a threshold value,  $\Delta K_{th}$  can be used.

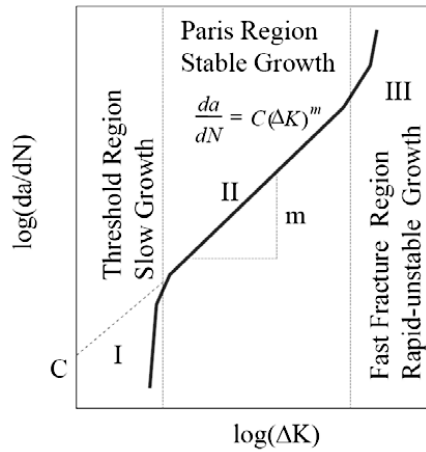


**Fig. 14** Fatigue crack growth law

## 6. Summary of the papers

**Paper I:** Fatigue behaviour study of laser hybrid welded eccentric fillet joints – Part II: State-of-the-Art of fracture mechanics and fatigue analysis of welded joints

**Abstract:** Simplified fatigue and fracture mechanics based assessment methods are widely used by the industry to determine the structural integrity significance of postulated cracks, manufacturing flaws, service-induced cracking or suspected degradation of engineering components under normal and abnormal service loads. In many cases, welded joints are the regions most likely to contain original fabrication defects or cracks initiating and growing during service operation. The welded joints are a major component that is often blamed for causing a structure failure or for being the point at which fatigue or fracture problems initiate and propagate. Various mathematical models/techniques for various classes of welded joints are developed by analytically or by simulation software's that can be used in fatigue and fracture assessments. This literature survey compiled useful information on fracture and fatigue analysis of various welded joints. The present review is divided into two major sections- fracture mechanics and fatigue analysis with widely used models. A survey table is also introduced to get the outlook of research trend on fatigue and fracture over last 3 decades. Although tremendous research effort has been implemented on fatigue and fracture analysis of conventional welding, research on relatively new welding technology (laser welding, hybrid laser welding) is still limited and unsatisfactory. In order to give guarantee or make welding standard for new welding technology, further research is required in the field of fatigue and fracture mechanics including FEM and multi-scale modeling.

### Conclusion

- Finite element modelling is a powerful method for calculating fracture and fatigue of welded joints.
- ANSYS and ABAQUS are widely accepted commercial simulation software.
- Stress intensity factor (K) is one of the most important parameter in fracture mechanics for the mathematical model of welded joints.
- Recent trends of fracture research include dynamic and time-dependent fracture on nonlinear materials, fracture mechanics of microstructures, and models related to local, global, and geometry-dependent fractures.
- LEFM is capable to describe crack growth and crack propagation in welded structures in a physically correct way.
- An engineering value of initial crack size at weld toe would be 0.1 mm.
- From the publication survey, it can be said that the critical weld location is at the toe for different joint.
- More research effort is required on hybrid laser welded joints.

**Paper II:** The influence of surface geometry and topography on the fatigue cracking behaviour of laser hybrid welded eccentric fillet joints.

**Abstract:** Laser hybrid welding of an eccentric fillet joint causes a complex geometry for fatigue load by four point bending. The weld surface geometry and topography were measured and studied in order to understand the crack initiation mechanisms. The crack initiation location and the crack propagation path were studied and compared to Finite Element stress analysis, taking into account the surface macro- and micro-geometry. It can be explained why the root and the upper weld toe are uncritical for cracking. The cracks that initiate from the weld bead show higher fatigue strength than the samples failing at the lower weld toe, as can be explained by a critical radius for the toe below which surface ripples instead determine the main stress raiser location for cracking. The location of maximum surface stress is related to a combination of throat depth, toe radius and sharp surface ripples along which the cracks preferably propagate.

## Conclusion

- The toe radius does not always dominate fatigue performance, as ripples can become local stress raisers.
- If the toe radii are large enough, the stress peak can be shifted to the weld bead; the weld re-solidification ripple pattern guides the cracks.
- Welds which fail in the bead show higher fatigue strength than those which fail in the toe.
- The toe radius and surface topography can vary along the weld.
- The lower toe radius is more critical than the upper toe in this eccentric joint, as its shorter distance to the root generally causes higher stress
- The surface ripples significantly raise stress, but those in the toe normally causes the highest stress, except when the toe radius is small.
- The cracks in this case always started in the weld, not in the HAZ, nor at the fusion interface.
- The complex geometrical interactions involved can be explained by a theoretical illustration.

**Paper III:** Fatigue cracking behaviour for laser hybrid welded eccentric fillet joints including lack of fusion

**Abstract:** Fatigue cracking of laser hybrid welded eccentric fillet joints has been studied for stainless steel. Two-dimensional linear elastic fracture mechanics (LEFM) analysis was carried out for this joint geometry for four point bending load. The numerical simulations explain for the experimental observations why cracking is initiated preferably at the lower weld toe and why the crack gradually bends towards the root. The tendency to Lack of Fusion (LOF) is explained by the restricted positioning of the laser beam along with the thermal barrier of the joint interface. LOF turned out to be uncritical for the initiation of cracks due to its compressive stress conditions. The LEFM analysis has demonstrated, in good qualitative agreement with

fatigue test results, that LOF slightly ( $<10\%$ ) reduces the fatigue life by accelerating the crack propagation. For the here studied geometrical conditions improved understanding of the crack propagation was obtained and in turn illustrated. The elaborated design curves turned out to be above the standard recommendations.

## Conclusion

- In good agreement between simulation (LEFM) and experiments, the crack first propagates normal to the local weld surface, preferably at the lower toe, but then gradually bends to the root
- Lack-of-Fusion (LOF) is likely to take place for this kind of weld; oxide layers and small gaps as the thermal barrier causing LOF can be overcome by very accurate laser beam positioning or by an excess of line energy
- LOF is not critical to initiate cracking, as mainly under compressive stress. When a crack propagates closer to LOF, the interaction increases the stress around the crack and accelerates it, slightly ( $< 10\%$ ) reducing the fatigue life for the here studied case
- The effective notch stress design curves for the batch were above the IIW recommendation. Higher slope ( $m=3.16$ ) of the S-N curves than the corresponding standard was obtained for hybrid laser welded eccentric fillet joints

## Paper IV: Generalising fatigue stress analysis of different laser weld geometries

**Abstract:** Two dimensional elastic-plastic finite element analyses was carried out on a laser welded box beam in order to study the impact of the geometrical aspects of the joint type and weld root on the fatigue performance. Different experimental and hypothetical weld geometries were studied. Characteristic root shapes, measured by the plastic replica method, and critical geometrical aspects were classified and then studied by FE-analysis with respect to their impact on the maximum stress. The simulation of hypothetical transition geometries facilitated the identification of trends and the explanation of part of the phenomena. However, quantitative geometry criteria were only partially suitable to describe the relations. From the results, preferable joint and root types can be recommended. Beside the contribution by multiple throat dimensions and by the root surface curvature, the local opening angle can be essential. The explanations were developed in a generalising manner, accompanied by illustrative and flow chart description.

## Conclusion

From the numerical study of the stress field of four laser welding joint geometries and manifold similar surface geometries the following conclusions can be drawn:

- (i) The combination of throat depths (anchors), local surface curvature (including roughness and sharp corners) and its opening angle determines the peak stress value and its location, as was discussed for a series of joint types and root shapes studied

(ii) Basic relations, derived from inverting the above key geometrical properties, widely explained the qualitative trends, but only to a limited extent the quantitative relations when comparing the stress peaks of different cases; the interacting origins are difficult to separate, even in the simulated stress field data, except when conducting sensitivity studies

(iii) Little surface radii, small opening angles or sharp corners (e.g. at the root or by surface ripples) can attract the maximum stress to a different location than the minimum throat depth location; small radii, the avoidance of sharp corners, of ripples or of small opening angles are highly efficient design guidelines for lowering the stress

(iv) Illustration of the main geometrical aspects and of the stress distribution is a suitable tool for qualitative stress analysis of different joint and surface geometries, particularly for the transition between similar kinds; a modified flow chart method was developed for formulating and documenting the findings, suitable for extension

## 7. General conclusions of the thesis

From the appended papers in this thesis, the following general conclusion can be drawn

- Fatigue life of welded joints is greatly influenced by the competing mechanism between toe radii, root radii, weld angle and weld penetration depth (or other throat thickness).
- For complex root shapes, e.g. with two maxima the location of the maximum stress is often not obvious between them and depends on the confining joint geometry
- When comparing different joint types, often several short distances (anchor lengths) confining the stress distribution need to be considered, while only the side of the weld under tensile load is essential.
- Weld surface ripples i.e. undercut at the micro level, acts as initial crack that propagates along the weld resolidification pattern at bending load situation.
- Details of the shape of the top or root geometry can be essential stress raisers
- Cracks originating in the weld surface instead of the weld toe were associated with increased fatigue life.
- The internal welding defect of lack of fusion does not propagate at compressive stress situation and only slightly reduces ( $< 10\%$ ) fatigue life by interacting stress flow with the crack tip.
- Hybrid laser welded joint obtained higher fatigue strength than the standard recommendation for conventional arc welding.
- Illustration of the phenomena and flow chart formulations were suitable to transfer and generalize new findings.

## 8. Future outlook

Laser and hybrid laser welding are advanced welding technologies nowadays for which numerous researches have already been carried out. Still research on stress analysis of laser welded joint is unsatisfactory. More and more complex welded products are invented by the designers, including the use of high strength metals, which requires proper investigation to achieve the desired mechanical strength. Thus the future outlook for this work can be

- Additional comparison with same weld joint types but by improving the weld geometry with the aid of BFC and with different numerical analysis
- Numerical study of the elastic plastic fracture mechanics (EPFM) regime (typically below  $10^5$  cycles)
- Improved understanding of the impact of microscopic surface details on the fatigue behaviour, particularly by three dimensional fatigue analysis with a real 3D surface texture for complex joints
- Three dimensional analysis of complex product structures and load cases
- Development of design rules for the laser and hybrid laser welding process and thus standardized fatigue curves for different load situation
- Innovation of new techniques which correlate the welding process with the fatigue strength by means of controlling the weld defects for various weld geometries
- Improved understanding of the material properties, particularly for ultra high strength steels
- Isolated analysis of the interacting mechanisms contributing to the stress formation in order to better judge the origins of stress raisers
- On-line measurement of the essential surface properties during production, quantitatively related to monitoring the weld quality related to suitable standards
- Improved guidelines for the welding process parameters for how to avoid critical weld quality details
- Converging knowledge by improved and more frequent use of standardised, generally applicable methods (like the BFC or illustrative methods) for gradually combining and generalising the findings

## 9. References

- [1] V. Caccese, P.A. Blomquist, K.A. Berube, S.R. Webber, N.J. Orozco, Effect of weld geometric profile on fatigue life of cruciform welds made by laser/GMAW processes, *Mar. Struct.* 19 (2006) 1-22.
- [2] M. Ring, W. Dahl, Fatigue properties of laser-beam weldments on the high strength Steels, *Steel Research*. 65(1994) 505-510.
- [3] Z. Barsoum J. Samuelsson, Fatigue Assessment of Cruciform Joints Welded with Different Methods, *Steel Research International*, Vol.77, No.12, 2006.
- [4] W. W. Duley, *Laser welding*, Newyork Wiley 1999 ISBN 0.471-24679-4.
- [5] X. Jin, P. Berger, Th. Graf, Multiple reflections and Fresnel absorption in an actual 3D keyhole during deep penetration laser welding, *J. Phys. D: Appl. Phys.* 39(2006) 4703-4712.
- [6] A.F.H. Kaplan, A model of deep penetration laser welding based on calculation of the keyhole profile, *J. Phys. D: Appl. Phys.*, 27(1994), 1805-1814.
- [7] U. Dilthey, H. Keller, A. Ghandahari, Laser beam welding with filler metal, *Steel Research* 70(1999) 198–202.
- [8] J. Matsuda, A. Utsumi, M. Hamasaki, S. Nagata, TIG or MIG arc augmented laser welding of thick mild steel plate, *Joining and Materials*, (1988) 31–34.
- [9] J. Alexander, W. M. Steen, Arc augmented laser welding-process variables, structure and properties, *The Joining of Metals: Practice and Performance*, (2000) 155–160.
- [10] W.M. Steen, M. Eboo, Arc augmented laser welding, *Metal Construction*, (1979) 332–335.
- [11] N. Abe, Y. Agamo, M. Tsukamoto, T. Makino, M. Hayashi, T. Kurosawa, High speed welding of thick plates on laser-arc combination system, *JWRI* 26(1997) 69 -75.
- [12] C. Bagger, F. Olsen, Review of laser hybrid welding, *J. L. App.*, 17(2005).
- [13] K.H. Magee, V. E. Merchant, C. V. Hyatt, Laser assisted gas metal arc weld characteristics, *Proceedings of the Laser Materials Processing - ICALEO '90*, Nov 4-9 1990, Boston, MA, USA, LIA (Laser Institute of America), v 71, 1991.
- [14] C. Miki, K. Homma, T. Tominaga, High strength and high performance steels and their use in bridge structures, *J. of Const. Steel Research*, (2002) 3 – 20.

- [15] R. Bjorhovde, Development and use of high performance steel, *Journal of Constructional Steel Research*, (2004) 393–400.
- [16] T. Dahle, Design fatigue strength of TIG-dressed welded joints in high-strength steels subjected to spectrum loading, *Int. J. of Fatigue*, (1998) 677-681.
- [17] K. J. Kirkhope, R. Bell, L. Caron, R. I. Basu, K. T. Ma, Weld detail fatigue life improvement techniques, part 1: review, *Marine Structures*, 2(1999) 447-474.
- [18] K. J. Kirkhope, R. Bell, L. Caron, R. I. Basu, K. T. Ma Weld detail fatigue life improvement techniques, part 2: application to ship structures, *Marine Structures*, 12(1999) 477-496.
- [19] Z. Xiulin, L. Baotong, C. Tianxie, L. Xiaoyan, L. Chao, Fatigue tests and life prediction of 16 Mn steel butt welds without crack-like defect, *Int. J. Frac.*, 68 (1994) 275–85.
- [20] C.Y. Hou, Fatigue analysis of welded joints with the aid of real three-dimensional weld toe geometry, *Int. J. of Fatigue*, 29(2007) 772-785.
- [21] M.D.Chapetti, J.L.Otegui, Importance of toe irregularity for fatigue resistance of automatic welds, *Int. J. of Fatigue*, 17(1995) 531-538.
- [22] F. Ellyin, *Fatigue damage, crack growth and life prediction*, ISBN 0-412-59600-8.
- [23] G. Pettersson, *Fatigue assessment of welded structures with non-linear boundary conditions*, Licentiate Thesis, Dept. of Aeronautical and Vehicle Engineering, KTH, Sweden, ISBN 91-7283-948-1 (2004).
- [24] D. Radaj, *Design and analysis of fatigue resistant welded structures*, Abington Publishing, ISBN 1 85573 004 9 (1990).
- [25] J. Samuelsson, *Fatigue design of vehicle components: methodology and applications*, report 88-23, Dep. Of Aeronautical Structures and Materials, The Royal Institute of Technology, Stockholm, (1998).



## **Paper I**

### **FATIGUE BEHAVIOUR STUDY OF LASER HYBRID WELDED ECCENTRIC FILLET JOINTS – PART II: STATE-OF-THE-ART OF FRACTURE MECHANICS AND FATIGUE ANALYSIS OF WELDED JOINTS**

M. M. Alam, A. F. H. Kaplan, P. Jonsén

Proceedings of NOLAMP 12 Conference, Copenhagen, Denmark 24-26 August 2009



# **FATIGUE BEHAVIOUR STUDY OF LASER HYBRID WELDED ECCENTRIC FILLET JOINTS – PART II: STATE-OF-THE-ART OF FRACTURE MECHANICS AND FATIGUE ANALYSIS OF WELDED JOINTS.**

**M. M. Alam, A. F. H. Kaplan, P. Jonsén**

<sup>1)</sup> Luleå University of Technology, Dept. of Applied Physics and Mechanical Engineering, Sweden, [www.ltu.se/tfm/produktion](http://www.ltu.se/tfm/produktion)

## **ABSTRACT**

Simplified fatigue and fracture mechanics based assessment methods are widely used by the industry to determine the structural integrity significance of postulated cracks, manufacturing flaws, service-induced cracking or suspected degradation of engineering components under normal and abnormal service loads. In many cases, welded joints are the regions most likely to contain original fabrication defects or cracks initiating and growing during service operation. The welded joints are a major component that is often blamed for causing a structure failure or for being the point at which fatigue or fracture problems initiate and propagate. Various mathematical models/techniques for various classes of welded joints are developed by analytically or by simulation software's that can be used in fatigue and fracture assessments. This literature survey compiled useful information on fracture and fatigue analysis of various welded joints. The present review is divided into two major sections- fracture mechanics and fatigue analysis with widely used models. A survey table is also introduced to get the outlook of research trend on fatigue and fracture over last 3 decades. Although tremendous research effort has been implemented on fatigue and fracture analysis of conventional welding, research on relatively new welding technology (laser welding, hybrid laser welding) is still limited and unsatisfactory. In order to give guarantee or make welding standard for new welding technology, further research is required in the field of fatigue and fracture mechanics including FEM and multi-scale modeling.

**Keywords:** Fracture mechanics, fatigue, welded joints, welding standards, FEM, multi-scale modeling.

## **1. INTRODUCTION**

This paper is a literature survey which compiled useful information regarding fracture and fatigue analysis of various welded joints. The main objective was on to analyze fracture mechanics and fatigue life prediction on hybrid laser welded joints. Since hybrid laser welding is a new technology and very few researches have been done on this area, this literature survey has to restrict on conventional welding process from where fracture and fatigue analysis are shortly presented. Around 550 publications are illustrated in [1].

This paper is mainly divided into two major section- fracture mechanics and fatigue analysis. In fracture mechanics, a basic study on fracture mechanics is given followed by three different approaches on three types welding joints and fatigue analysis section is oriented by four fatigue assessment method from where two methods are described briefly.

Nowadays, the trend is to use the welded structures to the maximum of their life potential. To achieve this aim, considerable effort should be paid on design of welded joints. Weld joints are characterized by differences in mechanical properties produced by geometrical, material and metallurgical discontinuities. The heat-affected zone is usually a source of failure of welded parts/structures. The quality of welding has strong influence on the strength of whole structure beside the welding depth and the geometry of the weld surface. The presence of cracks, defects and residual stresses is a danger to structure in service.

To determine residual stresses, cracks, defects, there are several approaches based on fracture mechanics. Two main approaches are mostly used: *Linear Elastic Fracture Mechanics (LEFM)* and *Elastic Plastic Fracture Mechanics (EPFM)* [4]. In this literature survey, these two approaches have been focused on.

A material fractures when sufficient stress and work are applied on the atomic level to break the bonds that hold atoms together. The bond strength is supplied by the attractive forces between atoms. Figure 1 shows schematic plots of the potential energy and force versus separation distance between atoms.

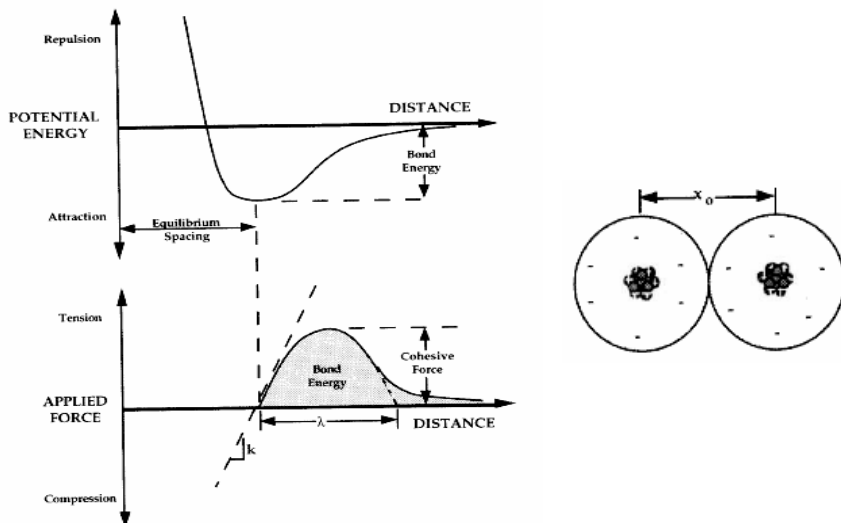


**Fig. 1:** Potential energy and force as a function of atomic separation [4]

The equilibrium spacing occurs where the potential energy is at a minimum. At the equilibrium separation,  $x_0$ , the potential energy is minimized and the attractive and repelling forces are balanced. A tensile force is required to increase the separation

distance from the equilibrium value; this force must exceed the cohesive force to sever the bond completely.

Fatigue is a mechanism of failure which involves the formation and growth of cracks under the action of repeated stresses. Ultimately, a crack may propagate to such an extent that total fracture of the member may occur. It is known that the local weld geometry, toe angle, toe radius, undercuts and cracks strongly influence the fatigue strength. The local geometry affects the local stress concentration and together with defects of different types fatigue cracks may form during cyclic loading and lead to large scatter in fatigue life [46]. At present, there are two primary approaches used for predicting fatigue life, namely, the fracture mechanics approach and the S-N curve approach. See Fig 21. The relationship between these approaches as depicted in Fig.2

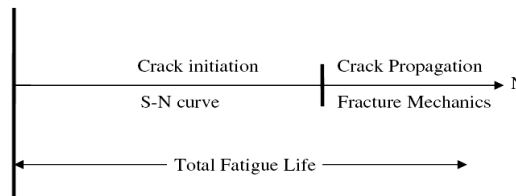


**Fig. 2:** Relationship between the characteristics S-N curve and fracture mechanics approaches [22]

## 2. SURVEY OF JOURNALS

**Table1.** Survey of publications on fracture mechanics and fatigue analysis

No.	Author name	Country	Welding types	Joint types	Critical weld location	Mathematical Models /Techniques	Simulation software	Estimation /Goal	Year
7	B. Chang	China	S	L		Experimental		Hardness distribution	1999
8	P. Dong	USA		L,T	T	FEM		Structural Stress	2001
9	El-Sayed	USA	S	S	T	FEM	NA	Fatigue life estimation	1996
10	H.F.Henrysson	Sweden	S	S	T	Coarse FEM		Fatigue life prediction	2000
11	H.Remes	Finland	L	B	R	Theoretical		Fatigue strength	2003
12	S.K.Cho	S. Korea	L	T	T	Thermo-elastic-plastic FEM	AB	Fatigue strength	2003
13	S.J.Maddox	UK		C	T	Fracture mechanics		Fatigue cracks	1973
14	M.S.Alam	USA		B	T	FEM	AN	Simulation-fatigue crack growth	2004
15	L.S.Etube	UK		U		Statistical		Y correction	2000

								factor	
16	M.A.Sutton	Columbia	F	B		FEM	AN	Residual stress	2006
17	B.Guha	India	F	C	R	Strain Energy density approach		Crack growth behavior	1999
18	P.J.Haagensen	Norway	T	L,T	R	Ultrasonic impact treatment		Introduction of fatigue test	1998
19	T.L.Teng	Taiwan	T	B	T	Strain based		Prediction-fatigue crack initiation	2003
20	X.Y.Li	Finland		T	T	LEFM		Fatigue strength	2001
21	Y. Jiang	USA				Elastic-Plastic	AB	Crack growth rate and crack direction.	2006
22	V.Caccese	USA	L	C	T	Conventional FEM	AN	Weld geometric profile	2006
23	Chris Hsu	USA	L	L	T	Cyclic stress-strain		Joint stress calculation	1991
24	Z.Barsoum	Sweden	H	C	T	LEFM	AN	Fatigue assessment	2005
25	G.Pettersson	Sweden				LEFM	AN	Non-linear effects	2004
26	P.Andersson	Sweden		X		Creep ductility-based damage	AB	Creep crack growth investigation	1999
27	A. Assire	France		X		FEM		Creep crack initiation and creep growth assessments	2000
28	Y.C.Hou	USA			C	J-Integral		Fracture parameter	1998
29	Infante, V	Portugal		T	T	Elastic-Plastic	AB	Residual Stress analysis	2002
30	J.M. Ferreira	Portugal	A	T,C	T, M	FEM		Fatigue life prediction	1994
31	G.Cam	Turkey	L	B	R	Experimental		Mechanical & fracture properties	1999
32	B.Atzori	Italy		C	T	LEFM		Fatigue strength	1998
33	P.J.Budden	UK			C	Fracture mechanics	BE	Creep crack growth	1999
34	P.C. Wang	USA	L	T		J- Integral	AB	Fracture mechanics parameter	1994
35	C.Maosheng	China	A	B	T	Fracture mechanics		Crack growth & fatigue life estimation	1990
36	H.P.Lieurade	France	A	B,C	T	Fracture mechanics		Fatigue life estimation	1983
37	J.C. Newman	USA				Weight function		Stress intensity factor	1996
38	H.J.Schindler	Switzerland		T,B	R	LEFM		Fatigue endurance	2006
39	Chang K.H.	Korea	A	B	C	Elastic-Plastic		Residual stress	2006
40	Y.Lei	UK			C	J- Integral	AB	Residual stress	2000

41	H.Y.Lee	S.Korea		T,B		LEFM	AB	Stress intensity factor	2005
42	W.Muller	Germany			C	Elastic-Plastic	AD	Weld material properties	1988
43	W.Dahl	Germany	A	T	C	Elastic-Plastic	AB	Fracture mechanics	1986
44	M. Chiesa	Norway	A		C	J-Integral	AB	Fracture analysis	2000
45	T. Nykänen	Finland		T,B	T	LEFM	FR	Fracture mechanics study	2005

**LEGEND:****Joint Type**

L : Lap

T : T

S : Spot

B : Butt

C : Cruciform

U: Tubular

X : Cross Weld

F : Fillet

**Welding type**

S : Spot

L : Laser

F : Friction Stir

A : Arc

T : TIG

H : Hybrid Laser

**Critical Location**

T : Toe

R : Root

C : Crack tip

M : Mid. of weld

**Simulation Software**

AB : ABAQUS

AN : ANSYS

BS : BERSAFE

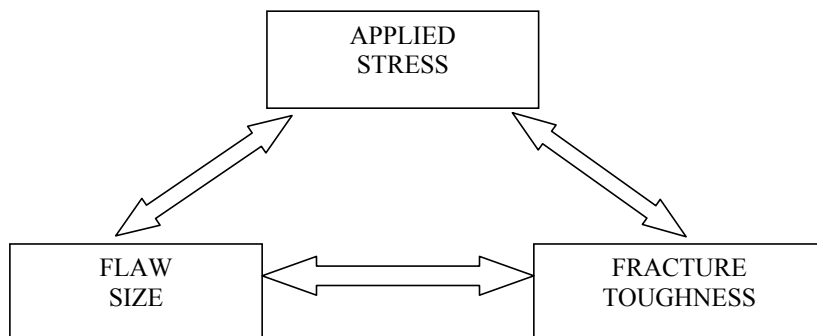
FR : FRANC 2D

NA : NASTRAN

AD : ADINA

**3. FRACTURE ANALYSIS****3.1 Fundamental knowledge on fracture mechanics**

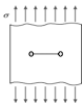
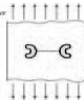
Fracture mechanics is the study of mechanical behaviour of cracked materials subjected to an applied load. Crack growth behavior due to fatigue, stress corrosion, creep, or some combination thereof can be simulated and predicted with the appropriate software and experimental data. [49].The fracture mechanics approach has three important variables:

**Fig. 3:** The fracture mechanics approach

Fracture mechanics can be approached from a number of points of view, including energy to cause failure, stress analysis, micro mechanisms of fracture, applications of

fracture, computational approaches and so on. A simplified table for the analysis of fracture mechanics depending on the material properties on fracture shows below:

**Table 2:** Simplified table for the field of fracture mechanics [2]

Category	Material Property	Parameter	Effective Regime
Linear Elastic Fracture Mechanics (LEFM)	Linear, time-independent	Stress intensity factor(K), Energy release rate(G)	
Elastic Plastic Fracture Mechanics	Non-linear, time-independent	J- Integral, Crack tip opening displacement (CTOD)	

### 3.1.1. Linear elastic fracture mechanics

Linear Elastic Fracture Mechanics (LEFM) first assumes that the material is isotropic and linear elastic. Based on the assumption, the stress field near the crack tip is calculated using the theory of elasticity. When the stresses near the crack tip exceed the material fracture toughness, the crack will grow.

#### THE GRIFFITH ENERGY BALANCE

According to the First Law of Thermodynamics, when a system goes from a non equilibrium state to equilibrium, there will be a net decrease in energy. In 1920 Griffith applied this idea to the formation of a crack. Griffith observed that the strain energy in a body is partly released by the propagation of a crack. At the same time, new surfaces are created in the body, which are associated with a certain surface energy, which in turn is characteristic for a material. According to Griffith, a necessary condition for failure is that the released strain energy, corresponding to a certain crack growth, is greater than the consumed surface energy.

Griffith considered a plane plate of a linear elastic material with a through-thickness crack of length  $2a$ , **Fig. 4**. The in-plane dimensions of the plate are much larger than the length of the crack and in the theory the plate is assumed to be infinite. The boundary of the plate is subjected to a constant and uni-axial stress  $\sigma$  perpendicular to the plane of the crack.



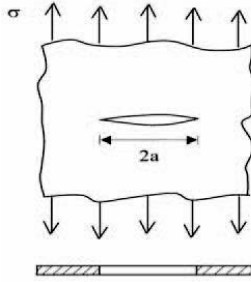


**Fig. 4:** The Griffith crack [4].

From the stress state in a plate with an elliptic hole (Inglis, 1913), Griffith determined the elastic strain energy  $U(a)$  as a function of crack length for a plate with crack:

$$U(a) = U_0 - \frac{\pi \sigma^2 a^2}{E} \quad (1)$$

Where  $U_0$  is the strain energy in the plate without regard to the crack,  $\sigma$  the nominal stress in the crack plane and  $E$  is Young's modulus.

Through crack growth, material close to the newly formed crack surfaces is unloaded and the corresponding elastic energy released. The energy released per unit length of crack growth at a crack tip, or the *crack extension force*  $G$ , is:

$$G = -\frac{dU(a)}{da} = \frac{\pi \sigma^2 a^2}{E} \quad (2)$$

In the crack propagation process, energy is required to create new crack surfaces and for plastic deformation and other dissipative processes adjacent to the new surfaces. The energy required per unit crack length is called the *critical crack extension force*  $G_c$ .

The condition for fracture is then  $G = G_c$

i.e. fracture occurs at a critical value of the crack extension force.

Thus it can be concluded that failure occurs when the stress, crack length and critical crack extension force are related as follows:

$$G_c = \frac{\pi \sigma_c^2 a_c}{E} \quad (3)$$

Here  $\sigma_c$  is the nominal, or critical, stress at fracture and  $a_c$  the critical crack length.

## STRESS INTENSITY FACTOR

While the energy-balance approach provides a great deal of insight to the fracture process, an alternative method that examines the stress state near the tip of a sharp crack directly has proven more useful in engineering practice. A plane plate with a crack can in the general case be loaded in three different ways, in accordance to the nominal stress components  $\sigma_{yy}$ ,  $\tau_{xy}$  and  $\tau_{yz}$  in the plane of the plate. In **Fig. 5** is shown the stress components and the orientation of the coordinates and of the crack. The plane of the crack is situated in the  $xz$ -plane and the crack front is along the  $z$ -axis.

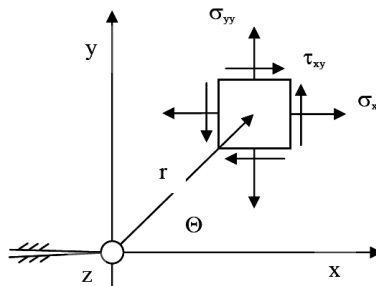


**Fig. 5:** Stress components at a crack tip [4]

Along the  $x$ -axis and ahead of the crack  $\sigma_{yy}$  is the normal stress in the plane of the crack. This stress component tends to open the crack and the corresponding mode of deformation is denoted Mode I.  $\tau_{xy}$  is the shear stress in the plane of the plate and corresponds to in-plane shear, or Mode II deformation. This stress component tends to slide the crack surfaces relative to each other in the plane of the plate.

$\tau_{yz}$  is the shear stress acting perpendicular to the plane of the plate and corresponds to transverse shear, or Mode III deformation. In **Fig. 6** there different crack tip deformation modes are shown: opening, sliding, and tearing:

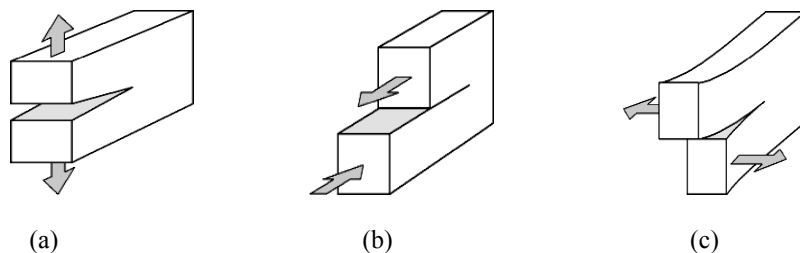


**Fig. 6:** Three basic modes of crack tip deformation. (a) mode I-opening; (b) mode II-sliding; (c) mode III-tearing [2]

In practise Mode I is the most important case and therefore only this mode will be dealt with further here. For Mode I the asymptotic stress field at the tip of a crack in a

linear elastic material is given in the following equation. The origin of the coordinates is located at the crack tip.  $x, y, z$  are Cartesian coordinates and  $r, \theta$  polar coordinates.

$$\begin{aligned}\sigma_{xx} &= \frac{K_I}{\sqrt{2\pi r}} \cos \frac{\theta}{2} \left( 1 - \sin \frac{\theta}{2} \sin \frac{3\theta}{2} \right) \\ \sigma_{yy} &= \frac{K_I}{\sqrt{2\pi r}} \cos \frac{\theta}{2} \left( 1 + \sin \frac{\theta}{2} \sin \frac{3\theta}{2} \right) \\ \tau_{xy} &= \frac{K_I}{\sqrt{2\pi r}} \cos \frac{\theta}{2} \sin \frac{\theta}{2} \cos \frac{3\theta}{2}\end{aligned}\quad (4)$$

In the crack plane  $y = 0$ , where  $r = x$  and  $\theta = 0$  ahead of the crack, (4) reduces to the simpler form:

$$\begin{aligned}\sigma_{xx} &= \sigma_{yy} = \frac{K_I}{\sqrt{2\pi x}} \\ \tau_{xy} &= 0\end{aligned}\quad (5)$$

In (4) all stress components are proportional to the factor  $K_I$ , which accordingly is denoted the *stress intensity factor*.

By applying a virtual crack extension model Irwin (1957) showed that the energy released per unit crack length is:

$$-\frac{dU}{da} = \frac{K_I^2}{E} \quad (6)$$

Eqs. (3) and (6) provides a relation  $G$  and  $K_I$

$$G = \frac{K_I^2}{E} \quad (7)$$

From (3) and (7) the stress intensity factor for the Griffith plate is further obtained as

$$K_I = \sigma \sqrt{\pi a} \quad (8)$$

In practice the general form of the stress intensity factor is

$$K_I = \sigma \sqrt{\pi a} f(g) \quad (9)$$

Where  $f(g)$  is a dimensionless function which depends on the geometry of the cracked body considered.

Expressions for  $K_I$  for some additional geometries are given in Table 3.

**Table 3:** Stress intensity factor for several common geometry

Type of Crack	Stress Intensity Factor, $K_I$
Edge crack, length $a$ , in a semi-infinite plate	$1.12\sigma\sqrt{\pi a}$
Central penny-shaped crack, radius $a$ , in infinite body	$2\sigma\sqrt{\frac{a}{\pi}}$
Center crack, length $2a$ in plate of width $W$	$\sigma\sqrt{W \tan \frac{\pi a}{W}}$
2 symmetrical edge cracks, each length $a$ , in plate of total width $W$	$\sigma\sqrt{W \left[ \tan\left(\frac{\pi a}{W}\right) + 0.1 \sin\left(\frac{2\pi a}{W}\right) \right]}$

These stress intensity factors are used in design and analysis by arguing that the material can withstand crack tip stresses up to a critical value of stress intensity, termed  $K_{Ic}$ , beyond which the crack propagates rapidly. *This critical stress intensity factor* is then a measure of material toughness. The failure stress  $\sigma_f$  is then related to the crack length  $a$  and the fracture toughness by

$$\sigma_f = \frac{K_{Ic}}{\alpha\sqrt{\pi a}} \quad (10)$$

where,  $\alpha$  is a geometrical parameter equal to 1 for edge cracks and generally on the order of unity for other situations. Expressions for  $\alpha$  are tabulated for a wide variety of specimen and crack geometries, and specialty finite element methods are available to compute it for new situations.

### 3.1.2 ELASTIC PLASTIC FRACTURE MECHANICS

Elastic Plastic Fracture Mechanics (EPFM) assumes isotropic and elastic-plastic materials. Based on the assumption, the strain energy fields or opening displacement near the crack tips are calculated. When the energy or opening exceeds the critical value, the crack will grow

For almost all materials, including steel, the engineering stress-strain curve is initially linear, i.e. stress is proportional to strain. A transition to non-linear behavior follows as the material is loaded beyond a limit of proportionality, called the *yield strength* of the material. Within the linear part of the stress-strain curve, deformation is purely *elastic*. If a specimen is unloaded before the yield strength was attained, the unloading curve is identical to the loading curve; see **fig 7 (a)**. After unloading, the specimen returns to its original shape, without any permanent deformation.

A material is said to *flow* when deformed beyond the yield strength. Consider a specimen loaded to the point *A* in **Fig. 7(c)** and then unloaded. The unloading will not follow the loading curve backward, but instead a linear curve with the same slope as the initial, elastic curve. The unloading curve is in fact elastic. After unloading a permanent or *plastic* deformation remains in the material. [2]

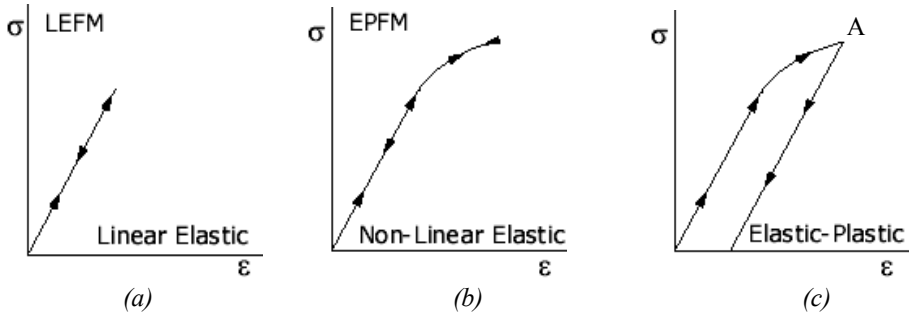


**Fig. 7:** Relationship between LEFM & EPFM. (a) linear elastic curve; (b) non-linear elastic curve; (c) elastic-plastic curve[2]

## NON LINEAR ENERGY RELEASE RATE

In 1956, Irwin proposed an energy approach for fracture. Irwin defined an energy release rate,  $G$ , which is a measure of the energy available for an increment of crack extension:

$$G = -\frac{d\Pi}{dA} \quad (11)$$

where,  $G$  is the rate of change in potential energy with crack area. Equation (11) defines the energy release rate for linear materials. The same definition holds for nonlinear elastic materials except  $G$  is replaced by  $J$ :

$$J = -\frac{d\Pi}{dA} \quad (12)$$

where,  $\Pi$  is the potential energy and  $A$  is crack area. The potential energy is given by

$$\Pi = U - F \quad (13)$$

where,  $U$  is the strain energy stored in the body and  $F$  is the work done by external forces. Considering a cracked plate which exhibits a nonlinear load-displacement curve, as illustrated in **Fig. 8**

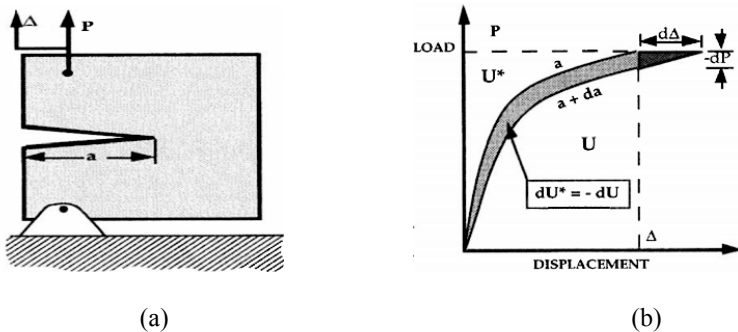


**Fig. 8:** Non-linear energy rate. (a) Cracked plate; (b) Load-displacement curve [4]

In **Fig. 8(b)**, the area under the curve is the strain energy  $U$ , and the area above the curve, called the complementary strain energy,  $U^*$ .

For load control

$$\Pi = U - P\Delta = -U^* \quad (14)$$

where, complementary strain energy is defines as

$$U^* = \int_0^P \Delta dP \quad (15)$$

Thus, if the plate in **Fig. 8 (a)** is in load control,  $J$  is given by

$$J = \left( \frac{dU^*}{da} \right)_P \quad (16)$$

If the crack advances at a fixed displacement,  $F=0$ , and  $J$  is given by

$$J = - \left( \frac{dU^*}{da} \right)_\Delta \quad (17)$$

According to **Fig. 8**,  $dU^*$  for load control differs from  $-dU$  for displacement control by the amount  $\frac{1}{2}dP\Delta$ , which vanishingly small compared to  $dU$ . There fore,  $J$  for load control is equal to  $J$  for displacement control.

## J INTEGRAL

For a two-dimensional body of area,  $A$ , with surface traction,  $T_i$  prescribed over a portion of the bounding surface,  $\Gamma$ , the potential energy of the body is given by

$$\Pi = \int_A W dA - \int_\Gamma T_i u_i ds \quad (18)$$

By differentiating Eqn. 18

$$J = - \frac{d\Pi}{dA} = \frac{1}{B} \int_A \frac{dW}{da} dA - \frac{1}{B} \int_\Gamma T_i \frac{du_i}{da} ds \quad (19)$$

After some manipulations, this equation can be written in the form

$$J = \int_\Gamma \left( W dy - T_i \frac{\partial u_i}{\partial x} ds \right) \quad (20)$$

Where,  $\Gamma$  is arbitrary counter-clockwise path around crack tip as illustrated in **Fig.9**.  $W = \int \sigma_{ij} d\varepsilon_{ij}$  is the strain energy density where  $\sigma_{ij}$  is the stress tensor and  $\varepsilon_{ij}$  the

strain tensor,  $T_i = \sigma_{ij}n_j$  is the stress vector where  $n_j$  is positive outward unit normal and  $u_i$  the displacement vector and  $ds$  an increment of the length along the path.

$J$  can be evaluated on an arbitrary contour around a crack tip. Because of the property of path independence of the integral, it always yields the same value for any path enclosing the crack tip. Thus  $J$  is called a *path-independent* integral.

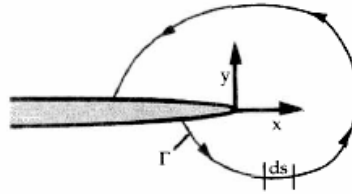


**Fig. 9:** Arbitrary contour around the tip of a crack [4]

### 3.2 WELDED JOINTS ANALYSIS BASED ON FRACTURE MECHANICS

#### 3.2.1 T-JOINTS (Stress Intensity approach)

In service cracks may form at the weld toe due to the stress concentration there. Such cracks tend to be along the line A-A in **Fig 10**, i.e. normal to the transverse stress. A fracture assessment for such a crack will generally require the linear elastic stress intensity factor,  $K$ , due to the weld residual stress and any additional primary (mechanical) loading. [3]

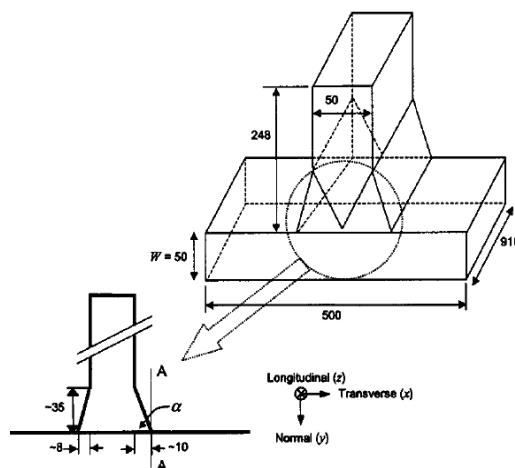


**Fig.10:** Geometry of T-plate weld [3]

The stress intensity factors for the cracked T-plate have been calculated using linear superposition.

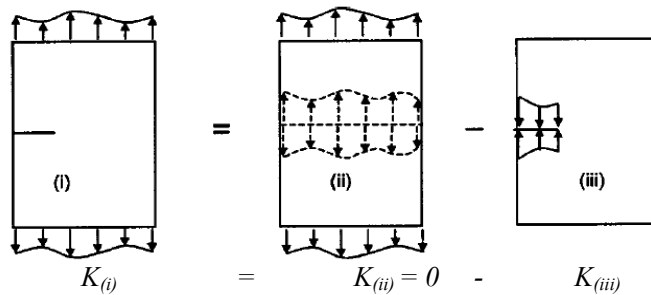


**Fig. 11:** Superposition method to determine stress intensity factor [4]

As illustrated in **Fig.11**, to determine the value of  $K$  only the stress distribution over the crack face is required, i.e.,  $K(i) = -K(iii)$ . For the current problem, the crack face loading is simply the measured (or approximated) residual stress at the weld toe. The approach taken here is analogous to the weight function method, except for the fact that the  $K$  value from the crack face loading is obtained directly using a finite element analysis, rather than by using a weight function.

**FEM Simulation** A typical finite element mesh, which contains 13,000 plane strain four noded elements, is illustrated in **Fig. 12**.

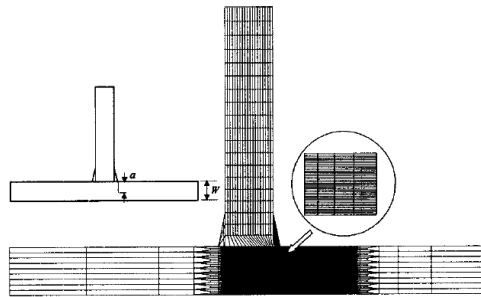


**Fig. 12:** Finite element mesh used in stress intensity factor calculation [3]

The (un-cracked) T-plate is assumed symmetric with weld angle,  $\alpha = 80^\circ$ . A crack of length,  $a$ , is included at the right hand weld toe, as indicated in the inset to **Fig. 12**, thus losing the symmetry of the problem. Because of the very dense mesh near the weld toe the element boundaries are not visible in this region of the figure. The smallest element size is 0.03 mm. The fracture mechanics parameters  $J$  and  $K$  can be calculated from any FEM software— $J$  is calculated using a standard domain integral implementation and  $K$  is obtained using an interaction integral approach. The advantage of the latter approach is that for mixed mode problems, both the mode I and



mode II intensity factors,  $K_I$  and  $K_{II}$ , respectively, are calculated. For a mode I linear elastic problem  $K=K_I$  can be evaluated from  $J$  using the relationship (for plane strain),

$$K = \sqrt{\frac{JE}{1-\nu^2}} \quad (21)$$

where  $E$  and  $\nu$  are the Young's modulus and Poisson ratio, respectively.[3]

### 3.2.2 BUTT JOINT (J-Integral)

A finite element analysis method which can calculate the J-integral for a crack in a residual stress field is developed to evaluate the J-integral for a centre crack when mechanical stresses were applied in conjunction with residual stresses. In this case, double 'V' butt joint configuration has been showed for joining the plates in **Fig. 13**.

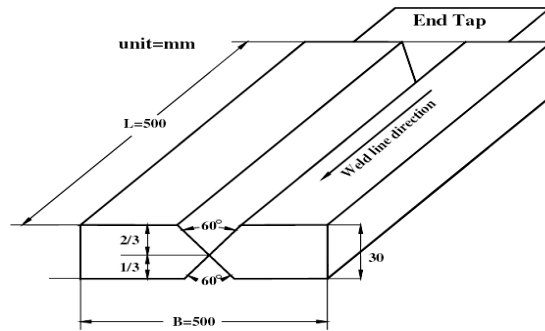


**Fig. 13:** Joint configuration [39]

The J-integral has emerged over the last years as one of the leading parameters to characterize crack-propagation in solids. The J-integral derived by Rice was proposed as the strain energy release rate at the crack tip in linear or nonlinear solid and written as

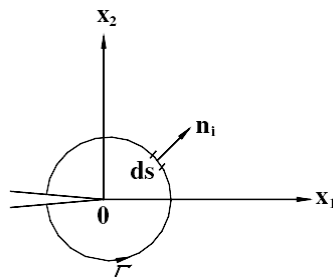


**Fig. 14:** Typical contour for evaluation of J-integral [40]

$$J = -\frac{d\Pi}{da} = \int_{\Gamma} \left( W \delta_{1i} - \sigma_{ij} \frac{\partial u_j}{\partial x_1} \right) n_i ds \quad (22)$$

where  $\Pi$  is the potential energy,  $\sigma_{ij}$  and  $u_j$  are components stress and displacement in Cartesian coordinate respectively,  $\Gamma$  is a curve surrounding the crack tip which begins at the lower face of the crack and ends at the upper one,  $n_j$  is the unit vector normal to  $\Gamma$  and  $ds$  is the path length along  $\Gamma$  (**Fig. 14**) and  $W$  is the strain energy density and defined as

$$W = \int_0^{\varepsilon_{ij}} \sigma_{ij} d\varepsilon_{ij}^m \quad (23)$$

### The J-Integral in a three-dimensional residual stress field

By applying the divergence theorem to above J-Integral equation and generalizing the results for three dimensions subject to in plane displacement yields

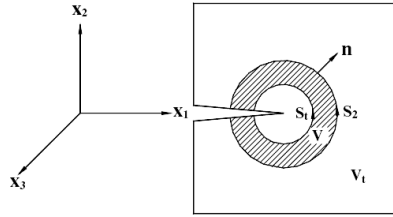


**Fig.15:** Volume V formed by  $S_1$  &  $S_2$  [40]

$$(J)_{volume} = -\int_V \left( W \frac{\partial q}{\partial x_1} - \sigma_{ij} \frac{\partial u_i}{\partial x_1} \frac{\partial q}{\partial x_j} \right) dV - \int_V \frac{\partial W}{\partial x_1} - \sigma_{ij} \frac{\partial \varepsilon_{ij}}{\partial x_1} \quad (24)$$

where,

$$\frac{\partial W}{\partial x_1} = \frac{\partial W}{\partial \varepsilon_{ij}^m} \frac{\partial \varepsilon_{ij}^m}{\partial x_1} = \sigma_{ij} \frac{\partial \varepsilon_{ij}^m}{\partial x_1} \quad (25)$$

When initial strain is absent, the second term in the above integral is zero. Otherwise,  $\varepsilon_{ij}^m$  is then written as

$$\varepsilon_{ij}^m = \varepsilon_{ij}^e + \varepsilon_{ij}^p + \varepsilon_{ij}^o \quad (26)$$

where,  $\varepsilon_{ij}^e$  and  $\varepsilon_{ij}^p$  are the total elastic and plastic strains, respectively and  $\varepsilon_{ij}^o$  is the initial plastic strain.

Inserting Eqs. (25) and (26) into Eq. (24) lead to a path-independent J-integral definition considering residual stress and initial strain as follows:

$$(J)_{\text{volume}} = - \int_v \left( W \frac{\partial q}{\partial x_i} - \sigma_{ij} \frac{\partial u_i}{\partial x_i} \frac{\partial q}{\partial x_j} \right) dV + \int_v \sigma_{ij} \frac{\partial \varepsilon_{ij}^p}{\partial x_i} q dV \quad (27)$$

And  $W$  must be adjusted to account for the initial strain energy density i.e.

$$W = W^{\text{total}} - W^P \Big|_{\text{initial}}$$

where,  $W^P \Big|_{\text{initial}}$  is the plastic work done before the initial state [39]

### 3.2.3 TUBULAR JOINTS (Stress intensity approach)

The accurate evaluation of SIF for surface cracks in tubular joints is a difficult task due to complex geometry of the joint and crack configuration.

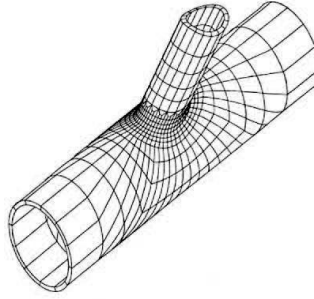


**Fig. 16:** Geometry of Tubular joints [47]

Well established procedures commonly used for evaluating SIF in arbitrary cracked bodies are, displacement extrapolation technique, strain energy release rate (SERR) method and J-integral method. In this paper, displacement extrapolation technique has been used for computing SIF. Bowness and Lee [5] reported an investigation on the prediction of SIF in tubular joints for semi-elliptical surface cracks by using displacement extrapolation technique. The method uses the elastic displacements in the vicinity of the crack front for computing SIF. For the case of plane strain conditions at crack front, the displacement fields are expressed as: [4]

$$\begin{aligned} v_n &= \frac{K_I}{G} \sqrt{\frac{r}{2\pi}} \sin \frac{\theta}{2} \left[ 2 - 2\nu - \cos^2 \left( \frac{\theta}{2} \right) \right] \\ \text{Mode I: } u_r &= \frac{K_I}{G} \sqrt{\frac{r}{2\pi}} \sin \frac{\theta}{2} \left[ 1 - 2\nu + \sin^2 \left( \frac{\theta}{2} \right) \right] \\ w_t &= 0 \end{aligned} \quad (28)$$

$$\begin{aligned} v_n &= \frac{K_{II}}{G} \sqrt{\frac{r}{2\pi}} \sin \frac{\theta}{2} \left[ -1 + 2\nu + \sin^2 \left( \frac{\theta}{2} \right) \right] \\ \text{Mode II: } u_r &= \frac{K_{II}}{G} \sqrt{\frac{r}{2\pi}} \sin \frac{\theta}{2} \left[ 2 - 2\nu + \cos^2 \left( \frac{\theta}{2} \right) \right] \end{aligned} \quad (29)$$

$$w_t = 0$$

$$v_n = 0$$

$$\text{Mode II: } u_r = 0 \quad (30)$$

$$w_t = \frac{K_{III}}{G} \sqrt{\frac{r}{2\pi}} \sin \left( \frac{\theta}{2} \right)$$

where,  $K_I$ ,  $K_{II}$  and  $K_{III}$  are the SIF for Modes I, II and III, respectively;  $G$ , the shear modulus;  $\nu$ , the Poisson's ratio; and  $u_r$ ,  $v_n$  and  $w_t$  denote the local radial, normal and tangential displacements, respectively, as shown in **Fig. 17**. The plane stress form of these equations is obtained by substituting  $\nu$  by  $\nu / (1 + \nu)$

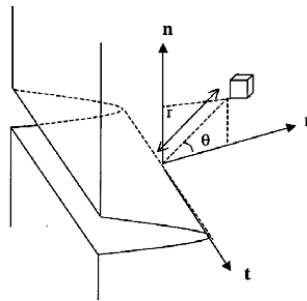


**Fig.17:** Local axes system at crack front [47]

Using the displacements near the crack front obtained from FE analysis, the corresponding SIF may be calculated by using equations (28)-(30). The SIF for a particular radial path are then plotted against the distance from the crack tip. The crack front SIF may then be found by extrapolating the linear part of the distribution back to the crack front. In order to apply the displacement extrapolation technique to a doubly curved crack in a tubular joint, the local radial, normal and tangential directions must be defined for each point on the crack front. This is achieved by first calculating the vectors defining the local directions, which is quite straightforward as the crack is planar and lies in one of the global planes. The radial direction is calculated from the co-ordinates of the nodes on the radial paths along the crack front. The tangential direction is determined from the derivative of the equation defining the elliptical crack front. The two vectors defining these directions are then mapped to vectors defining the local radial and tangential directions for the doubly curved weld toe crack. The third vector in the normal direction is then generated from a cross product of the other two. Having determined these local directions, the global displacements from the FE analysis may then be transformed into local displacements as:

$$\begin{Bmatrix} u_r \\ v_n \\ w_t \end{Bmatrix} = \begin{bmatrix} l_1 m_1 n_1 \\ l_2 m_2 n_2 \\ l_3 m_3 n_3 \end{bmatrix} \begin{Bmatrix} \delta X \\ \delta Y \\ \delta Z \end{Bmatrix}$$

where  $\delta X$ ,  $\delta Y$  and  $\delta Z$  are the global displacements and  $l_1, m_1, n_1$  etc are the direction cosines of the local directions with respect to the global axes X, Y and Z. To evaluate SIF, the largest displacement in the vicinity of the crack, obtained from the radial paths up the crack front, i.e.  $q = \pm 180^\circ$  is generally chosen[48].

## 4. FATIGUE ANALYSIS

### 4.1 FUNDAMENTAL KNOWLEDGE ON FATIGUE ANALYSIS

Fatigue is the progressive and localized structural damage that occurs when a material is subjected to cyclic loading. The maximum stress values are less than the ultimate tensile stress limit, and may be below the yield stress limit of the material. Failure of a material due to fatigue may be viewed on a microscopic level in three steps:

1. **Crack Initiation** - The initial crack occurs in this stage. The crack may be caused by surface scratches caused by handling, or tooling of the material; threads (as in a screw or bolt); slip bands or dislocations intersecting the surface as a result of previous cyclic loading or work hardening.
2. **Crack Propagation** - The crack continues to grow during this stage as a result of continuously applied stresses
3. **Failure** - Failure occurs when the material that has not been affected by the crack cannot withstand the applied stress. This stage happens very quickly.

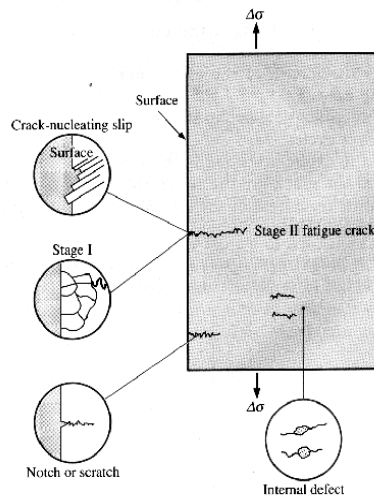


**Fig. 18:** Crack Propagation Due to Fatigue [52]

The **Fig. 18** illustrates the various ways in which cracks are initiated and the stages that occur after they start. This is extremely important since these cracks will ultimately lead to failure of the material if not detected and recognized. The material shown is pulled in tension with a cyclic stress in the y, or horizontal direction. Cracks can be initiated by several different causes. There are several methods for fatigue assessment which are frequently used in fatigue life prediction or fatigue crack propagation of welded structures and components. They can be divided as global approaches- *Nominal* and *Geometric Stress Method* and local approaches-*Effective Notch Stress Method* and *LEFM (Linear Elastic Fracture Mechanics)*. [24] All these methods are described briefly in this paper:

#### 4.1.1 NOMINAL STRESS

Nominal stress can, in simple cases, be calculated analytically using elementary theories of structural mechanics, based on linear-elastic behavior. In general the simple formula can be used:

$$\sigma_{nom} = \frac{F}{M} + \frac{M}{W} \quad (31)$$

#### 4.1.2 GEOMETRIC STRESS

The geometric stress (**Fig. 19**) incorporates all the stress raising effects on a structural detail, with the exception of stress concentration originating from the weld itself. In fatigue calculation, the geometric stress must be determined in the critical direction and location on the welded joint. The approach is not appropriate for joints where the crack would develop from the root of the weld or from an internal defect. Geometric stress is calculated by taking the stress provided by the finite element analysis or calculated from the deformation measured by gauges at specified distances from the bead toe, as shown in **Fig. 19b**. The geometric stress at the bead toe is extrapolated from the values obtained at the measuring points using a two- or three-point formula, in accordance with the following equations:

$$\begin{aligned} \sigma_{HS} &= 1.67\sigma_{0.4t} - 0.67\sigma_{1.0t} \\ \sigma_{HS} &= 2.52\sigma_{0.4t} - 2.24\sigma_{0.9t} + 0.72\sigma_{1.4t} \end{aligned} \quad (32)$$

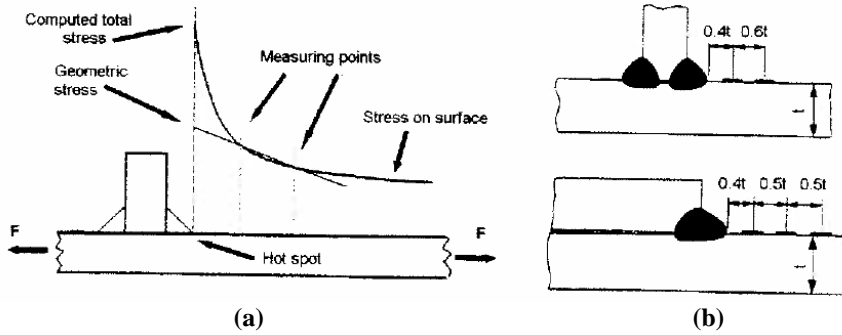


**Fig. 19:** Definition of geometric stress (a) and extrapolation points (b) [25]

#### 4.1.3 EFFECTIVE NOTCH STRESS METHOD

The effective notch stress is the maximum stress measured at the notch, corresponding to a radius of 1 mm, as shown in **Fig. 20**, assuming linear elastic behaviour in the material. One essential benefit of this method is that the notch stress is independent of the geometry, so that a common fatigue strength curve can be used.

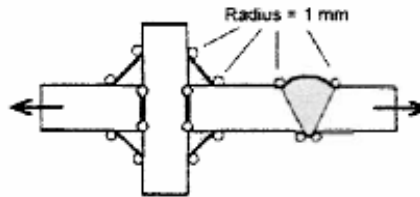


**Fig. 20:** Principle of applying 1 mm notch radius at the bead toe and root [25]

#### 4.1.4 LINEAR ELASTIC FRACTURE MECHANICS

The basic procedure of fracture mechanics used for fatigue crack propagation based on the following two equations:

- fatigue crack growth equation,  $da/dN$  (in m/cycle)

$$\frac{da}{dN} = C(\Delta K)^m \quad (33)$$

- stress intensity factor range,  $\Delta K$  (in  $\text{MPa}\sqrt{\text{m}}$ )

$$\Delta K = F(a)\Delta\sigma\sqrt{\pi a} \quad (34)$$

where,  $a$  = initial crack size in the direction of the crack growth,  $C$ ,  $m$  = material

constant,  $\Delta\sigma$  = applied nominal stress,  $F(a)$  = correction factor for the stress intensity factor.

In the literature some engineering values for initial crack sizes in welds in steel can be found. Radaj (50) give the value  $a = 0.1-0.5$  mm for a line crack and for a semi elliptical crack, he give  $a/c = 0.1 - 0.5$  for the depth/width ratio. In a literature survey by Samuelsson (51) the following typical flaw sizes were found for use in conjunction with welds. At the surface, welding causes defects with depths from 0.01 to 0.05 mm.

When the applied stress range,  $\Delta\sigma$ , is constant during crack propagation, fatigue crack growth equation can be written as follows

$$dN = \frac{da}{C[F(a)\Delta\sigma\sqrt{\pi a}]^m} \quad (35)$$

Then, the fatigue crack propagation life,  $N_p$ , from an initial crack size  $a_i$  to a final crack size  $a_f$  can be computed as follows:

$$N_p = \int_{N_i}^{N_f} dN = \int_{a_i}^{a_f} \frac{da}{C[F(a)\Delta\sigma\sqrt{\pi a}]^m} \quad (36)$$

The stress intensity factor range,  $\Delta K$ , for a crack initiating at the weld toe may conveniently express as follows:

$$\Delta K = F_S \cdot F_E \cdot F_G \cdot F_T \cdot \sigma \sqrt{\pi a} \quad (37)$$

where,  $F_S$  = correction factor for free surface,  $F_E$  = correction factor for crack shape,  $F_G$  = geometry correction factor accounting for the effect of stress concentration due to geometrical discontinuity,  $F_T$  = correction factor for finite thickness or finite width. [46].

## 4.2 WELDED JOINTS ANALYSIS BASED ON FATIGUE ANALYSIS

### 4.2.1 BUTT JOINT (Theoretical Model)

The process of the fatigue failure in the welded joints can be divided into two main periods: micro cracks nucleation, growth and coalescence (stage I fatigue crack) and macro crack propagation to a length, which causes fracture (stage II fatigue crack). The boundaries of the periods are poorly defined, but it is useful to think that the total fatigue life  $N_F$  consist of macro crack initiation period  $N_I$  and macro crack propagation period  $N_P$ :

$$N_F = N_I + N_P \quad (38)$$

Macro crack initiation S- $N_I$  curve can be now written on the basis of the fatigue



strength on  $N=500$  load cycles  $\Delta\sigma_{500}$  and fatigue strength on  $N=2 \cdot 10^6$  load cycles  $\Delta\sigma_E$ :

$$N_I = \left( \frac{\Delta S \cdot K_f}{\Delta\sigma_E} \right) 2 \cdot 10^6 \quad (39)$$

where,  $\Delta S$  is nominal stress range. The slope of  $S-N_I$  curve  $m_I$  is

$$m_I = \frac{\log(2 \cdot 10^6) - \log(500)}{\log\left(\frac{\Delta\sigma_E}{K_f}\right) - \log(\Delta\sigma_{500})} \quad (40)$$

The material fatigue strength,  $\Delta\sigma_{500}$  and  $\Delta\sigma_E$  can be estimated using Basquin-Morrow equation:

$$\begin{aligned} \Delta\sigma_{500} &= 2 \cdot (\sigma_f' - \sigma_m) \cdot 500^b \\ \Delta\sigma_E &= 2 \cdot (\sigma_f' - \sigma_m) \cdot 2 \cdot 10^6^b \end{aligned} \quad (41)$$

where  $\sigma_m$  is the mean stress,  $\sigma_f'$  is fatigue-strength coefficient and  $b$  is fatigue-strength exponent. The fatigue strength parameters can be determined most accurately by experimental testing. The testing of a narrow HAZ zones is very difficult or impossible. Alternative, the fatigue strength parameters can be estimated from the material tensile properties or hardness values. Lawrence et al (1981) purposed the Brinell hardness based estimation for steel with hardness between 150 HB and 700 HB:

$$\sigma_f' \approx 3.42 \cdot HB + 342 \text{ MPa} \quad (42)$$

$$b \approx -\frac{1}{6} \log\left(\frac{2 \cdot (HB + 100)}{HB}\right)$$

The relationship between the Brinell hardness HB and Vickers hardness HV can be carried out using the conversion table from Metals handbook (Boyer and Gall, 1985):

$$HB \approx 0.98 HV^{0.994} \quad (43)$$

A reduction of fatigue strength by notch i.e. fatigue notch factor can be calculated using Peterson's equation:

$$K_f = 1 + \frac{K_t - 1}{1 + \frac{a_p}{\rho}} \quad (44)$$

where,  $K_t$  is elastic stress concentration factor,  $\rho$  is notch root radius and  $a_p$  is Peterson's material parameter relating to the material ultimate strength (Peterson, 1974). The notch radius is determined so that  $K_f$  gets the maximum value using analytical formulations developed for butt welds (Anthes et al., 1994). The ultimate strength for a narrow HAZ is estimated from material hardness value HV (Boyer and Gall, 1985).

Hardness based estimation for steel is:

$$S_u \approx 3.074HV - 25 \quad HV \leq 340 \quad (45)$$

The advantage of the approach is that S-N curve for macro crack initiation can be calculated from the material hardness at the macro crack initiation point i.e. weld root or toe.

Macro crack propagation period is calculated using the Paris Law and the propagation equation by Forman et al. (1967):

$$N_P = \int_{a_i}^{a_c} \frac{1-R}{C \Delta K^n} da \quad (46)$$

Where,  $\Delta K$  is the stress intensity factor,  $a_i$  is the initiated crack size,  $a_c$  critical crack length and  $C$ ,  $n$  are material constants.

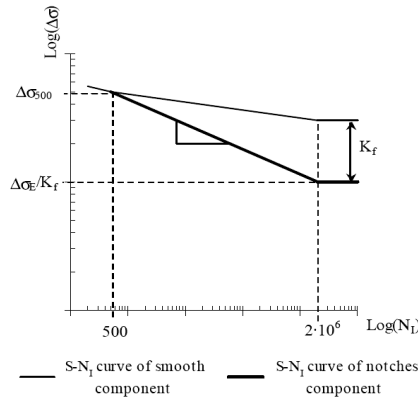


**Fig. 21:** Schematic presentation for determination of S-N<sub>I</sub> curve for notched component [11]

#### 4.2.2 LAP JOINT (Static Stress and Local Stress-Strain Analysis)

##### Static Stress Analysis

An idealized lap joint configuration is employed in the analysis (Fig.22). The overlap length ( $2c$ ), the sheet thickness ( $t$ ), and the interlayer gap width ( $n$ ) are the three essential geometric variables. The local stresses at the sheet-to-sheet interface are

assumed to be in a state of plane strain because the sheet width is very large compared to either the sheet thickness or the gap width.

In order to analyse the stresses at the lap joint interface, it is necessary to determine the loading that must be transmitted through the joint. These loads consist of a tension,  $T$ , a moment,  $M_0$ , and a shearing force,  $V_0$ , each per unit of joint width (**Fig. 22**).

The critical location for failure initiation is most often at the edge of the interlayer. Thus employing the Von Mises distortion energy criterion to give a combined stress parameter,  $J$ , given by:

$$J = (\sigma_y^2 + \tau_{xy}^2)^{1/2} \quad (47)$$

The failure stress concentration,  $J/P$  ( $P$  being the normal stress in the sheet away from the joint) is thus considered to be the theoretical stress concentration factor (TSCF),  $K_t$ .

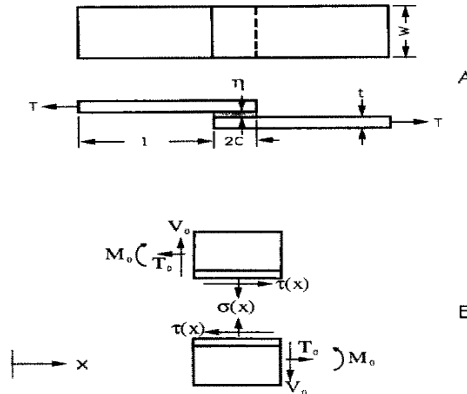


**Fig 22:** Loads and symbol definition of joint: A-Joint dimensions and end load, B-Resolved loads and stresses at joint ends and mid plate [23]

### Local Stress-Strain Analysis

During fatigue testing the local stress amplitude at the joint interface is higher than the stress in the sheet away from the joint due to stress concentration effects. Conventionally the nominal stress in the sheet is plotted against cycles to failure in developing S-N curves. Local stress concentrations thus decrease the observed fatigue strength. The stress concentration is so severe with welded lap joints that the observed fatigue strength is very low using this technique.

The concept of local stress-strain behaviour has been developed to account for geometric stress concentration effects.

$$\sigma_a \left[ \frac{\sigma_a}{E} + \left( \frac{\sigma_a}{\sigma'_f} \right)^{1/n'} \right] = \frac{(K_t S_a)^2}{E} \quad (48)$$

where,

$\sigma_a$  = local stress amplitude,  $E$  = Young's Modulus,  $\sigma'_f$  = fatigue strength co-efficient,  $n'$  = fatigue strain hardening exponent,  $S_a$  = nominal stress amplitude,  $K_t$  = theoretical concentration factor.

Combining above two equations allows one to calculate a stress or a stress concentration under static loading at the critical location at the edge of the layer between sheets, and then to modify this stress level for fatigue loading conditions. The combined model thus provides a prediction of welded lap joint behaviour from smooth sheet fatigue data. [23]

## 5. MULTI-SCALE MODELLING

In every day engineering, many failures are due to the pre-existence of various types of defects in the material's micro-scale [53]. The propagation and coalescence of micro cracks, micro voids and similar defects in the micro-scale leads eventually to the complete rapture of the component [54]. One of the principal objectives of micro/nanomechanics of materials is to account for the observed phenomena and properties of macroscopic solid bodies, such as strength and fracture toughness of metals, on the basis of the quantum mechanical theory of the behaviour of atomic particles. Success will have been achieved when it becomes possible to calculate the quantities that describe the constitution of materials and their response to alterations of macroscopic mechanical boundary conditions from the knowledge of the component elements and their hierarchical structures from atomistic–electronic scales to micro- and macro scales [55]. Therefore, it is seen that there is a need for modelling materials in different scales and actually monitoring their behaviour simultaneously.

### 5.1 Multi-scale approaches

A series of different multi-scale approaches have been established, however only some of them for high strength steel. Multi-scale approaches introduced modelling at the mesoscale, like the Cellular Automation model or the Monte Carlo Potts model. These approaches are particularly suitable for welding and hot forming processes, as they consider the recrystallization process by adding small embryos with new re-orientation, provided the local net energy is reduced [56]. As an alternative to FEA, the Boundary Element Method is meanwhile established for multi-scale modelling, particularly for fracture problems, as it reduces the dimensionality and thus the computation time/storage. E.g. for  $Al_2O_3$ -cracking a multi-scale model was developed [55] by employing a fully frictional contact analysis (contacting, sliding, sticking, separation) at the grain scale, allowing at the macro-scale for multiple intergranular crack initiation and propagation under mixed-mode failure conditions, **Fig. 23**.

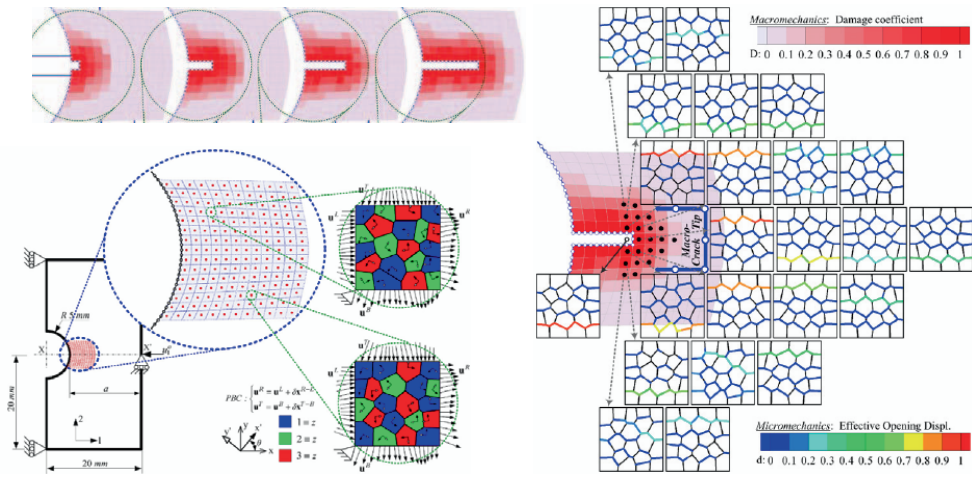


**Fig. 23:** Multi-scale model for crack propagation: stress formation in the macro scale (upper left), average properties mesoscale (right), RVE grain scale (lower left) [55]

### 5.1.1 Macro continuum scale

Finite Element simulation of the stress formation and the strain response of a weld under load conditions is a common method often applied at the macro continuum scale. The difficulties are meshing at locations with small dimensions/curvatures or strong deformations. Moreover, valid material properties are needed, often by empirically identified material models. For single phase metals the stress-strain curve is often developed by an empirical model based on the chemical composition, while modelling of the physics is based on the density of dislocations and mobility of the grain boundaries.

However, for multi phase materials like high strength steels (DP, TRIP) and for the different zones of a weld the identification is difficult as the micro polycrystal structure is heterogeneous, which demands for modelling of the material properties at one or several micro-scale levels.

### 5.1.2 Microstructure and RVE-scale

A recently often applied method for modelling the formability at the micro-scale is the Representative Volume Element (RVE) method for solving the crystal plasticity constitutive equations. The RVE can be determined by SEM-EBSD measurement. **Fig. 24** shows the different phases of an RVE model

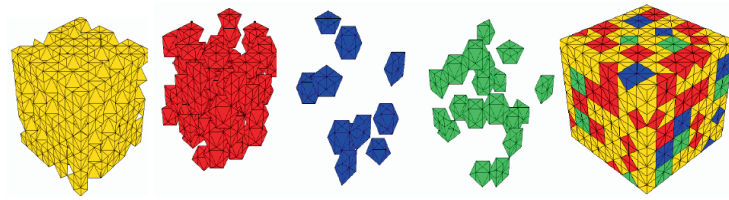


**Fig. 24:** Four phases (ferrite, bainite, retained austenite, martensite) of the RVE (cube size e.g. of the order of 100  $\mu\text{m}$ ) of a TRIP steel

Many RVE models have been developed, but they suffer from lack of describing the grain location, size or orientation accurately in 3D space, due to the strong interaction with adjacent grains to be considered.

### 5.1.3 Crystallic/atomic scale

Both, plastic deformation and fracture have their origin at the atomic scale. While deformation is caused by the propagation of dislocations (atomistic sliding), governed by the Rice criterion, during fracture of a crystal atomic aggregates are split into two parts, as can be calculated by a universal relation for the binding energy leading to a newly created surface energy. The imperfections of real crystals have to be taken into account, such as impurity or interstitial atoms, vacant lattice site and dislocations. Calculation of these lattice-particle interactions at the atomic level is complicated, but essential for understanding and control of separation or dislocation propagation, as it is the key for setting goals for the development of advanced high strength steel types.

## 6. WELDING STANDARD

Welding standard in Hybrid laser welding is not prepared yet by any international organization. The available welding standards are ISO 5817 (Welding-Fusion welded joints in steel, nickel, titanium and their alloys-Quality levels of imperfections), ISO 9692-1 (Welding and allied processes- recommendations for joint preparation, BS EN ISO 6520-2 (Welding and allied processes- Classification of geometric imperfections in metallic materials - Welding with pressure) etc. Therefore separate standards, based on existing welding standards, have to be prepared.

## 7. CONCLUSION

- Finite element modelling is a powerful method for calculating fracture and fatigue of welded joints.
- ANSYS and ABAQUS are widely accepted commercial simulation software.

- Stress intensity factor (K) is one of the most important parameter in fracture mechanics for the mathematical model of welded joints.
- Recent trends of fracture research include dynamic and time-dependent fracture on nonlinear materials, fracture mechanics of microstructures, and models related to local, global, and geometry-dependent fractures.
- LEFM is capable to describe crack growth and crack propagation in welded structures in a physically correct way.
- An engineering value of initial crack size at weld toe would be 0.1 mm.
- From the publication survey, it can be said that the critical weld location is at the toe for different joint.
- More research effort is required on hybrid laser welded joints.

## 8. ACKNOWLEDGEMENTS

The authors are grateful to VINNOVA – The Swedish Innovation Agency (project HYBRIGHT, no. 27382-2) for funding the research.

## 9. LITERATURE

1. Jaroslav M, **Finite element analysis and simulation of welding – an addendum: a bibliography (1996-2001)**, Modelling Simul. Mater. Sci. Eng., Vol. 10, pp. 295-318 (2002).
2. [http://www.efunda.com/formulae/solid\\_mechanics/fracture\\_mechanics/fm\\_intro.cfm](http://www.efunda.com/formulae/solid_mechanics/fracture_mechanics/fm_intro.cfm)
3. O'Dowd N P, Nikbin K M, Lee H-Y, Wimpory R, Biglari F, **Stress intensity factors due to residual stresses in T-plate welds**, J. Press Vessel Technol, pp.6-12 (2004).
4. Anderson T L, **Fracture Mechanics fundamentals and applications**, ISBN 0-8493- 4260-0.
5. Bowness D, Lee M M K, **A finite element study of stress fields and stress intensity factors in tubular joints**, Journal of Strain Analysis, Vol. 30, pp. 135-142 (1995).
6. HSU C, Albright C E, **Fatigue analysis of laser welded lap joints**, **Engineering Fracture Mechanics**, Vol. 39, No. 3, pp. 575-580 (1991).
7. Baohua C, Yaown S, Liangqing L, **Studies on the stress distribution and fatigue behaviour of weld-bonded lap shear joints**, Journal of Materials Processing Technology, pp. 307-313 (2001).

8. Dong P, **A structural stress definition and numerical implementation for fatigue analysis of welded joints**, International Journal of Fatigue, Vol. 23, pp. 865-876, (2001).
9. El-Sayed M E M, Stawiariski T, Frutiger R, **Fatigue analysis of spot-welded joints under variable amplitude load history**, Engineering Fracture Mechanics, Vol. 55, No. 3, pp. 363-369 (1996).
10. Henrysson H F, **Fatigue life predictions of spot welds using coarse FE meshes**, Fatigue Fracture Engineering Material Structure, Vol. 23, pp. 737-746 (2000).
11. Remes H, **A theoretical model to predict fatigue life of laser welded joints**, Ship laboratory, Helsinki University of Technology, Finland.
12. Cho S K, Yang Y S, Son K J, Kim J Y, **Fatigue strength in laser welding of the lap joint**, Finite Elements in Analysis and Design, Vol. 40, pp. 1059-1070 (2004).
13. Maddox S J, **An analysis of fatigue cracks in fillet welded joints**, International Journal of Fracture, Vol. 11, No. 2, pp. 221-243 (1975).
14. Alam M S, Wahab M A, **Modeling the fatigue crack growth and propagation life of a joint of two elastic materials using interface elements**, International journals of pressure vessels and piping, Vol. 82, pp. 105-113 (2005).
15. Etube L S, Bremen F P, Dover W D, **A new method for predicting stress intensity factors in cracked welded tubular joints**, International Journal of Fatigue, Vol. 22, pp. 447-456 (2000).
16. Sutton M A, Reynolds A P, Ge Y Z, Deng X, **Limited weld residual stress measurements in fatigue crack propagation: Part II FEM based fatigue crack propagation with complete residual stress fields**, Fatigue Fracture Engineering Material Structure, Vol. 29, pp. 537-545 (2006).
17. Balasubramanian V, Guha B, **Effect of weld size on fatigue crack growth behaviour of cruciform joints by strain energy density factor approach**, Theoretical and Applied Fracture Mechanics, Vol. 31, pp. 141-148 (1999).
18. Haagenzen P J, Statnikov E S, Martinez L L, **Introductory fatigue tests on welded joints in high strength steel and aluminium improved by various methods including ultrasonic impact treatment**, IIW Doc. XIII- 1748-98.



19. Teng T L, Chang P H, **Effect of residual stresses in fatigue crack initiation life for butt-welded joints**, Journal of Materials Processing Technology Vol. 145, pp. 325-335 (2004).
20. Li X Y, Partanen T, Nykänen T, Björk T, **Finite element analysis of the effect of weld geometry and local condition on fatigue strength of lap joint**, International Journal of Pressure Vessels and Piping, Vol. 78, pp. 591-597 (2001).
21. Ding F, Zhao T, Jiang Y, **A study of fatigue crack growth with changing loading direction**, Engineering Fracture Mechanics, Vol. 74, pp. 2014-2029 (2007).
22. Caccese V, Blomquist P A, Berube K A, **Effect of weld geometric profile on fatigue life of cruciform welds made by laser/GMAW processes**, Marine Structures, Vol. 19, pp. 1-22 (2006).
23. Hsu C, Albright C E, **Fatigue analysis of laser welded lap joints**, Engineering Fracture Mechanics Vol. 39, No. 3, pp. 575-580 (1991)
24. Barsoum Z, **Residual Stress Analysis and fatigue of Welded Structures**, Licentiate Thesis, Dept. of Aeronautical and Vehicle Engineering, KTH, Sweden 2006. ISBN 91-7178-264-8
25. Pettersson G, **Fatigue assessment of welded structures with non-linear boundary conditions**, Licentiate Thesis, Dept. of Aeronautical and Vehicle Engineering, KTH, Sweden 2004. ISBN 91-7283-948-1.
26. Andersson P, Segle P, Samuelson L Å, **Numerical investigation of creep crack growth in cross-weld CT specimens. Part II: influence of specimen size**, Fatigue Fract. Engng. Struct. Vol. 23, pp. 533-540 (1999).
27. Assire A, Michel B, Raous M, **Creep crack initiation and creep crack growth assessments in welded structures**, Nuclear Engineering and Design, Vol. 206, pp. 45-56 (2001).
28. Hou Y C, Pan J, **A fracture parameter for welded structures with residual stresses**, Computational Mechanics, Vol. 22, pp. 281-288 (1998).
29. Infante V, Branco C M, Baptista R, Gomes E, **A residual stresses and fracture mechanics analysis of welded joints repaired by hammer peening**, 8<sup>th</sup> Portuguese Conference on Fracture (2002).
30. Ferreira J M, Pereira A H, Branco C M, **A fracture mechanics based fatigue life prediction for welded joints of square tubes**, Thin Walled Structures, Vol. 21, pp. 107-120 (1995).

31. Cam G, Erim S, Yeni C, Kocak M, **Determination of mechanical and fracture properties of laser beam welded steel joints**, Welding Research Supplement (1999).
32. Atzori B, Lazzarin P, Tovo R, **From a local stress approach to fracture mechanics: a comprehensive evaluation of the fatigue strength of welded joints**, Fatigue Fract. Engng. Struct., Vol. 22, pp. 369-381 (1998)
33. Budden P J, Curbishley I, **Assessment of creep crack growth in dissimilar metal welds**, Nuclear Engineering and Design, Vol. 197, pp. 13-23 (2000).
34. Wang P C, **Fracture mechanics parameter for the fatigue resistance of laser welds**, International Journal of Fatigue, Vol. 17, No. 1, pp. 25-34 (1995).
35. Maosheng C, Shan W, Shaofu L, **Crack growth and fatigue life estimation in welded T- Tubular joints based on fracture mechanics**, Proceedings of the International Offshore Mechanics and Arctic Engineering symposium, Vol. 3, pp. 351-358, (1990).
36. Lieurade H P, **Application of fracture mechanics to the fatigue of welded structures**, Welding in the world, Vol. 21, No. 11, pp. 272-295, (1983).
37. Zaho W, Newman J C, Sutton M A, Shivkumar K N, Wu X R, **Stress intensity factors for surface cracks at a hole by a three dimensional weight function method with stresses from the finite element method**, Fatigue & fracture of engineering materials and structures, Vol. 21, pp. 229-239 (1996).
38. Schindler H J, Martens H J, Sönnichsen S, **A fracture mechanics approach to estimate the fatigue endurance of welded t-joints including residual stress effects**, Fatigue Fract. Engng. Mater. Struct., Vol. 30, pp. 206-213 (2006).
39. Chang K H, Lee C H, **Residual stresses and fracture mechanics analysis of a crack in welds of high strength steels**, Engineering Fracture Mechanics, Vol. 74, Issue 6, pp 980-994 (2007).
40. Lei Y, Dowd N P, Webster G A, **Fracture mechanics analysis of a crack in a residual stress field**, International Journal of Fracture, Vol. 106, pp. 195-216 (2000).
41. Lee H Y, Nikbin K M, Dowd N P, **A generic approach for a linear elastic fracture mechanics analysis of a components containing residual stress**, Int. Journal of Pressure Vessels and Piping, Vol. 82, pp. 797-806 (2005).
42. Muller W, Veith H, **Influence of weld material properties on fracture mechanics parameters in welds analysed by FEM calculations**, Int. J. Pres. Ves. & Piping, Vol. 33, pp. 285-300 (1988)

43. Dahl W, Ehrhardt H, Heuser A, Hubo R, Twickler R, Uwer D, **Determination of fracture mechanics properties of welded joints and comparison with the failure behaviour of wide plates**, Nuclear Engineering. and Design Vol. 102, pp. 451-461 (1987).
44. Chiesa M, Skallerud B, Thaulow C, **Fracture analysis of strength-mismatched welded wide plates by line spring elements**, Engineering Fracture Mechanics, Vol. 68, pp. 987-1001 (2001).
45. Nykänen T, Li X, Björk T, Marquis G, **A parametric fracture mechanics study of welded joints with toe cracks and lack of penetration**, Engineering Fracture Mechanics, Vol. 72, pp. 1580-1609 (2005).
46. Ellyin F, **Fatigue damage, crack growth and life prediction**, ISBN 0-412-59600-8.
47. Cao J J, Yang G J, Packer J A, Burdekin F M, **Crack modelling in FE analysis of circular tubular joints**, Engineering Fracture Mechanics, Vol. 61, pp. 537-553 (1998)
48. Murthy A R C, Palani G S, Iyer N R, Appa Rao T V S R, **An efficient FE modelling strategy for fracture analysis of tubular joints**, Vol. 85, pp. 17-51 (2004).
49. <http://www.mpmtechnologies.com/Finite-Element-Fracture-Mechanics.htm>.
50. Radaj D, **Design and analysis of fatigue resistant welded structures**, Abington Publishing (1990), ISBN 1 85573 004 9.
51. Samuelsson J, **Fatigue design of vehicle components: methodology and applications, report 88-23**, Dep. Of Aeronautical Structures and Materials, The Royal Institute of Technology, Stockholm (1998).
52. [http://www.sv.vt.edu/classes/MSE2094\\_NoteBook/97ClassProj/anal/kelly/fatigue.html](http://www.sv.vt.edu/classes/MSE2094_NoteBook/97ClassProj/anal/kelly/fatigue.html).
53. Gagg C R, **Failure of components and products by 'engineered-in' defects: case studies**, Engrg. Fail. Anal., pp. 1000–1026 (2000).
54. Scutti J J, McBrine W J, **Failure Analysis and Prevention**, in: W.T. Becker, R.J. Shipley (Eds.), ASM Handbook, vol. 11, ASM, USA (2002).
55. Hao S, Liu W K, Moran B, Vernerey F, Olson G B, **Multi-scale constitutive model and computational framework for the design of ultra-high strength**

**high toughness steels**, Comput. Meth. Appl. Mech. Eng, v 193, pp 1865-1908 (2004).

56. Yu Q, Esche S K, **A multi-scale approach for microstructural prediction in thermomechanical processing of metals**, J Mat Proc Tech, v 169, pp 493-502 (2005).

## **Paper II**

### **THE INFLUENCE OF SURFACE GEOMETRY AND TOPOGRAPHY ON THE FATIGUE CRACKING BEHAVIOUR OF LASER HYBRID WELDED ECCENTRIC FILLET JOINTS**

M. M. Alam, Z. Barsoum, P. Jonsén, H. A. Häggblad, A. Kaplan

Applied Surface Science, 2009 (in press available online)



## **The influence of surface geometry and topography on the fatigue cracking behaviour of laser hybrid welded eccentric fillet joints**

**Authors:** M. M. Alam<sup>1\*</sup>, Z. Barsoum<sup>2</sup>, P. Jonsén<sup>1</sup>, A. F. H. Kaplan<sup>1</sup>, H. Å. Häggblad<sup>1</sup>

### **Affiliation:**

<sup>1</sup>Luleå University of Technology, Dept. of Applied Physics and Mechanical Engineering,

SE-971 87 Luleå, Sweden

Email: minhaj.alam@ltu.se, par.jonsen@ltu.se, alexander.kaplan@ltu.se, hans-ake.haggblad@ltu.se

<sup>2</sup>Royal Institute of Technology, Dept. of Aeronautical and Vehicle Engineering, SE-100 44 Stockholm, Sweden

Email: zuheir@kth.se

\*Corresponding author: minhaj.alam@ltu.se

Phone: +46(0)920 493917

Fax: +46(0)920 49 22 28

### **Abstract**

Laser hybrid welding of an eccentric fillet joint causes a complex geometry for fatigue load by four point bending. The weld surface geometry and topography were measured and studied in order to understand the crack initiation mechanisms. The crack initiation location and the crack propagation path were studied and compared to Finite Element stress analysis, taking into account the surface macro- and micro-geometry. It can be explained why the root and the upper weld toe are uncritical for cracking. The cracks that initiate from the weld bead show higher fatigue strength than the samples failing at the lower weld toe, as can be explained by a critical radius for the toe below which surface ripples instead determine the main stress raiser location for cracking. The location of maximum surface stress is related to a combination of throat depth, toe radius and sharp surface ripples along which the cracks preferably propagate.

**Keywords:** Surface geometry; Surface ripples; Topography; Crack; Fatigue; Hybrid weld.

## 1. Introduction

Fatigue is a mechanism of material failure which involves the formation and growth of cracks under the action of cyclic stresses. Ultimately, a crack will propagate to such an extent that total fracture of the component occurs. Welded joints are regions of stress concentration where fatigue cracks are often initiated. Macro- and micro-geometrical features of the weld can act as stress raisers which govern the fatigue life [1-3]. Thus, smooth weld geometry with minimal defects will optimise the fatigue strength of a welded joint. The welding process and its parameters influence the geometry of the weld. For example, the manual metal arc welding process tends to form a highly irregular weld toe, which leads to sharp transitions between the weld and the base metal. Unusual joint geometries, load situations and new welding techniques can produce new, complex situations from the point of view of fatigue behaviour. This paper studies laser hybrid welding of an eccentric fillet joint under a 4-point bending load. Hybrid welding [4, 5] combines a laser beam with an electric arc (MAG) and creates a narrow deep weld (by the laser beam) but also has the freedom to shape the surface (by MAG parameters).

Fatigue failure comprises two phases: fatigue crack initiation (short crack nucleation, growth and propagation up to a macro-crack threshold length) and fatigue (macro) crack propagation [4, 6]. For an accurate calculation of the fatigue life of a component, a detailed investigation of the probable fatigue crack initiation characteristics is required. The initiation of cracks at the weld toe due to sharp transitions (between the weld and base metal), root cracks, cold laps and surface cracks in the weld bead are the most common reasons for fatigue failure of welded joints while internal defects are less critical [3]. Fatigue crack initiation is difficult to observe [7, 8] and is usually estimated by the weld toe stress concentration factor (SCF). Crack propagation is analysed by stress intensity factors (SIF) employing a linear elastic fracture mechanics approach [9]. The estimation of fatigue life usually approximates the weld toe geometry to a weld angle, and a circle defines the weld toe radius. The SCF or the SIF of the crack initiated from the weld toe can then be calculated. The analysis is usually performed on a two-dimensional plane strain basis [10-14]. But there is no direct evidence that the fatigue cracks are really initiated from the toe of the assumed geometry. Some researchers have tried to perform fatigue strength assessment of welded joints whilst ignoring the irregularity of weld toes. Radaj [15] used the concept of a micro-structural support effect and assumed a weld toe radius of 1 mm for the weld fatigue analysis of steel structures. This approach has been adopted in the fatigue design recommendations of the International Institute of Welding [16]. Several fatigue analysis approaches have been described in [17-18], all concentrating on the weld macro-surface geometry, i.e. weld toe radius and weld angle.

The influence of the weld geometry on the fatigue strength of laser-welded joints has been investigated with the help of a nominal stress-based approach (however, this assumes that short crack nucleation and propagation periods are negligible) to create S-N curves for fatigue design [19-21]. However, previous



investigations have revealed that the S-N curves of laser-based joints can differ significantly from arc-welded joints. A slope of S-N curves equal to 3 is commonly used for arc-welded joints [25], but for laser-welded joints; slopes up to a value of 10 have been observed but this phenomenon so far only partially understood (in a complex component structure the laser weld also ends up in 3-4, but locally the laser weld has lower stiffness and is often thinner). Laser welded joints often have 50% higher fatigue strength than conventional arc welds due to their advantageous weld geometries and also for metallurgical reasons [1], [7], [21], [26-27]. Research into the fatigue life of laser welded joints has generally concentrated on the weld macro-geometry, while the impact of weld surface waviness or ripples is usually ignored. Recently [4] the fatigue crack initiation of laser hybrid welded low carbon steel was studied in depth, considering notch radius and depth as critical surface dimensions. Chapetti and Otegui [28] investigated the effect of toe irregularities on the fatigue resistance of automated arc welds and concluded that the period of toe waves as well as the local toe geometry strongly influences the fatigue crack initiation and propagation life. Long toe wave periods were gave the longest fatigue life. An arc rotation method was introduced to control the degree of waviness on the weld surface [29]. Surface ripples or waviness can also be considered as undercut [30]. The crack initiation point on the weld bead was identified at the intersection of two weld ripples or at the secondary undercut along any point along the surface ripples path or a combination of both situations.

## 2. Methodology

The goal of this research is an improved knowledge of the impact of weld surface macro-geometry and topography on fatigue crack initiation (and in a subsequent paper on crack propagation) for the complex case selected here. The methodological approach applied is: (i) prepare joint edges and carry out the welding for suitable parameters, (ii) measure the surface macro- and micro-geometry, (iii) carry out 4-point bending fatigue testing for a series of samples with identical welding parameters, (iv) microscopic analysis of the cracked samples, (v) FE-stress analysis for measured micro- and macro-surface geometries, (vi) quantitative and qualitative analysis and discussion of the results. In particular conclusions on the mechanism and contributions from the joint geometry in competition to the weld macro-shape and the topography shall be drawn and described by a theory. As outlined above, knowledge of the influence of both the surface geometry and the topography on fatigue cracking is still limited, particularly for complex geometries. To measure the surface topography and surface geometry, 3D optical profilers and the plastic replica method were used in this study. Based on the data from the 3D optical profilers and the plastic replica, Finite Element (FE) stress analysis was performed. Four point bend fatigue tests were carried out for several welded specimens under constant amplitude stress ratio. Subsequently, analysis of specimen fracture surfaces was carried out to identify the crack initiation points and the crack propagation paths.

### 3. Welding

#### 3.1. Joint design

The joint type studied involves two 10 mm thick steel plates in butt configuration, but with  $m = 5$  mm eccentricity, see Fig. 1. This design was stipulated for a specific industrial application. Structural stainless steel SS2333 was used with sample dimensions of  $w \times l \times t = 50 \times 100 \times 10 \text{ mm}^3$ , prepared by milling and grinding of the joint surface to give zero gap. Fillet welds were made between two base plates with 5 mm eccentricity using the hybrid laser metal inert gas (L/MIG) welding technique, see Fig. 1. The chemical composition and mechanical properties of the base metal and the filler wire are presented in Tables 1 and 2. After the welding had been completed, all specimens were milled to cut about 12.5 mm from both ends of the weld to remove start and stop defects. Consequently, a small square plate with  $25 \times 25 \times 5 \text{ mm}^3$  dimensions was attached by manual arc weld under the eccentric base metal to facilitate sample attachment to the fatigue testing machine. The load condition was 4-point bending (see later), applying the force from the bottom.

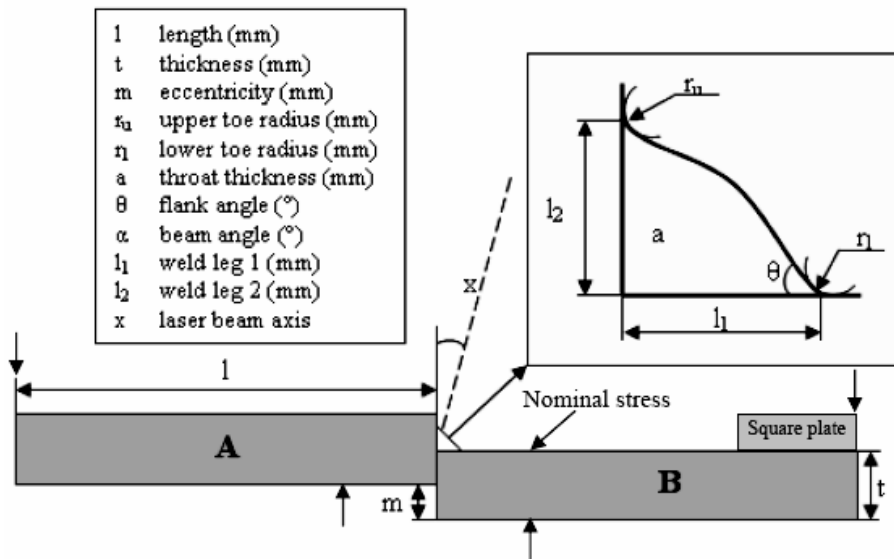


**Fig. 1** Eccentric fillet joint: geometrical properties

**Table 1:** Chemical composition [%] of the materials used for the sheets and for the filler wire

Material	C	Si	Mn	Cr	Ni	P	S	N
SS142333 (sheets)	0.05	1.0	2.0	19.0	11.0	0.045	0.030	-
Avesta 253MA (wire)	0.07	1.6	0.6	21.0	10.0	-	-	0.15

**Table 2:** Mechanical properties of the materials used

Material	$R_{p0.2}(\text{N/mm}^2)$	$R_m(\text{N/mm}^2)$	$A_5(\%)$	Hardness,
HB	min		min	max
SS142333 (sheets)	210	490 – 690	45	200
Avesta 253MA (wire)	440	680	38	210

### 3.2. Welding set-up

An Ytterbium Fiber Laser (IPG Laser YLR 15000) with a maximum power of 15 kW (wavelength 1070 nm), beam parameters product 10.4 mm·mrad delivered through a 200  $\mu\text{m}$  fiber core, was in used for these experiments. The optics (focusing collimating length = 300:150 = 2:1) created a beam with a focal diameter of 400  $\mu\text{m}$  and a Rayleigh length of  $\pm 4$  mm, with a focal plane position on the top surface of the weld. The laser was combined with a MIG-welding source (ESAB ARISTO). The filler wire, see Tables 1 and 2, had a diameter of 1.2 mm. During the hybrid laser/MIG welding process, the laser beam was traveling 2 mm in front of the MIG torch. Further process parameters are summarized in Table 3.

**Table 3:** Hybrid welding parameters

Parameter	Value / type
MIG current (constant)	328 A
MIG voltage (resulting)	27 V
Pulse time	2.4 ms
Frequency	90 Hz
Wire stick out length	16 mm
Wire feed rate	4.2 m/min
Shielding gas	Ar
Shielding gas flow	20 l/min
Laser beam angle, $\alpha$	10 °
Welding speed	1.05 m/min
Laser power	3.25 kW

### 3.3. Welding samples

For statistical purpose, 13 samples were welded under identical conditions. Figure 2 shows a typical top surface and weld cross section. The effective weld throat thickness is 6-7 mm and the leg length is 4 mm. As the bending force acts from the bottom, the weld root shape is not important, as this area is under compressive stress. In contrast, the shape of the top of the weld is critical to the fatigue performance of the specimen.

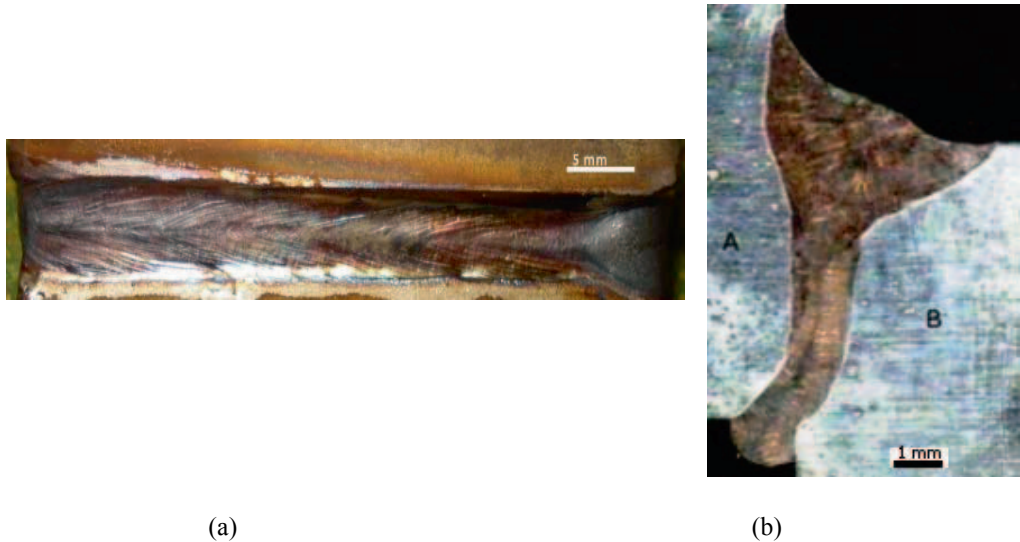


**Fig. 2** Typical resulting weld: (a) top surface appearance, (b) cross section

#### 4. Weld surface shape analysis

##### 4.1. Shape measurement

The surface geometry is mainly determined by the toe radii and toe angles (see Fig. 1), and these were measured by the non-destructive plastic replica method [7, 31]. The specimen surface was first polished to remove surface oxides. Afterwards the surface of the weld toes was filled with liquid silicon rubber. The rubber hardened within a few minutes, generating an inverted accurate 3D-profile of the weld surface. The hardened profile was detached from the surface and sliced in four positions. The cross sections thus generated which were used to measure the toe radii and angles by optical microscopy. The measured data (radius and angle) were then used to create a two-dimensional FE-model to calculate the stress concentration factor;  $K_t$ . Figure 3 shows the relationship between all toe radii and toe angles. The values were measured at the positions 1, 8, 16 and 25 mm along the weld per sample. In this figure all the measured values from plastic replicas are plotted. Smooth toe radii and smaller toe angle gives lower stress concentration factor [25]. Due to smooth toe surface geometry, weld failure shifted from the toe region towards the weld bead. Though many researchers have shown that toe radius is the most significant parameter for the stress concentration [7, 32-33], out of our thirteen samples, only four specimens were cracked at the lower toe region whereas the rest of the specimens cracked at the weld bead, i.e. in the weld surface ripples. Therefore, the topography (micro-geometry) of the welds was also studied.

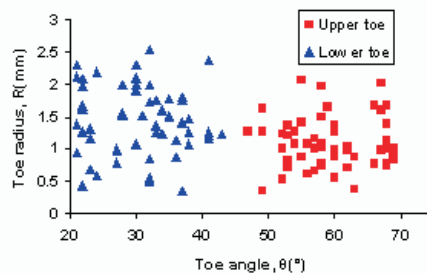


**Fig. 3** Measured local weld geometry

#### 4.2. Analysis of stress generated by a smooth surface shape

In order to calculate the stress fields and the stress concentration factors in the weld toes, stress analysis was carried out with the FEM using the ANSYS 11 software [34]. A linear elastic 2D model with the assumption of plane stress with thickness was applied, 25000 8-nodes quadrilateral elements were used, with mesh refinement around the toe regions. Residual stress was neglected due to the short weld length. The stress formation during loading conditions is basically superimposed by residual stresses from the welding process. In the present study the samples are kept very short (25 mm); moreover laser hybrid welding enables low heat input (line energy). Therefore residual stress is expected to be low and was thus neglected, particularly for the FE-analysis. Barsoum [21] carried out extensive FE welding simulation and measurement in order to characterize the residual stresses for various types of welding processes.

For laser hybrid (MAG) welding Barsoum measured residual stresses of approx. 50 MPa for 13 mm thick specimens, whereas the residual stresses were 130-160 MPa for conventional MAG welding at the weld toe fatigue failure site. The investigations of Otha [22] for 10 mm wide specimens cut out from a 250 mm wide cruciform plate had residual stresses in the range of 100 to -50 MPa 3 mm from the weld toe. Chon [23] carried out comprehensive welding simulation on cruciform joints with fillet welds. The welding techniques investigated were gas metal arc welding (GMAW) and flux cored arc welding (FCAW). Also the cool saw cutting of the full-width (102 mm) specimens, cut out from the 610 mm cruciform plate to a half-width specimen was simulated. It was concluded that the residual stresses across the weld toe are significantly relieved by the cutting. The longitudinal residual stresses 25 mm away from the weld toe, which can be considered to cause the considerable effects in fatigue crack propagation, dropped from 282 MPa to 193 MPa; a 30 % drop.

Since fatigue was tested in the low-mid cycle regime, in addition the small residual stress magnitude will relax/redistribute early in the fatigue life of the specimens due to the high stress amplitude applied. Barsoum and Gustafsson [24] showed in a recent investigation that the residual weld stresses (tensile or compressive) have very little effect on the fatigue life in the low-mid cycle regime. Hence no effect

of the residual stresses could be expected on the fatigue life predictions. We would also like to emphasize that the present study tries to isolate the different stress raising contributions, thus even for significant residual stress as an additional contribution the basic findings about topography and geometry would remain valid.

According to the large scatter of the toe radii, Fig. 3, different radii-combinations were studied. Figure 4 shows how a smaller lower toe radius induces a much a higher stress peak than the upper toe, but for increasing radius this becomes less pronounced. Nevertheless, the lower toe has a shorter distance (throat) to the root and thus remains dominant. Stress concentration factor,  $K_t$  as a function of the toe radius is plotted in Fig. 5. The stress concentration factor was calculated based on the nominal stress method. The nominal stresses were taken from the top surfaces, 24 mm away from the joint edge, thus where the load was applied to both plates, see Fig. 1. This indicates that the lower toe for eccentric fillet joints in a four point bend situation is critical at the macro geometry level.

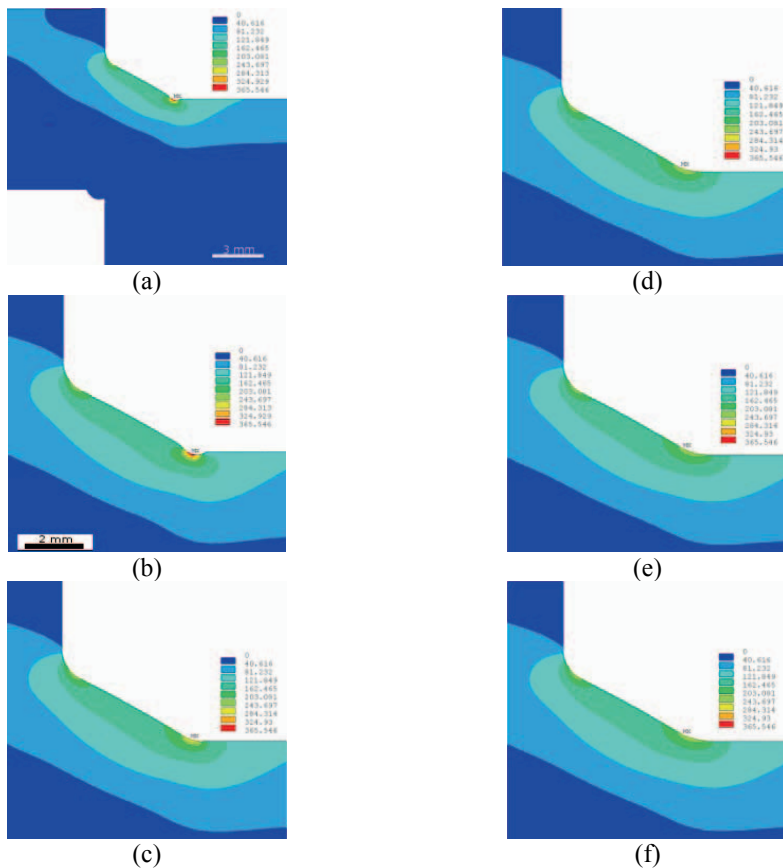


**Fig. 4** Calculated stress fields for a smooth surface for various lower toe radii, LTR (UTR=1 mm) combinations: (a) total cross section, (b) 0.5 mm, (c) 1 mm, (d) 1.5 mm, (e) 2 mm and (f) 2.5 mm

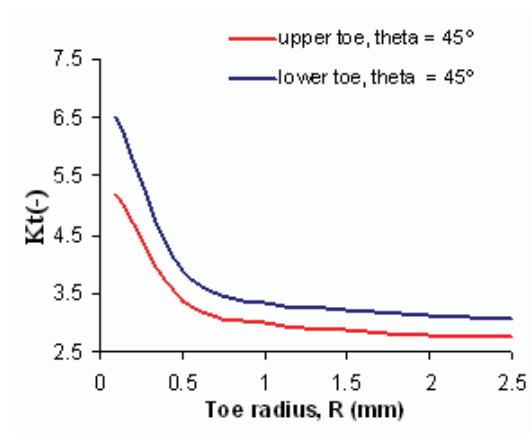


**Fig. 5** Stress concentration factor as a function of the upper and of the lower toe radius (Upper toe radius kept constant at 1 mm)

## 5. Weld surface topography analysis

### 5.1. Topography measurement

Beside the toe radii macro-geometry, the impact of the topography (micro-geometry) is expected to be critical and was therefore studied, too. A Wyko NT1100 was used as 3D optical profiler. It utilizes vertical scanning/white light interferometry. A typical topography scan taken from the lower toe is shown in Fig. 6, showing the resolidification patterns which cover the surface. The surface was free of larger welding defects such as cracks or cold laps. The roughness was typically  $R_t = 253.44 \mu\text{m}$  across and  $R_z = 200.35 \mu\text{m}$  along the weld, thus very rough due to the surface ripples. This data can be used for FE analysis. The software of the profiler was Vision32. The height resolution was set to 1 nm. The measurement was taken in the middle of the lower toe.

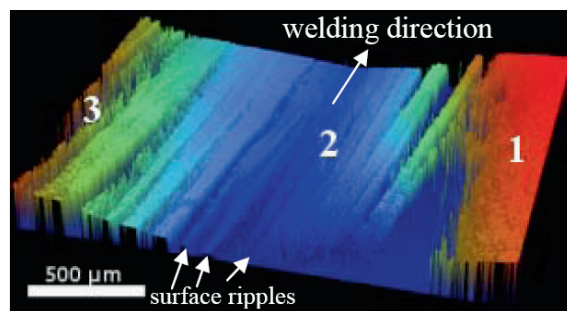


**Fig. 6** Typical measured weld surface topography, here ranging from the base metal (1) across the lower toe (2) to the weld bead (3); the ripples see also Fig. 2(a), are surface curvatures on a micro-scale

## 5.2. Analysis of stress concentration generated by topography

The FE analysis that was used and described for smooth surface shape analysis, Section 4.2, was also utilized here. Instead of giving smooth toe radii, in this FE model surface topography (roughness of the ripples across the weld) was introduced. From the measured data for three rough surface profiles, three surface meshes were generated. While on the lower toe radii for smooth surface shape analysis, 8 quadrilateral elements were applied along the toe region (0.125 mm wide); in the topography analysis 1092 quadrilateral elements (0.92  $\mu\text{m}$  wide) were used across the same region. The other mesh of the sample and the loading conditions remained unchanged. The FE-analysis for smooth surfaces with different lower toe radii was then compared with three FE-analysis results for the three typical roughness profiles. From the FE analysis the large topography scatter in the weld toe results in stress peaks. Compared to the ideal toe radii, the highest stress peak are almost four times higher, see Figure 7(a)-(d) and 8 where stress peaks above  $K_t = 4$  were classified as unrealistic. The definition of surface curvature, the corresponding FE- mesh resolution and result interpretation is critical and not completely understood yet. The present study aims to indicate the importance of stress raising resulting from features of the measured topography (compared to a smooth surface) for crack initiation. Once a crack is initiated, the stress level rapidly decays to the typical crack tip raiser values, thus the values of surface curvature and their stress peaks lose importance. Compared to the stress peaks from the toe radii the welding ripples can cause significantly higher stress concentration. However, in the cases studied the difference between the ripples were not so significant, therefore a ripple in the toe showed highest stress, as combined with the toe radius and neck impact. However low toe radii will shift the peak value to the most critical ripple in the weld bead.

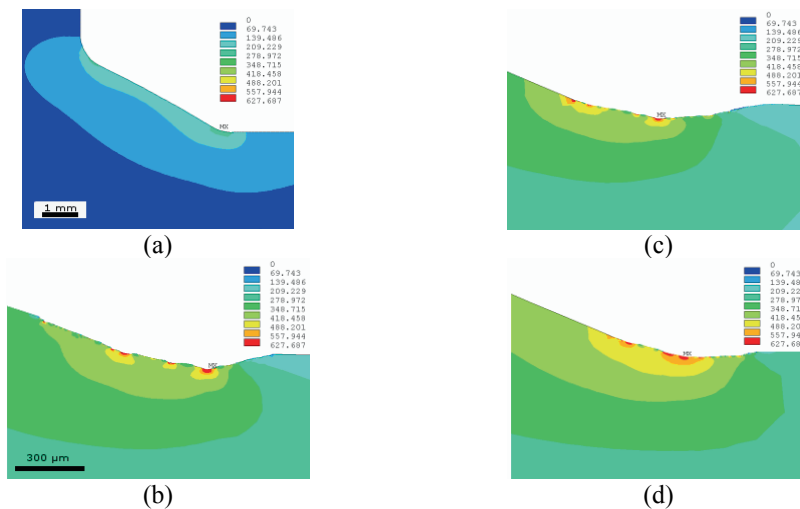


**Fig. 7:** Stress fields calculated by FEA for a simplified cross section for (a) a smooth surface (toe radius 1.5 mm) and by taking into account the measured topography profile (b) case 1, (c) case 2, (d) case 3



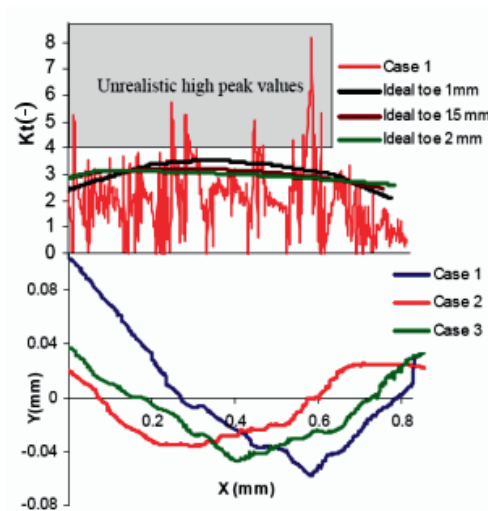


**Fig. 8** Stress concentration factors across the (simplified) weld surface for smooth surfaces for three radii and when considering the roughness (case 1, 1.5 mm, cut-off above  $K_t=4$ ) and corresponding roughness distribution for three cases

## 6. Fatigue analysis

### 6.1. Testing set-up

The four point bend fatigue testing was performed, using a servo- hydraulic machine (Instron 1272 max  $\pm 50$  kN). The welded joints were tested by keeping a constant amplitude stress ratio,  $R = 0$  at a frequency of 45 Hz as shown in Fig. 9. The specimens were tested in the range from 2.5 kN to 4 kN until complete failure or to an endurance of 2 million cycles if there was no evidence of fatigue cracking. A thicker beam than the base metal was specially prepared and hardened for fatigue testing with two different grooves so that the roller can fit the groove.

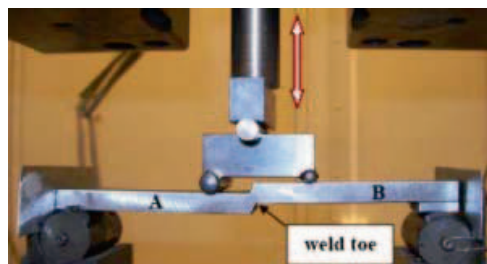


**Fig. 9** Four-point fatigue bending test (note: the weld is upside down)

## 6.2. Fatigue test evaluation

In this fatigue analysis, the nominal stress approach was used. The stresses were calculated by FEA [16]. The fatigue resistance data and stresses were then compiled into a logarithmic S-N curve (Wohler curve) as shown in Fig. 10 to describe the fatigue strength. The equation for SN-curves can be written as [16];

$$\log N = \log C - m \log \Delta \sigma \quad (1)$$

or simply as

$$N = \frac{C}{\Delta \sigma^m} \quad (2)$$

where, N is the number of cycles to failure,  $\Delta \sigma$  is the stress range, m is the slope of the S-N curve and C is the load intensity value (Capacity). Since no standard definitions exist so far for fillet joints with 5 mm eccentricity under a four point bending condition, all the calculations for fatigue strength were stand alone and not comparable [16], [35]. The fatigue test properties identified are shown in Table 4. The mean value (Pf 50%) of the fatigue strength was calculated with a slope of m=3, excluding the run outs. Also, the fatigue classes FAT on 50% and 95% survival probability levels were calculated according to IIW recommendations [16]. From the fatigue test data a mean linear regression analysis was carried out, assuming a straight line of the SN-curve. This gave a slightly higher natural slope m of the SN-curves of 3.16. The mean  $P_f$  50% was also increased to 141 MPa. The natural slope is calculated according to Equation (3) [35-36]. To calculate the natural mean curve,  $\log C$  has to be calculated, which is done by using Equation (4) where n is the number of failed specimens.

$$m_{natural} = \frac{n \cdot \sum (\log N \cdot \log \sigma) - \sum \log N \cdot \sum \log \sigma}{(\sum \log \sigma)^2 - n \cdot \sum (\log \sigma)^2} \quad (3)$$

$$\log C = \frac{\sum \log N + m_{natural} \cdot \sum \log \sigma}{n} \quad (4)$$

The  $K_t$  and C values of each specimen were calculated according to [16] and shown in Fig. 10. The tested samples can be divided into two groups, i.e. weld bead failure (WBF) and toe failure (TF). The majority of the cracks were formed in the weld bead even though the toe radius is traditionally considered the most significant influence on crack initiation. In Fig. 11, WBF specimens show higher fatigue strength and lower stress concentration at the toe than the TF specimens, indicating that a larger toe angle and smaller toe radius creates higher stress concentration. This is also confirmed by [2], [21]. This indicates that low toe radius and low toe angle shift the crack initiation from the weld toe to the weld bead, giving higher fatigue strength.

**Table 4:** Fatigue testing results

IIW norm property	Value
$K_t$ – mean / standard deviation	3.09 / 0.35
Log C (m=3) – mean / standard deviation	12.71 / 0.18
m – natural slope	3.16
Mean value, (N = 2.10 <sup>6</sup> , m = natural slope)	141
Mean value, P <sub>f</sub> 50% (N = 2.10 <sup>6</sup> , m = 3)	137
FAT, P <sub>f</sub> 5% (N = 2.10 <sup>6</sup> , m = 3)	95

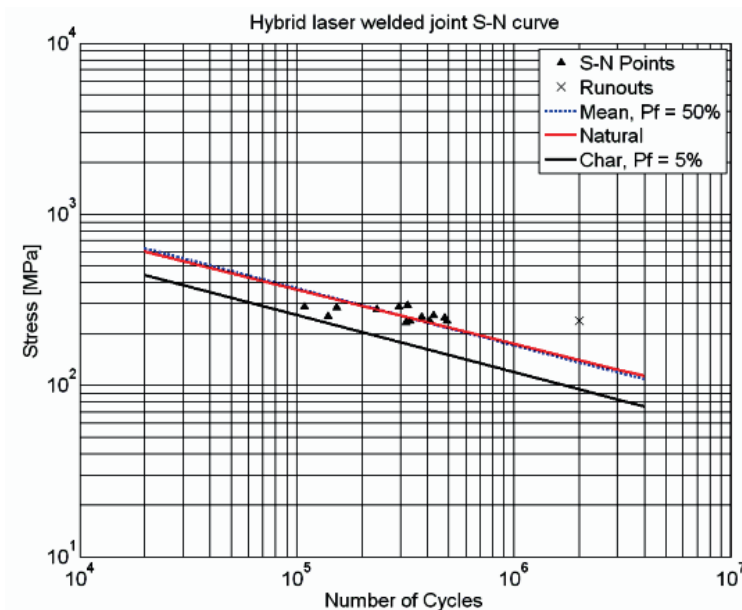


**Fig. 10** S-N-curve of the fatigue testing results, together with mean line (50% failure probability) evaluated with  $m=3$ , natural mean line with  $m$  evaluated with linear regression and the FAT (5% failure probability) line according to the IIW-standard

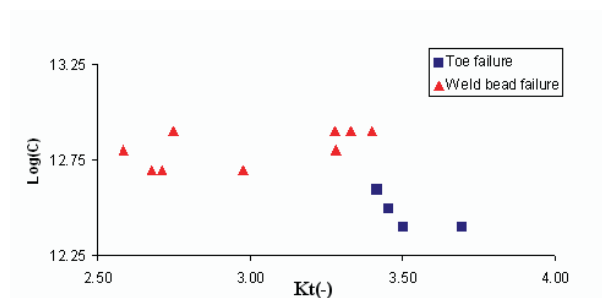


**Fig. 11** Capacitive value C ( $m=3$ ) as a function of the stress concentration factor  $K_t$ , distinguishing toe failure and weld bead failure specimens

## 7. Fractography

The fatigue crack initiation process involves the formation of microscopic flaws at grain boundaries, inclusions, micro-structural and chemical heterogeneities as well as microscopic and macroscopic stress concentrations [37]. As the welding processes create heterogeneous nucleation sites on the macroscopic level, a detailed study of microscopic aspects of fatigue crack initiation and propagation was not essential. Crack initiation and propagation patterns were observed after opening the cracks in the samples. Multiple crack initiation sites were found on the crack plane as shown in Fig. 12(c). In general, the number of crack initiation sites is proportional to the magnitude of the applied fatigue loading. This can be explained by taking the applied load on the surface source as the nominal strain, whereas the fatigue crack initiation is governed by the local strain which is much higher due to stress rising effects, i.e., inclusions, precipitates and micro structural defects[38]. Under a higher fatigue load more initiation sites activate as the local strain exceeds the elastic strain limit due to the microscopic stress concentration effect. As the fatigue cracks progress, they coalesce and develop into one or few dominating cracks leading to the final fracture.

When studying the fracture of a specimen with toe failure, a horizontal trace was observed below the surface, see Fig. 12(c). The distance to the surface was approximately 0.35 mm. As the fatigue crack initiated in the weld toe, this trace could be a transition from weld metal to base metal. This assumption was confirmed by H. Gripenberg [39]. Figure 12(b) shows at higher magnification some of the crack initiation sites associated with local toe radius. These initiation sites correspond to positions in which the weld ripples approach the toe of the hybrid weld. In this situation the ripples are following weld resolidification pattern. These defects are relatively long compared to their depth, and will cause a fairly constant stress concentration over most of their length. The initial aspect ratio (that is, the ratio of crack depth to half its surface length,  $a/c$ ) of cracks initiating from these defects tends therefore to be quite small, and oriented in a direction along the weld toe and normal to the plate surface. These orientations and aspect ratios are such that these cracks have the highest probability of becoming the dominant cracks that eventually lead to failure. Several chevron marks are observed in Fig. 12(c), with ratchet lines. Usually chevron marks point to the crack origin. Even though the specimen contains many initiation sites, only a few of them become predominant during the fatigue failure process. Each crack plane in Fig. 12(c) is separated by a ratchet line. Details for ratchet line formation at this state are discussed in [40]. When ratchet lines disappear after crack growth across the weld, the individual cracks coalesce and form a single crack plane. Figure 12 (a) shows fatigue crack propagation from a lower toe. The lower part of figure 12(c) shows tearing of the specimen after coalescence of the cracks. The weld top trace of the (longer) cracks of all 13 specimens is shown in Fig. 13. Many, but not all cracks follow the weld surface ripple pattern. Some cracks jump from an outer to an inner (with respect to the weld centre) ripple. Stress rising by the ripples obviously guides the cracks into a favored direction, as supported by the FE-simulation.

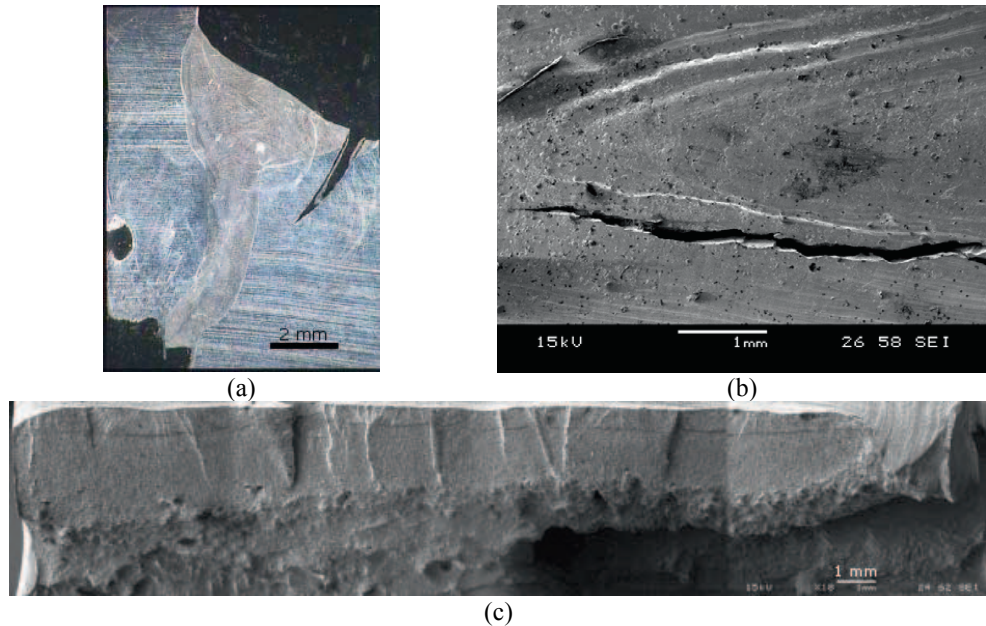


**Fig. 12** Typical fractography microscope images: (a) weld cross section with propagating crack, (b) weld surface with crack propagating along the ripples, (c) crack surface along the weld, showing crack initiation points, chevron marks and ratchet lines and the horizontal transition line weld bead-HAZ

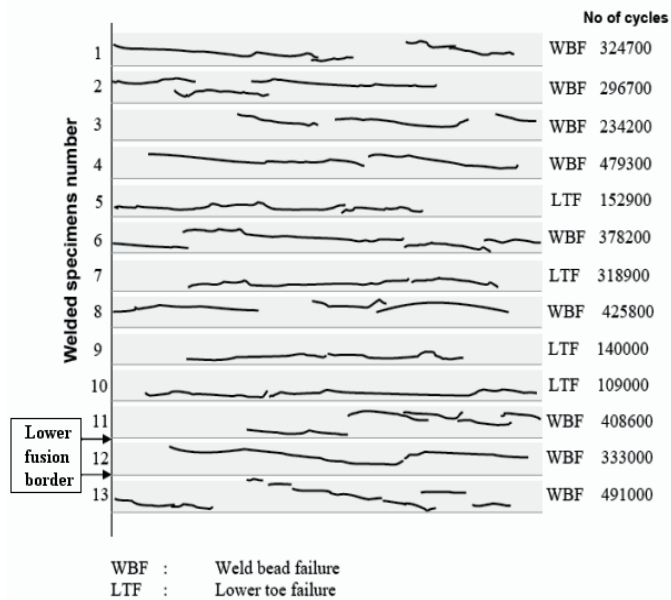


**Fig. 13** Crack trace at the weld top surface for all 13 samples

## 8. Discussion and theory

In this experiment, there are two different types of crack surfaces observed i.e. cracks in the weld toe and in the weld bead. Both cracks originated from undercuts according to Otegui et al [25]. Surface ripples or waviness are here considered as undercuts. Cracks initiated from the ripples near to weld toe propagate along the toe and formed ratchet marks which are shown in Fig. 14 (a). Corresponding to Otegui et al [21] crack initiation point on the weld bead is defined where two weld ripples intersect or secondary crack along any point in surface ripples path or at both situation which is shown in schematic diagram at Fig. 14 (b) and subsequently crack propagation path.

Owing to the presented findings, improvement of fatigue life by means of controlling the toe waviness is desirable, e.g. controlling the weld pool flow as origin of the ripples on by the post processing, e.g. surface remelting. The period of toe waves as well as particular features of the toe geometry strongly influence the fatigue crack initiation and propagation process [20]. Larger toe wave period and smaller internal toe angle gives the longest fatigue propagation live [21]. Large toe wave periods also mean large geometric mismatches in the internal toe points where toes corresponding to two adjacent waves intersect. On the one hand the geometry of these internal toe points makes them unsuitable for crack initiation; on the other hand cracks coalescence in these regions is delayed, increasing load shedding interactions between neighboring cracks and slowing crack propagation.

A theoretical description of the findings is illustrated in Fig. 15. Basically it shows that three mechanisms contribute to the maximum stress, namely the throat distance, the toe radius and the ripple radii. Those competing mechanisms determine which region is most critical. Moreover, the root of the weld is uncritical due to its compressive stress environment.

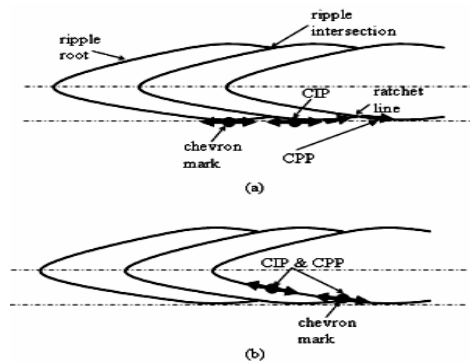


**Fig. 14** Theoretical description of cracking at the weld top surface: Schematic diagram of crack initiation point (CIP) and crack propagation path (CPP) for (a) straight propagation in the weld toe (b) propagation along the weld surface ripples

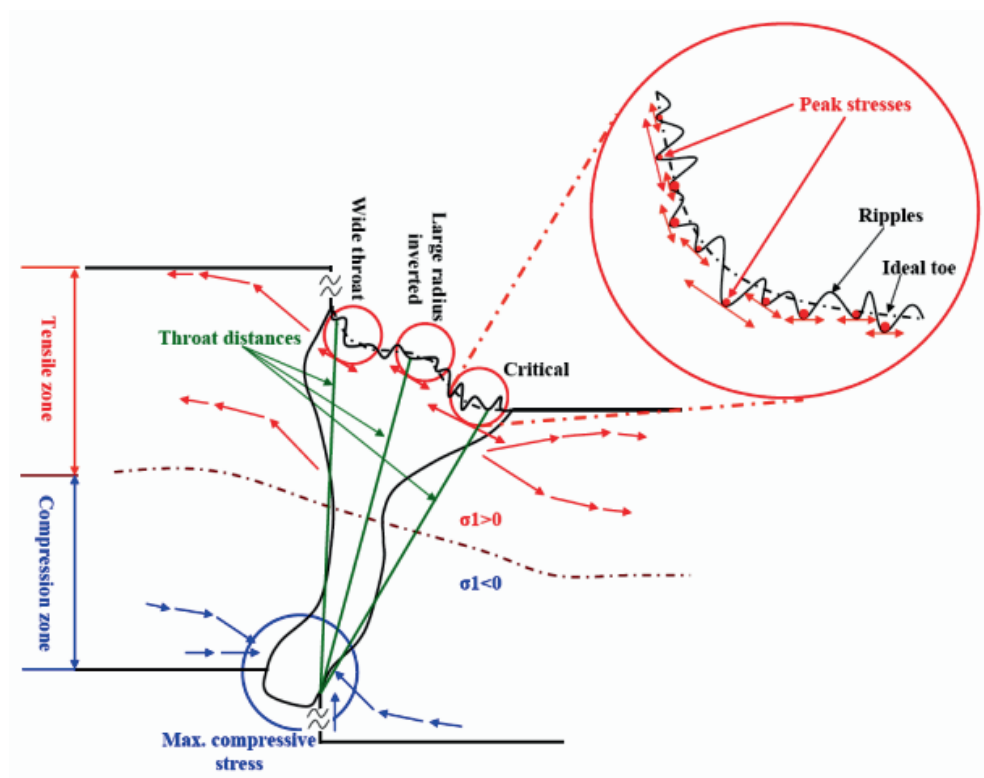


**Fig. 15:** Theoretical description of the competing stress raising mechanisms across the eccentric hybrid weld geometry, including surface ripple topography

## 9. Conclusions

- The toe radius does not always dominate fatigue performance, as ripples can become local stress raisers.
- If the toe radii are large enough, the stress peak can be shifted to the weld bead; the weld re-solidification ripple pattern guides the cracks.
- Welds which fail in the bead show higher fatigue strength than those which fail in the toe.
- The toe radius and surface topography can vary along the weld.
- The lower toe radius is more critical than the upper toe in this eccentric joint, as its shorter distance to the root generally causes higher stress
- The surface ripples significantly raise stress, but those in the toe normally causes the highest stress, except when the toe radius is small.
- The cracks in this case always started in the weld, not in the HAZ, nor at the fusion interface.
- The complex geometrical interactions involved can be explained by a theoretical illustration.

### Acknowledgements

The authors are grateful to VINNOVA – The Swedish Innovation Agency (project HYBRIGHT, no. 27382-2) and the Nordic Industry Centre (project NORHYB) for funding the research.

### References

- [1] V. Caccese, P.A. Blomquist, K.A. Berube, S.R. Webber, N.J. Orozco, Effect of weld geometric profile on fatigue life of cruciform welds made by laser/GMAW processes, *Mar. Struct.* 19 (2006) 1-22.
- [2] C.H. Lee, K.H. Chang, G.C. Jang, C.Y. Lee, Effect of weld geometry on the fatigue life of non-load carrying fillet welded cruciform joints, *Eng. Fail. Anal.* 16(2009) 849-855.
- [3] T.N. Nguyen, M.A. Wahab, A theoretical study of the effect of weld geometry parameters on fatigue crack propagation life, *Eng. Fract. Mech.* 51(1995) 1-8.
- [4] A. Fatemi, L. Yang, Cumulative fatigue damage and life prediction theories: a survey of the state of the art for homogeneous materials, *Int. J. Fatig.* 20(1998) 9-34.
- [5] Y. Yao, M. Wouters, J. Powell, K. Nilsson, A. Kaplan, Influence of joint geometry and fit-up gaps on hybrid laser-metal active gas (MAG) welding, *J. Laser Appl.* 18(2006) 283-288.
- [6] M. Wouters, J. Powell, A. Kaplan, The influence of joint gap on the strength of hybrid Nd:yttrium-aluminum-garnet laser-metal inert gas welds, *J. Laser Appl.* 18(2006) 181-184.
- [7] H. Remes, Strain-based approach to fatigue strength assessment of laser-welded joints, Doctoral dissertation, Department of Mechanical Engineering, Ship Laboratory, Helsinki University of Technology, Helsinki, 2007.
- [8] Z. Xiulin, L. Baotong, C. Tianxie, L. Xiaoyan, L. Chao, Fatigue tests and life prediction of 16 Mn steel butt welds without crack-like defect, *Int. J. Fract.* 68(1994) 275-285.
- [9] C.Y. Hou, Fatigue analysis of welded joints with the aid of real three-dimensional weld toe geometry, *Int. J. Fatig.* 29(2007) 772-785.
- [10] S. Kainuma, T. Mori, A study on fatigue crack initiation point of load-carrying fillet welded cruciform joints, *Int. J. Fatig.* 20(2008) 1669-1677.
- [11] F.P. Brennan, P. Peleties, A.K. Hellier, Predicting weld toe stress concentration factors for T and skewed T-joint plate connections, *Int. J. Fatig.* 22(2000) 573-584.
- [12] H.L.J. Pang, Analysis of weld toe profiles and weld toe cracks, *Int. J. Fatig.* 15(1993) 31-36.
- [13] H.L.J. Pang, Analysis of weld toe radius effects on fatigue weld toe cracks, *International J. Press. Vessels Piping.* 58(1994) 171-177.
- [14] J.A.M. Ferreira, C.A.M. Branco, Influence of the radius of curvature at the weld toe in the fatigue strength of fillet weld joints, *Int. J. Fatig.* 11(1989) 29-36.
- [15] D. Radaj, Design and analysis of fatigue resistant welded structures, Cambridge: Abington Publishing, 1990.
- [16] A. Hobbacher, Fatigue design of welded joints and components, IIW document XIII- 2151-07 / XV-1254-07.



- [17] W. Fricke, Fatigue analysis of welded joints: state of development, *Mar. Struct.* 16(2003)185–200.
- [18] S.J. Maddox, Fatigue strength of welded structures, Abington publishing limiter, 2<sup>nd</sup> edition, 2002
- [19] P. Kujala, G. Socha K. Koli, T. Toivonen, Characteristics of stake laser welded Joints, *Proceedings 7th Nordic Conference in Laser Processing of Materials Lappeenranta, Finland, (1999) 120-133.*
- [20] J. Weldingh, J.K. Kristensen, Hybrid YAG-laser/MAG welding quality and stability, *Proceedings 9th Conference on Laser Materials Processing in the Nordic Countries. Trondheim, Norway, (2003) 15–24.*
- [21] Z. Barsoum, Residual Stress Analysis and fatigue assessment of welded steel structures, Doctoral dissertation, Department of Aeronautical and Vehicle Engineering, Royal Institute of Technology, Stockholm, 2007.
- [22] A. Otha, Y. Maeda, N. Suzuki, Residual stress effect on fatigue strength of non-load- carrying cruciform welded joints of SM570Q steel for welded structures, *Welding in the World*, 46(2002) 20-25.
- [23] C-L., Tsai, C-M., Tso, W-C., Mohr, Geometry effect on fatigue life of fillet welds under tensioncompression loading, *EWI Material Joining Technology, Report No. MR0306, 2003.*
- [24] Z. Barsoum, M. Gustafsson, Fatigue of high strength steel joints welded with low temperature transformation consumables, *J. of Eng. Fail. Anal.*, 16(2009) 2186 2194.
- [25] R.F. Ricondo, Fatigue and quality analysis of cruciform joints welded with different methods, Master thesis, Department of Aeronautical and Vehicle Engineering, Royal Institute of Technology, Stockholm, 2006.
- [26] M. Ring, W. Dahl, Fatigue properties of laser-beam weldments on the high strength, *Steels, Steel Research.* 65(1994) 505-510.
- [27] F. Weichel, H. Petershagen, Fatigue strength of laser welded structural steels with thicknesses between 8 and 20 mm. *IIW Document XIII-1590-95. Germany: University of Hamburg. (1995).*
- [28] M.D. Chapetti, J.L. Otegui, Importance of toe irregularity for fatigue resistance of automatic welds, *Int. J. Fatig.* 17(1995) 531-538.
- [29] M.D. Chapetti, J.L. Otegui, Controlled toe waviness as a means to increase fatigue resistance of automatic welds in transverse loading, *Int. J. Fatig.* 19(1997) 667-675.
- [30] J. L. Otegui, H. W. Kerr, D. J. Burns, U. H. Mohaupt, Fatigue crack initiation from defects at weld toes in Steel, *Int. J. Press Vessels Piping.* 38(1989) 385-417
- [31] L. L. Martinez, Fatigue behaviour of welded high-strength steels, Doctoral dissertation, Department of Aeronautical and Vehicle Engineering, Royal Institute of Technology, Stockholm, 1997.
- [32] J. Martinsson, Fatigue Assessment of complex welded steel structures, Doctoral dissertation, Department of Aeronautical and Vehicle Engineering, Royal Institute of Technology, Stockholm, 2005.
- [33] R. Bell, O. Vosikovsky, S. A. Bain, Significance of weld toe undercuts in the fatigue of steel plate T-joints, *Int. J. Fatig.* 11(1989) 3-11.
- [34] ANSYS guide, ANSYS release 11. Houston : Swanson Analysis Systems

- [35] H. Narimani, Fatigue strength of laser hybrid welded high strength steel, Master's thesis, Department of Applied Physics and Mechanical Engineering, Luleå University of Technology, Luleå, 2008.
- [36] T. Gurney, Cumulative damage of welded joints, Woodhead publishing limited, 2006
- [37] S. Suresh, Fatigue of materials, Cambridge solid state science series, Cambridge university press, second ed., 1998.
- [38] R.W. Hertzberg, Deformation and fracture mechanics of engineering materials, John Wiley and Sons, INC. 4th Edition, USA, 1996.
- [39] H. Gripenberg, A Study of Submerged Arc, Laser and Hybrid Weld Properties, Residual Stresses, CSS-Curves and Fractography. Espoo, Finland: Helsinki University of Technology, Laboratory of Engineering Materials. Research report TKK-MTR-2/03.2003.
- [40] Y. Verreman, B. Nie, Short crack growth and coalescence along the toe of a manual fillet weld, *Fatig. Fract. Eng. Mat. Struct.* 14(1991) 337-349.

## **Paper III**

### **FATIGUE CRACKING BEHAVIOUR FOR LASER HYBRID WELDED ECCENTRIC FILLET JOINTS INCLUDING LACK OF FUSION**

M. M. Alam, Z. Barsoum, P. Jonsén, H. A. Häggblad, A.F.H. Kaplan

Engineering Fracture Mechanics, 2009 (submitted)



## **Fatigue cracking behaviour for laser hybrid welded eccentric fillet joints including lack of fusion**

**Authors:** M. M. Alam<sup>1\*</sup>, Z. Barsoum<sup>2</sup>, P. Jonsén<sup>1</sup>, A. F. H. Kaplan<sup>1</sup>, H. Å. Häggblad<sup>1</sup>

**Affiliation:**

<sup>1</sup>Luleå University of Technology, Dept. of Applied Physics and Mechanical Engineering,

SE-971 87 Luleå, Sweden

Email: minhaj.alam@ltu.se, par.jonsen@ltu.se, alexander.kaplan@ltu.se, hans-ake.haggblad@ltu.se

<sup>2</sup>Royal Institute of Technology, Dept. of Aeronautical and Vehicle Engineering, SE-100 44 Stockholm, Sweden

Email: zuheir@kth.se

\*Corresponding author: minhaj.alam@ltu.se

Phone: +46(0)920 493917

Fax: +46(0)920 49 22 28

### **Abstract**

Fatigue cracking of laser hybrid welded eccentric fillet joints has been studied for stainless steel. Two-dimensional linear elastic fracture mechanics (LEFM) analysis was carried out for this joint geometry for four point bending load. The numerical simulations explain for the experimental observations why cracking is initiated preferably at the lower weld toe and why the crack gradually bends towards the root. The tendency to Lack of Fusion (LOF) is explained by the restricted positioning of the laser beam along with the thermal barrier of the joint interface. LOF turned out to be uncritical for the initiation of cracks due to its compressive stress conditions. The LEFM analysis has demonstrated, in good qualitative agreement with fatigue test results, that LOF slightly (<10%) reduces the fatigue life by accelerating the crack propagation. For the here studied geometrical conditions improved understanding of the crack propagation was obtained and in turn illustrated. The elaborated design curves turned out to be above the standard recommendations.

**Keywords:** crack, fatigue, weld, LEFM, lack of fusion

## 1. Introduction

The level of complexity of the mechanisms responsible for fatigue cracking of welds further increases in case of complex geometry of the joint, of the weld shape and of the loading conditions. Welding strongly affects the material by the heating and cooling cycle as well as by the fusion process with additional filler wire, resulting in inhomogeneous materials and different phases. Furthermore, a weld is usually far from perfect, containing inclusions, pores, cavities, undercuts, etc. The top and root shape of the weld can create versatile geometrical properties and high stress concentration. As a consequence, fatigue failures appear in welded structures mostly at the welds rather than in the base metal, even if the latter contains notches such as openings or re-entrant corners. For this reason, fatigue analyses are of high practical interest for all welded structures exposed for cyclic loads e.g. ships, offshore structures, cranes, bridges, vehicles, railways, etc.

Fatigue failure usually includes three stages: crack initiation, propagation and instantaneous fracture [1]. At each stage, the corresponding fatigue behaviour can be affected by various factors, such as load conditions, geometry of the weld, constraint of the structure, material properties, environment, etc. Studies in the recent decades have shown that the initiation and propagation of cracks from welded joints is different from that in homogeneous base materials due to the high level of residual stresses, strength mismatching, complex microstructure, etc. found in welds [2-10]. It should be noted that the welding process always introduces cracks or other kinds of crack-like imperfections into welded joints in engineering practice. The existence of crack-like imperfections in the welded joint is normally considered to eliminate the crack initiation stage of fatigue life. Therefore, the emphasis of the fatigue assessment can often be focused on the crack growth stage of the fatigue life. The existence of crack-like flaws in the welded steel joints as a result of weld defects is unavoidable and its impact on fatigue crack initiation life has often been studied [11-18]. Under cyclic loading, fatigue cracks are initiated from these defects and propagate. However, so far limited analysis of the effect of weld geometry parameters on fatigue crack propagation has been carried out. In a wide variety of cases crack growth problems can be solved within the frame of linear elastic fracture mechanics (LEFM). This is the case when the yield zone at the crack tip is small with respect to both the crack size and the remaining ligament. By characterizing crack growth using concepts such as the stress intensity factor through the Paris-Erdogen power law [19], it is possible to predict the crack growth rate of a weld under cyclic loading, and hence the number of cycles necessary for a crack to extend from a certain initial size, i.e. the size of pre-existing cracks or crack-like defects, to a maximum permissible size to avoid catastrophic failures.

Lack of fusion (LOF) is normally considered as a very critical defect in a welded structure. Besides reducing the effective weld throat depth, because of its notch effect, a crack may further propagate even under small loads applied. The occurrence of lack-of-fusion and its characteristics is described for gas shielded arc welding processes in [20]. The main cause for the occurrence of lack of fusion is insufficient

energy input to the weld area. This means that the parent metal in the weld groove or previous runs have not heated to the melting point to make a uniform joint. This is mainly affected by the groove preparation, the welding technology and the welding parameters chosen [21]. Lack of fusion most often results from the weld pool part running ahead of the arc. An important influence is exerted by the welding parameters, i.e. welding current, voltage, welding speed, wire feeding rate, wire extension length, torch inclination, welding position, weld preparation and arc deflection [22].

Considerable research on the fatigue of welded joints and complex structures has been carried out and reported in the literature. However, there is no complete study available that considers the present combination of non-trivial conditions together for studying fatigue cracking behaviour, namely: (i) unusual joint geometry (eccentric fillet joint), (ii) advanced welding technique (hybrid laser welding), (iii) internal weld defects (lack of fusion or lack of penetration), (iv) four point bending load situation. Hybrid welding [23] combines a laser beam with an electric arc (MIG) and creates a narrow deep weld (from the laser beam) but also has the freedom to shape the surface (by the burning electrode).

The present study aims at improved understanding of the fatigue crack propagation behaviour for combination of the four above mentioned conditions.

## **2. Methodology**

While the initial stress conditions under load (at the surface, including also weld ripples) were investigated in [24] for identifying and understanding the crack initiation sites (for the same case), as a continuation (but independently) the present paper focuses for the same case on the crack propagation (in the volume, including possible LOF).

For achieving improved understanding of the fatigue cracking behavior, numerical Finite Element (FE) simulation of the stress field and of the propagating crack accompanies the experimental fatigue testing analysis. Based on measurement of the weld surface cross sections, FE-analysis is carried out. The research was conducted as follows: (i) Fatigue analysis of the tests was carried out by the nominal stress method, by the effective notch stress approach and others. (ii) The stress field as a function of time resulting from computed stepwise propagation of the crack (from the maximum stress location) just in the cross section then enables (iii) detailed analysis of competing mechanisms, e.g. interaction with LOF. (iv) The computed crack paths are compared with experimental ones. (v) The etched cross section and the surface of Lack-of-Fusion are metallurgically analysed. (vi) Simulated crack propagation cases with and without LOF are compared, also different origins of cracking (upper and lower toe, weld bead). The stress field enables detailed analysis of the mechanisms, and (vii) also comparison of the fatigue life. (viii) Eventually an illustrative phenomenological description was derived, both for the thermodynamic formation of LOF during welding and for the stress contributions determining the cracking behavior.

### 3. Welding

#### 3.1. Joint design

The joint type studied involves two 10 mm thick steel plates in eccentric fillet configuration, see Fig. 1. Structural stainless steel SS2333 was used with sample dimensions of  $w \times l \times t = 50 \times 100 \times 10 \text{ mm}^3$ , prepared by milling and grinding of the joint surface to give zero gap. Fillet welds were made between the two base plates with 5 mm eccentricity, see Fig. 1, using the hybrid laser metal inert gas (L/MIG) welding technique. The chemical composition and mechanical properties of the base metal and filler wire are presented in Table 1, 2. After the welding had been completed, all specimens were milled to cut off about 12.5 mm from both ends of the weld to remove the start and stop irregularities. A small square plate with  $25 \times 25 \times 5 \text{ mm}^3$  dimensions was attached (by manual arc welding) under the eccentric base metal; see Fig. 1, to facilitate sample attachment to the fatigue testing machine.

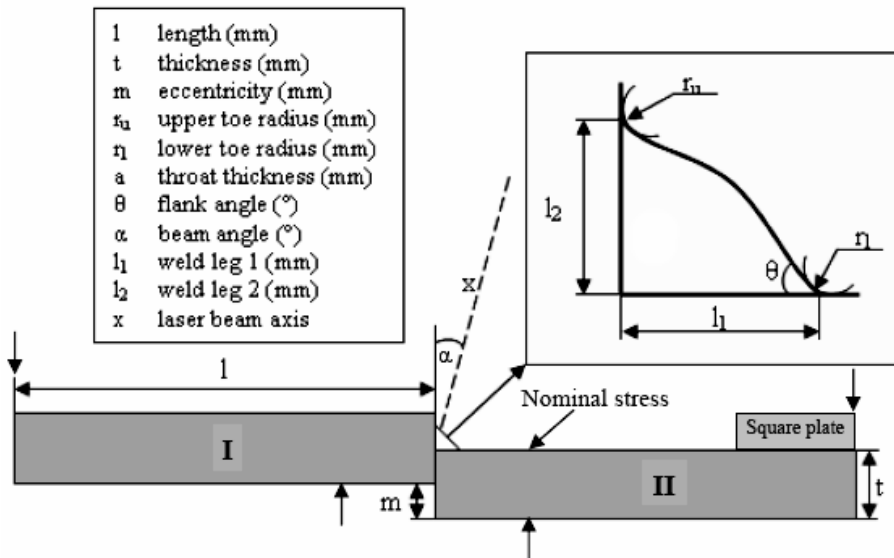


**Fig. 1:** Eccentric fillet joint: geometrical properties

#### 3.2. Welding set-up

An Ytterbium fibre laser (IPG Laser YLR 15000) with a maximum power of 15 kW (wavelength 1070 nm) was used for the experiments. The laser beam with a beam parameter product (beam quality) of  $10.4 \text{ mm} \cdot \text{mrad}$  was delivered through a  $200 \mu\text{m}$  fibre optics core. The optics (focusing to collimating length =  $300 \text{ mm} : 150 \text{ mm} = 2:1$ ) created a beam with a focal diameter of  $400 \mu\text{m}$  and a Rayleigh length (focal depth) of  $\pm 4 \text{ mm}$ , the focal plane positioned on the top surface of the weld. The laser was combined with a MIG-welding source (ESAB ARISTO). The filler wire, see



Table 1 and 2, had a diameter of 1.2 mm. During the hybrid laser welding process, the laser beam was traveling 2 mm in front of the MIG torch. Further process parameters (chosen to achieve a sound, stable weld) are summarized in Table 3.

**Table 1:** Chemical composition [%] of the materials used for the sheets and for the filler wire

Material	C	Si	Mn	Cr	Ni	P	S	N
SS142333 (sheets)	0.05	1.0	2.0	19.0	11.0	0.045	0.030	-
Avesta 253MA (wire)	0.07	1.6	0.6	21.0	10.0	-	-	0.15

**Table 2:** Mechanical properties of the materials used

Material	$R_{p0.2}$ (N/mm <sup>2</sup> ) min	$R_m$ (N/mm <sup>2</sup> )	$A_5$ (%) min	Hardness, HB max
SS142333 (sheets)	210	490 – 690	45	200
Avesta 253MA (wire)	440	680	38	210

**Table 3:** Hybrid welding parameters

Parameter	Value / type
MIG current (constant)	328 A
MIG voltage (resulting)	27 V
Pulse time	2.4 ms
Frequency	90 Hz
Wire stick out length	16 mm
Wire feed rate	4.2 m/min
Shielding gas	Ar
Shielding gas flow	20 l/min
Laser beam angle, $\alpha$	10 °
Welding speed	1.05 m/min
Laser power	3.25 kW

### 3.3. Resulting weld

For statistical purposes, 13 samples were welded under identical conditions. Figure 2 shows some resulting weld cross sections and indicates important locations (A-E). Lack of Fusion (LOF) was a typical defect that was difficult to suppress and therefore part of the study. The effective weld throat thickness is 6-7 mm and the leg length is 4 mm.

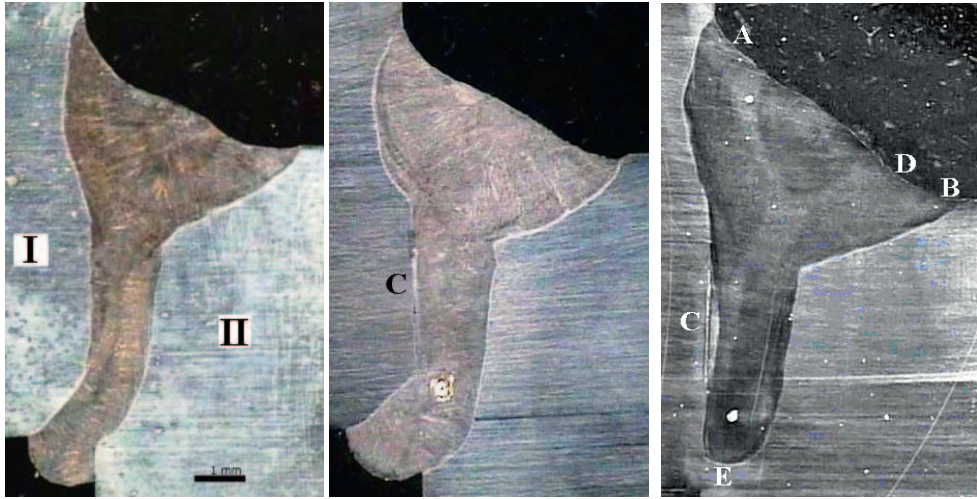


**Fig. 2:** Typical resulting weld: (a) defect-free weld cross section, (b) with lack of fusion-interface, (c) with distinct lack of fusion and lack of penetration

## 4. Fatigue analysis

### 4.1. Testing set-up

The four point bend fatigue testing was performed using a servo-hydraulic machine (Instron 1272, max  $\pm 50$  kN). The welded joints were tested by keeping a constant amplitude stress ratio,  $R = 0$  at a frequency of 45 Hz, as shown in Fig. 3. The specimens were tested in the range from 2.5 kN to 4 kN until complete failure. A thicker beam than the base metal was specially prepared and hardened for fatigue testing with two different grooves so that the roller can fit the groove.

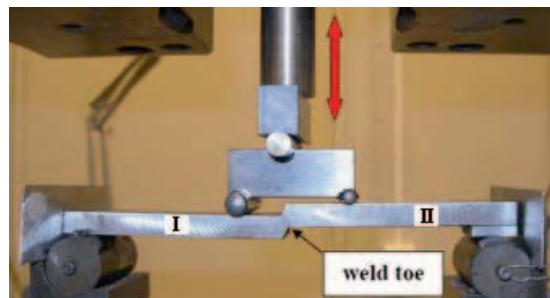


**Fig. 3:** Four-point fatigue bending test (note: the sample is upside down)

### 4.2. Fatigue test evaluation by the nominal stress method

In this fatigue analysis, the nominal stress approach was used. The stresses were calculated by FEA. The nominal stresses were taken from the top surfaces, 24 mm

away from the joint edge, thus where the load was applied to both plates, see Fig. 1. The fatigue resistance data and nominal stresses were then compiled into a logarithmic SN-curve (Wöhler curve) as shown in Fig. 4 to describe the fatigue strength. The equation for the SN-curves can be written as [25]

$$\log N = \log C - m \log \Delta \sigma \quad (1)$$

or simply as

$$N = \frac{C}{\Delta \sigma^m} \quad (2)$$

where  $N$  is the number of cycles to failure,  $\Delta \sigma$  is the stress range,  $m$  is the slope of the SN-curve and  $C$  is the load intensity value (Capacity). For comparison the numerically predicted values for fatigue life are also shown in Fig. 4. They will be described in Section 6.2. Since no standard definitions exist so far for fillet joints with 5 mm eccentricity under a four point bending condition, all the calculations for fatigue strength were stand alone and not comparable [25], [26]. The fatigue test properties identified are shown in Table 4. The mean value ( $P_f$  50%) of the fatigue strength was calculated with a slope of  $m=3$ , excluding one run out. Also, the fatigue classes FAT on 50% and 95% survival probability levels were calculated according to the IIW recommendations [25]. From the fatigue test data a mean linear regression analysis was carried out, assuming a straight line of the SN-curve. This gave a slightly higher natural slope of the SN-curves of  $m=3.16$ . The mean  $P_f$  50% was also increased to 141 MPa. The natural slope is calculated according to Equation (3) [26]. To calculate the natural mean curve,  $\log C$  has to be calculated, which is done by using Equation (4) where  $n$  is the number of failed specimens.

$$m_{\text{natural}} = \frac{n \cdot \sum (\log N \cdot \log \sigma) - \sum \log N \cdot \sum \log \sigma}{(\sum \log \sigma)^2 - n \cdot \sum (\log \sigma)^2} \quad (3)$$

$$\log C = \frac{\sum \log N + m_{\text{natural}} \cdot \sum \log \sigma}{n} \quad (4)$$

**Table 4:** Fatigue testing results

IIW norm property	Value
$K_t$ – mean / standard deviation	3.09 / 0.35
Log C ( $m=3$ ) – mean / standard deviation	12.71 / 0.18
$m$ – natural slope	3.16
Mean value, ( $N = 2 \cdot 10^6$ , $m = \text{natural slope}$ )	141
Mean value, $P_f$ 50% ( $N = 2 \cdot 10^6$ , $m = 3$ )	137
FAT, $P_f$ 5% ( $N = 2 \cdot 10^6$ , $m = 3$ )	95

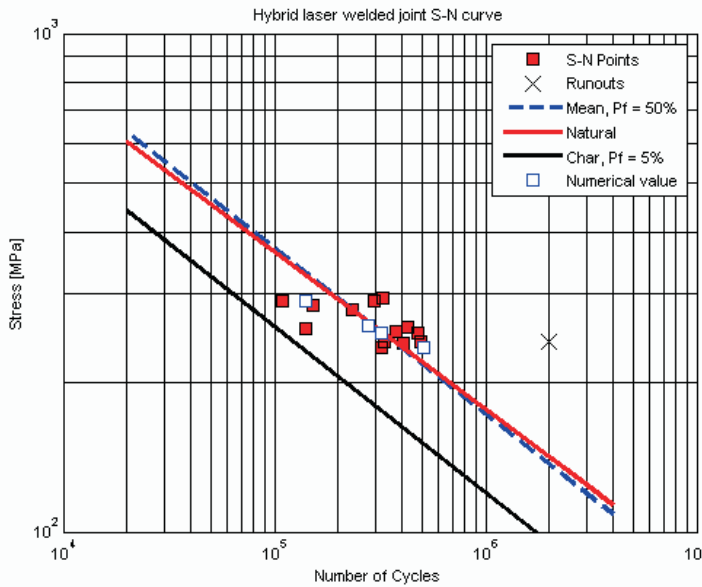


**Fig. 4:** SN-curve of the fatigue testing results, together with mean curve (50% failure probability) evaluated with  $m=3$ , natural mean curve with  $m$  evaluated with linear regression and the FAT (5% failure probability) curve according to the IIW-standard and numerical fatigue life.

#### 4.3. Fatigue test evaluation by the effective notch stress method

The effective notch stress is defined as the total stress at the root of a notch, obtained assuming linear-elastic material behavior. To take into account the statistical nature and scatter of the weld shape parameters as well as the non-linear material behavior at the notch root, the real weld contour is replaced by an effective notch root radius of 1 mm. This is considered to represent a normal weld that has not undergone any post-weld treatment. The effective notch radius is introduced such that the tip of the radius touches the root of the real notch. The approach is well suited for the FE-method even though the size of the elements at the notch has to be relatively small, approximately 0.25-0.35 mm, in order to achieve a good resolution of the stress field. A comprehensive review of notch stress methods can be found in Radaj et al. [27]

The effective notch stress was calculated for each specimen assuming an effective weld toe radius (1 mm) and excluding the actual notch radius as outlined in the recommendations in [25]. The toe angle was set to  $\theta = 45^\circ$  which has resulted in a mean stress concentration factor,  $K_t=3.36$ . The maximum principle stresses from the notch tip obtained from the FE-simulation are plotted against the experimentally observed fatigue cycles in Fig. 5. The effective notch stress fatigue assessment is summarized in Table. 5. The characteristic curve ( $P5\% = 279$  MPa) for all the specimens is above the characteristic curve, FAT 225 MPa, recommended by IIW [25]. The higher characteristic value than the recommendation might be due to

bending load situation and crack initiation from the weld bead [24]. Large scatter was observed at low cycles ( $<10^6$  cycles) in Fig. 5. This is due to the worst case assumption (toe radius: 1 mm) in connection with high scatter in the local weld geometry and observed life with a standard deviation of 0.249 for Log (C).

**Table 5:** Evaluation of fatigue test result of as welded specimens using effective notch stress method according to IIW.

IIW norm property	Value
Effective notch radius	1 mm
Log C (m=3) – mean / standard deviation	14.30 / 0.249
FAT at $P_f$ 50% ( $N = 2 \cdot 10^6$ , $m = 3$ )	465
FAT at $P_f$ 5% ( $N = 2 \cdot 10^6$ , $m = 3$ )	279
FAT (recommendation)	225

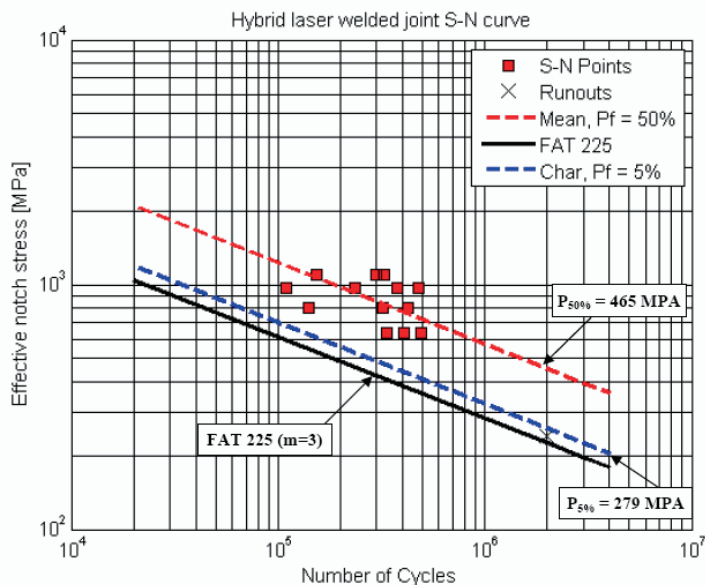


**Fig. 5:** Evaluation of the fatigue testing results using the effective notch stress method

## 5. Microscopic fracture mechanics analysis

### 5.1. Crack geometry and crack surface

Figure 6 shows a typical cracked weld top surface that failed at the lower toe. Figure 7 shows fatigue crack propagation from the lower and upper toes of welds with LOF defects. It is interesting to note that LOF opens and becomes more visible under load, but does not propagate as a crack.

Multiple crack initiation sites pointed by several chevron marks along with ratchet lines were found on the crack surface, as shown in Fig. 8. Even though the

specimen contains many initiation sites, only a few of them become predominant during the fatigue failure process. Each crack plane in Fig. 8 is separated by a ratchet line. Details for ratchet line formation at this stage are discussed in [28]. When ratchet lines disappear after crack growth across the weld, the individual cracks coalesce and form a single crack plane.

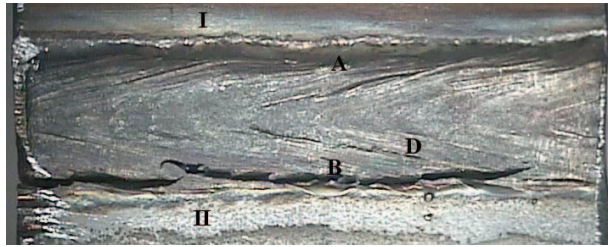


**Fig. 6:** Typical crack geometry at the top surface; cracking in the lower toe, partially propagating along the weld ripples

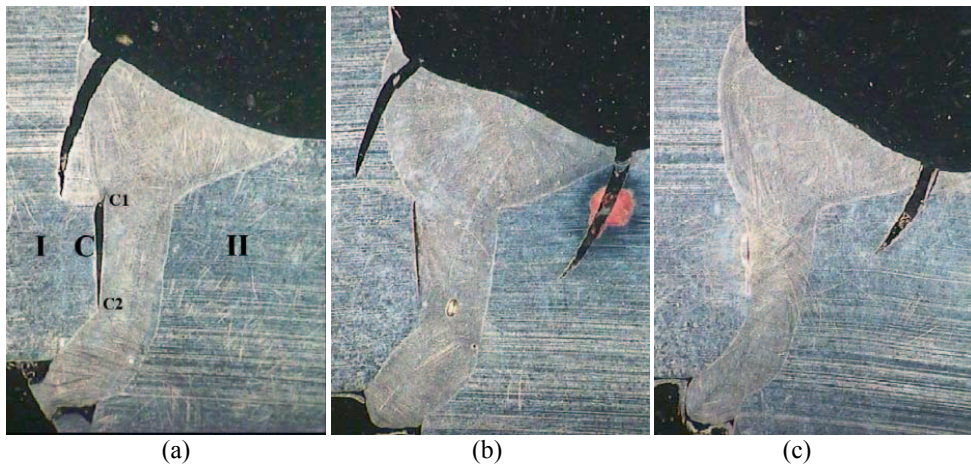


**Fig. 7:** Cross section of cracked welds (all with lack of fusion, C) after fatigue testing, with crack initiation (a) in the upper toe, (b) in the upper and lower toe, (c) in the lower toe

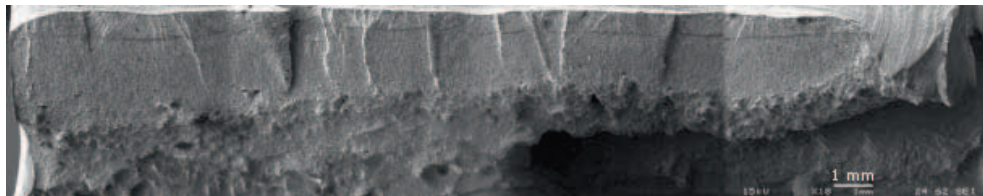


**Fig. 8:** Crack surface appearance along the weld: crack initiation points, chevron marks and ratchet lines and the horizontal transition line weld bead-HAZ

## 5.2. Joint surface, Lack-of-Fusion surface and metallurgy

Lack of fusion (LOF) is a weld discontinuity in which fusion has not occurred between the weld metal and the parent metal or between adjoining weld beads. Microscopic analysis was carried out to detect LOF on all as-welded and fractured specimens. LOF was observed in most of the welded specimens. The joint surfaces were prepared by milling, see Fig. 9(a), and compared to sawing. The two different surface preparations were not found to have any impact on the occurrence of LOF. After fatigue testing, the LOF surface was opened and examined. It was found that the parent metal surfaces were not melted in most cases; see Fig. 9(b), appearing different than the weld, Fig. 9(c). The microstructure of a fully welded weld-parent metal cross section is shown in Fig. 10(a), whereas Fig. 10(b) and 10(c) shows typical microstructures of LOF defects. Even almost invisible lack of fusion involves a sharp resolidification stop before the parent metal, see Fig. 10(b).

This occurs when the molten metal contacts the parent metal but does not melt it, due to the presence of oxides on the surface of the melt (and perhaps a gap). If, under the effect of internal stresses occurring during weld solidification and cooling, the two faces get separated, an open lack-of-fusion defect will be obtained. There is also LOF due to unmelted oxide inclusions, see Fig. 10(c), i.e. high melting point oxides or non-metallic inclusions are trapped between two adjoining faces. Oxides are arranged along the entire length of the LOF defect in a form of a thin layer. When they melt or when slag occurs in the lack-of-fusion defect, globular non-metallic inclusions will form [16]. The oxide layer and any gap create a thermal barrier between weld and parent metal which makes it more difficult to melt the parent metal. By accurate positioning of laser beam angle (restricted for eccentric joints) and higher line energy (higher power or lower welding speed), this effect can be minimized.

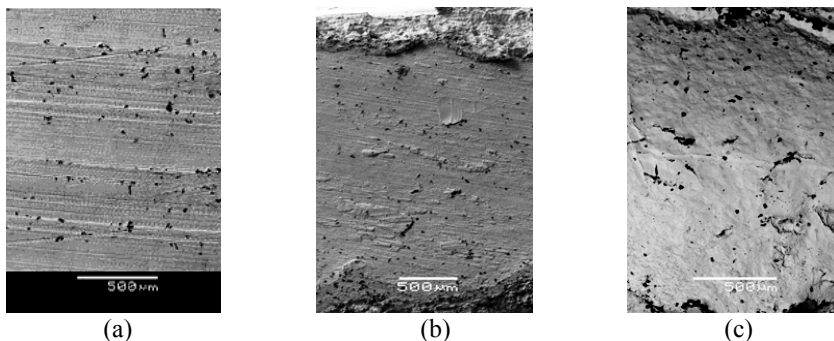


**Fig. 9:** Joint edge surface: (a) milled edge, (b) base metal side after opening the LOF, (c) weld bead side after opening the LOF



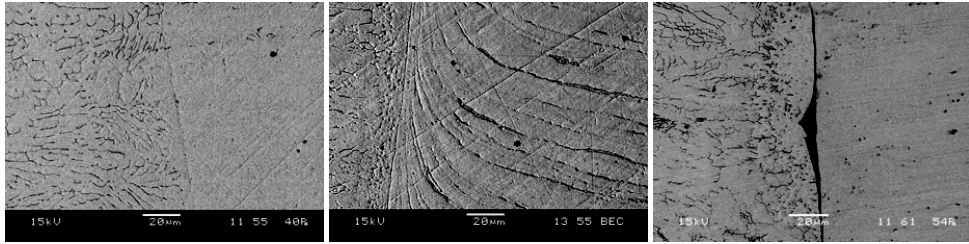


**Fig. 10:** Weld cross section metallurgy: (a) good weld (transition weld-HAZ), (b) lack of fusion: contact, but limited melting transition, (c) lack of fusion: distinct separation

## 6. Numerical fracture mechanics analysis

### 6.1. Numerical method

Linear elastic fracture mechanics (LEFM) crack growth analysis was carried out in order to understand the crack propagation for the here studied case, in particular the impact of the upper and lower weld toe shapes and of lack-of-fusion. The objective was to study the impact of crack propagation interaction and fracture avoidance from the different failure critical positions. The total fatigue life of welds involves both a crack initiation and a crack propagation stage. For welded joints an initial crack is assumed to exist due to the presence of weld defects. The major part of the fatigue life is consumed by propagation. This is a conservative way of predicting fatigue life in some cases, especially if a (large) defect is assumed to take the form of a straight-fronted ‘line’ crack (depth/surface length  $a/2c = 0$ ). However, the crack initiation phase is a negligible part of the fatigue life if accurate inspections are not utilized in the serial production of welds.

In a wide variety of cases crack growth problems can be solved within the frame of linear elastic fracture mechanics (LEFM). This is the case when the yield zone at the crack tip is small with respect to both the crack size and the remaining ligament. In the past decades, numerous investigations of fatigue crack growth of welded structures have been conducted, experimentally and numerically within the framework of LEFM [29-38]. In order to predict fatigue crack propagation, several equations were proposed by different researchers, usually semi- or wholly-empirical, to correlate fatigue crack growth rate data with the range of the single parameter  $\Delta K$ , the range of stress intensity factor. Among the proposed equations, the Paris-Erdogan relationship is commonly accepted and used in practice for a wide range of Mode I crack growth rates. The Paris-law [19] for the crack growth rate is

$$\frac{da}{dN} = C(\Delta K)^m, \quad (\Delta K_{th} \leq \Delta K \leq K_c, R=0) \quad (5)$$

where,  $da/dN$  is the crack growth rate per cycle,  $C$  and  $m$  are material constants. With respect to the crack propagation period  $Np$  and by integration of Eq. (5) we can obtain the number of loading cycles  $Np$ :



$$\int_0^{N_f} dN = \frac{1}{C} \int_{a_i}^{a_f} \frac{da}{[\Delta K]^m} \quad (6)$$

Equation (6) indicates that the required number of loading cycles  $N_f$  for a crack to propagate from the initial length  $a_i$  to the final crack length  $a_f$  can be explicitly determined if  $C$ ,  $m$  and  $\Delta K$  are known.  $C$  and  $m$  are material constants obtained experimentally [39-42]. For complicated geometries and loading cases it is necessary to use FE-simulation to predict the stress intensity factor.

### 6.1.1. Numerical computation of the stress-intensity factor

The accuracy of the obtained results in the numerical method depends on the fracture criteria used for calculating the fatigue crack growth rate and the crack growth direction. The crack growth rate is a function of the stress intensity factor (SIF;  $K_I$ ,  $K_{II}$ ,  $K_{III}$ ) [43]. In 2D FE models, four methods can be chosen to compute the stress-intensity factors along the (generally curved) crack path:

- (a) the displacement correlation technique (DCT) [44];
- (b) the quarter point displacement technique (QPDT) [45];
- (c) the potential energy release rate computed by means of a modified crack-closure (MCC) integral technique [46,47]; and
- (d) the J-integral computed by means of the equivalent domain integral (EDI) together with a mode decomposition scheme [48,49].

In this work the Finite Element Method in the framework of the program package FRANC2D [46] has been used for simulation of the fatigue crack growth. In this approach the determination of the stress intensity factor is based on the DCT using singular quarter-point, six node triangular elements around the crack tip, see Fig. 11. It is worth noting that in a quarter-point element (QPE) the mid-side node is located at the quarter distance away from the crack tip node ( $ab = 1/4 ac$ ) in order to provide more accuracy for the calculated stress and displacement fields around the tip. The DCT uses all four nodes on the crack faces of a QPE. The technique uses the differential displacements of the adjacent nodes across the crack to compute the stress intensity factors:

$$\begin{aligned} K_I &= \frac{2G}{(3-4\nu)+1} \sqrt{\frac{\pi}{2L}} [4V_d - V_e - 4V_b + V_c] \\ K_{II} &= \frac{2G}{(3-4\nu)+1} \sqrt{\frac{\pi}{2L}} [4u_d - u_e - 4u_b + u_c] \end{aligned} \quad (7)$$

where  $G$  is the shear modulus of the material,  $\nu$  is the Poisson ratio,  $L$  is the finite element length on crack face,  $u$  and  $V$  are displacements of the finite element nodes b, c, d and e, see Fig. 11. The combined stress intensity factor is then:

$$K = \sqrt{(K_I^2 + K_{II}^2) \cdot (1 - \nu^2)} \quad (8)$$

The displacement method can be applied to the plane strain condition to calculate the stress intensity factor:

$$K_I = \frac{E}{8(1-\nu^2)} \sqrt{\frac{2\pi}{L}} [4(V_b - V_d) - (V_c - V_e)] \quad (9)$$

where  $E$  is Young's modulus

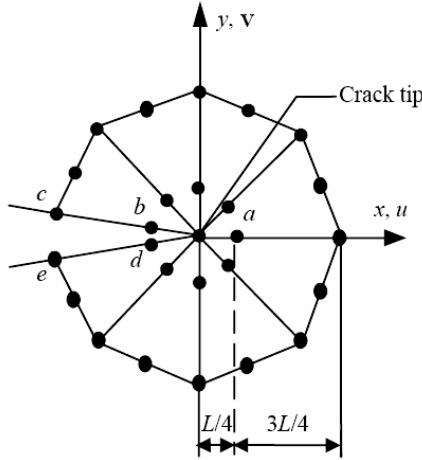


**Fig. 11:** Six-node triangular element around the crack tip [51]

### 6.1.2. Numerical computation of the crack growth direction

To simulate the crack growth direction in 2D FE-analysis, the most usual criteria for the computation of crack growth are: (a) maximum circumferential stress ( $\sigma_{\theta\max}$ ); (b) maximum potential energy release rate ( $g_{\theta\max}$ ); and (c) minimum strain energy density ( $S_{\theta\max}$ ).

For the first criterion, Erdogan and Sih [52] considered that a crack grows in the same direction as the maximum circumferential tensile stress around the crack tip. In the second criterion, Hussain et al [53] have suggested that the crack propagates in the direction with the highest energy relaxation rate and Sih [54] proposed the third criterion that crack grows in the direction that provides the lowest level of strain energy within the material. Although research has shown a close similarity between the results of these three methods for predicting the crack growth direction, most of the studies indicate that the first method (the maximum circumferential tensile stress method) has been preferred [55-58]. In the maximum circumferential stress theory, the direction of crack propagation  $\theta$  is computed from

$$K_I \sin \theta + K_{II} (3 \cos \theta - 1) = 0 \quad (10)$$

Analysis of Equation (10) for the two pure modes showed that for pure Mode I,  $K_{II} = 0$ ,  $K_I \sin \theta = 0$  and  $\theta = 0^\circ$ , and for pure Mode II,  $K_I = 0$  and  $\theta = \pm 70.5^\circ$ . These values of  $\theta$  are the extreme values of the crack propagation angles. The intermediary values are found by solving Eq. (10) for  $\theta$  considering the mixed mode, resulting in

$$\theta = 2 \arctan \left( \frac{1}{4} \frac{K_I}{K_{II}} \pm \frac{1}{4} \sqrt{\left( \frac{K_I}{K_{II}} \right)^2 + 8} \right) \quad (11)$$

### 6.1.3. Fatigue crack growth simulation

The concepts of numerical crack growth, as reviewed in the previous sections, are applied in the framework of simulation to predict the fatigue crack propagation behavior in an eccentric fillet joint. Simulation in this work consists of two individual processes: modeling and meshing, using ANSYS 11 [59] software, and simulating and analyzing, with the help of FRANC2D [50]. A 2D plane strain FE-model was used for the LEFM calculations. The weld toe radii (upper and lower) were modelled with a radius of 1 mm. The mesh used in the analysis consists of 6-node triangular QPEs for the crack region and 8-node quadrilateral elements for the remaining regions. 839 elements and 2684 nodes were used. A unity load (1 N) was used according to the loading positions in the fatigue test rig for four point bending test. For the here studied standard stainless steel a Poisson ratio of 0.3 and a Young Modulus of 210 GPa was used. The initial crack was placed perpendicularly to the surface at the point where the crack initiation has been determined. The assumption is that the initial crack in lower toe, upper toe and weld bead are surface ripples which are considered as undercuts [18], with initial size of  $a_{\text{initial}} = 0.1 \text{ mm}$  (also an initial size of 0.5 mm was studied but hardly led to any difference). The initial LOF size (C) is assumed to be 3 mm in the multiple crack growth interactions (also 1 mm and 5 mm were studied, correspondingly changing the impact by due to different weld throat confinements). The Paris-law constants  $m = 3$ ,  $C_{\text{char}} = 9.5 \cdot 10^{-12} \text{ MPa}\sqrt{\text{m}}$ , and  $C_{\text{mean}} = 4.75 \text{ MPa}\sqrt{\text{m}}$  are recommended by IIW and are used in this study.  $C_{\text{mean}}$  is considered to be the mean fatigue crack growth rate coefficient and  $C_{\text{char}}$  is the characteristic value corresponding to 95% survival probability value. Threshold effects were considered by assuming  $K_{\text{th}} = 2 \text{ MPa}\sqrt{\text{m}}$ . During numerical simulations the crack increment size  $\Delta a$  was 0.5 mm up to the crack length  $a_f = 3.5 \text{ mm}$ . In a fatigue crack investigation based on a numerical method, the nodal displacement field is obtained for the nodes around the crack tip applied to calculate the stress intensity factor for Modes I and II ( $K_I$ ,  $K_{II}$ ) using a displacement correlation technique based on Eq. (7). Numerical analyses have shown that the  $K_I$  stress intensity factor is much higher if compared with  $K_{II}$  ( $K_{II}$  was less than 3% of  $K_I$  for all load cases and crack lengths). Therefore, the  $K_I$  stress intensity factor is considered here which can be calculated by using Eq. (9) for plane strain condition. Finally, the number of cycles for each crack propagation step is predicted by applying the obtained  $\Delta K$  and  $\Delta a$  to the Paris-model into Eq. (6). In addition to the incremental crack length and the corresponding number of cycles for each  $\Delta a$ , the crack growth direction is also calculated by applying the obtained  $\Delta K$  to

Eq. (11). Note that all of the mentioned calculations are followed in segments prior to each crack propagation step in order to predict the crack growth rate and direction.

## 6.2. Numerical results and discussion

For the particular case studied here, the initiation of cracking takes place at the top surface; its location is most likely in the lower weld toe due to the shortest distance to the root. The competition between the distance to the root, the toe radii and possible micro radii by surface ripples can shift the initiation to the weld bead or upper toe [24]. Therefore different crack initiation sites are considered here which are upper toe (A), lower toe (B), LOF (C) and weld bead (D). Figure 12 shows a calculated crack that has propagated, in good agreement with an experimentally obtained crack. The LOF opens but normally does not propagate. The stress fields of the initial and final crack propagation stage, from the lower and upper toe, with and without LOF, are shown in Fig. 13.

Stress peaks can be clearly seen at the two weld toes but also at the ends of the LOF, while the root experiences compressive stress. Note that stresses above 10 MPa were cut off for better visibility of the interactions. When the crack propagates it comes closer to the LOF for a while, particularly when originating from the upper toe (A). The interaction between the stress fields from the crack tip and from the LOF-ends can be clearly seen in Fig. 13(e), (f). In particular they increase the crack tip stress compared to no LOF, Fig. 13(b), (c) and thus accelerate the crack and reduce the fatigue life. The stress distribution from the crack tip (originating from the upper toe, A) to the root is plotted in Fig. 14, both for the initial and propagated stage, with and without LOF in between. Here the quantitative impact of the LOF (causing two peaks) and the change to (negative) compressive domains can be well seen. The change of the deflection angle during the crack propagation is shown in Fig. 15. While the crack starts to propagate normal to the surface, due to the stress gradients it bends early, heading towards the root, see also Fig. 12. In the exceptional case that LOF propagates as crack (C), it experiences stronger, less stable variations of the deflection angle.

The maximum stress at the crack tip during its propagation is shown in Fig. 16. The stress is clearly lower in the upper toe than in the weld bead and particularly in the lower toe, in good coincidence with the probability of crack initiation per location. LOF increases the stress further, which corresponds to reduced fatigue life, see Fig. 17 (derived via the Paris-law), however only of the order of 10%. It is worthwhile to note the significantly higher lifetime from upper toe cracking which can be an important design criterion (avoid small radii in the lower weld toe).

Four numerically simulated fatigue lives for the as welded conditions at selected nominal stress ranges are inserted in Fig. 4 for comparison with the (scattering) values derived from the fatigue testing experiments. The local weld geometry and crack growth data used were the average values and a 0.1 mm long initial line crack is assumed as a starting crack at the weld toe. The crack initiation period and threshold effects could have an influence on the fatigue life prediction at

cycles larger than  $10^6$  cycles. The experimentally obtained mean fatigue strength for all tested as-welded specimens is 141 MPa while the numerical value is 137 MPa, thus in good agreement.

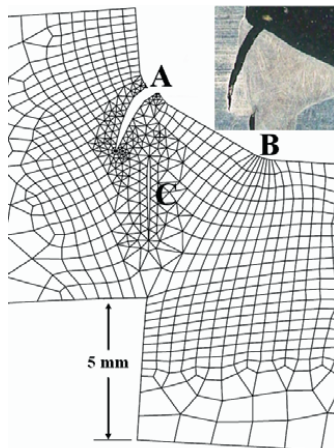


**Fig. 12:** Comparison of the calculated and experimental cross section of the crack (upper toe, LOF)

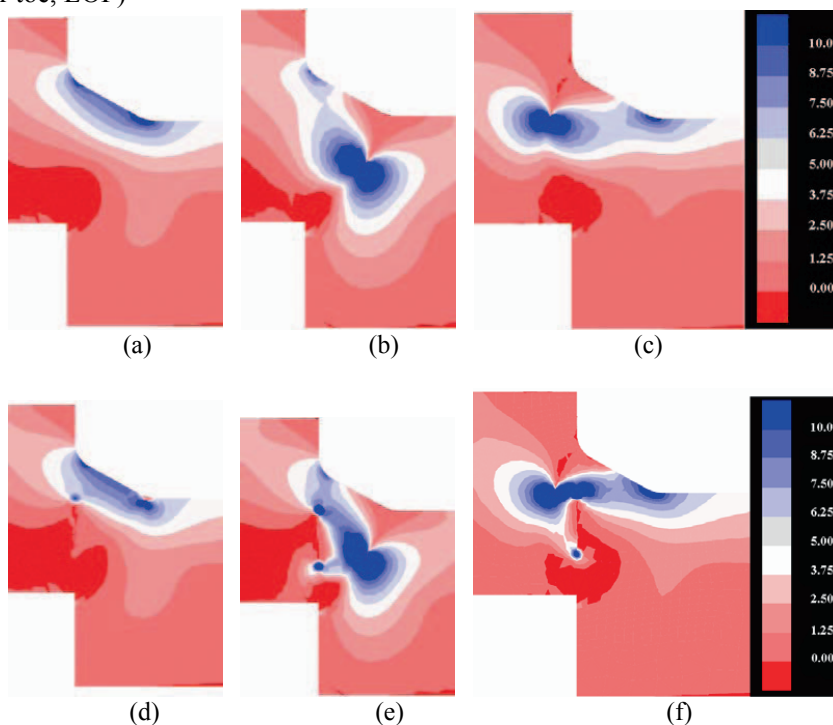


**Fig. 13:** Calculated normal stress field (in MPa) across the weld (toe radii 1 mm): (a) initially, no LOF, (b) after lower toe cracking, no LOF, (c) after upper toe cracking, no LOF, (d) initially, LOF, (e) after lower toe cracking, LOF, (f) after upper toe cracking, LOF

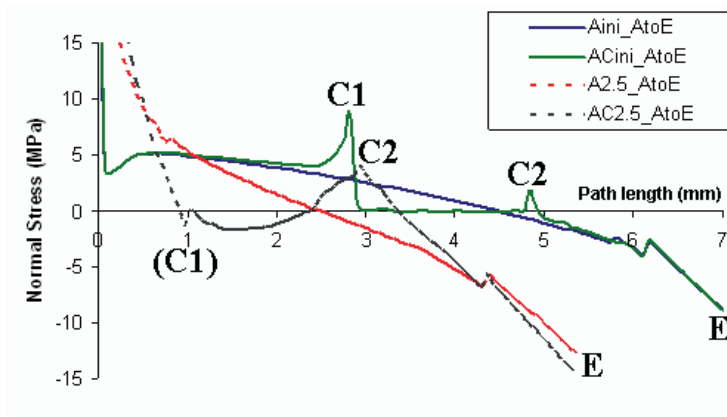


**Fig. 14:** Normal stress flow (in MPa) along the direct path from the crack tip (upper toe case, A) to the root (E), initially and after 2.5 mm crack propagation, with and without LOF (C)

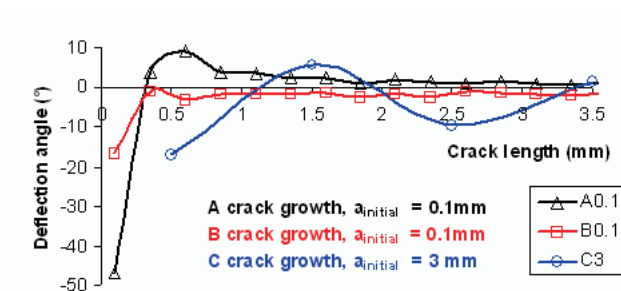


**Fig. 15:** Crack deflection angle during the crack growth for three initiations A, B and C

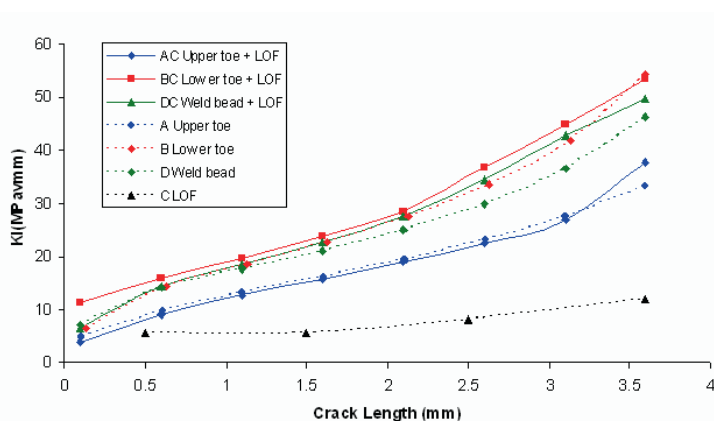


**Fig. 16:** Stress intensity factor at the key tips as a function of the crack propagation length for the different crack combination

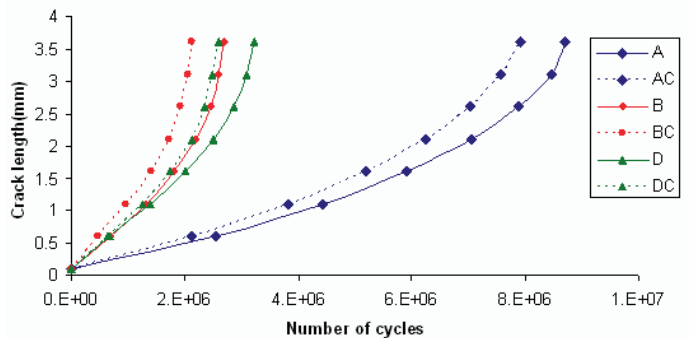


**Fig. 17:** Fatigue life comparison for different crack situations

## 7. Illustrative phenomenological description

In order to facilitate knowledge transfer we illustrate part of the above discussed phenomenological findings in Fig. 18. Figure 18(a) indicates the cross sectional heat flow conditions during welding. In laser hybrid welding the heat is generated at the weld pool surface by the MIG-arc and -wire and on the keyhole (vapor capillary) walls into the melt by the absorbed laser beam. The generated heat is continuously conducted across the geometry of the eccentric joint, leading to the typical nail-shaped cross-section. However, from metallographic we have seen that the oxide layers and possible gaps of the joint interface act as thermal barrier. While the upper part (arc) and the root region (crossing laser beam) provide enough energy to melt through this barrier, the central part bears the risk of remaining below the thermal threshold, i.e. Part I does locally not melt and LOF takes place. Measures to avoid LOF are particularly accurate positioning (difficult for an eccentric joint) of the laser beam and/or higher line energy (welding power/speed) than required (for welding through).

A phenomenological description of the above findings for fatigue crack propagation for eccentric hybrid welds is illustrated in Fig. 18(b) and schematically in Fig. 18(c). Cracking is initiated at the maximum stress concentration location, usually in the lower weld toe, propagating normal to the surface downwards, but then (following the stress gradients) gradually bending towards the root (that itself is uncritical, as under compressive stress here). The two edges of a possible LOF are mainly under compressive stress and rarely initiate cracks, but they interact with the propagating crack by enhancing its peak stress and accelerating it.

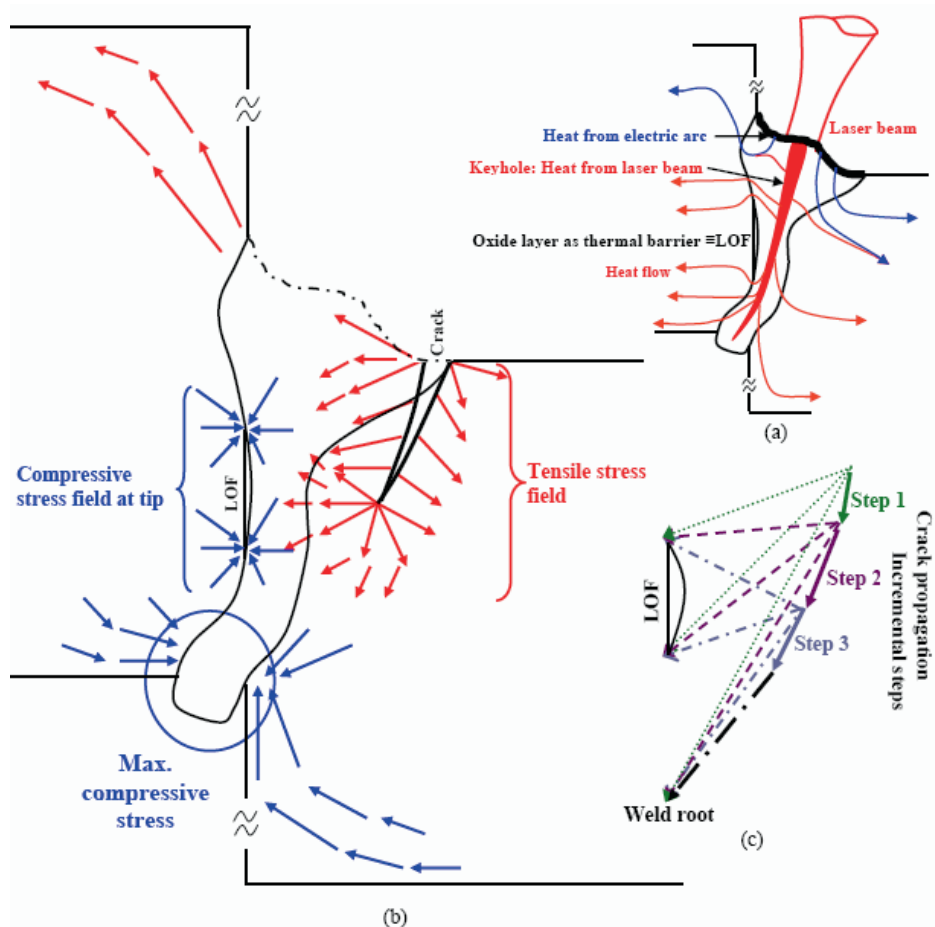


**Fig. 18:** Theoretical description of the competing mechanisms (a) during welding determining whether Lack of Fusion is caused, (b),(c) during fatigue load of an eccentric hybrid weld with lack of fusion, determining stress raising

## 8. Conclusions

We conclude:

- In good agreement between simulation (LEFM) and experiments, the crack first propagates normal to the local weld surface, preferably at the lower toe, but then gradually bends to the root
- Lack-of-Fusion (LOF) is likely to take place for this kind of weld; oxide layers and small gaps as the thermal barrier causing LOF can be overcome by very accurate laser beam positioning or by an excess of line energy
- LOF is not critical to initiate cracking, as mainly under compressive stress. When a crack propagates closer to LOF, the interaction increases the stress around the crack and accelerates it, slightly ( $< 10\%$ ) reducing the fatigue life for the here studied case



- The effective notch stress design curves for the batch were above the IIW recommendation. Higher slope ( $m=3.16$ ) of the S-N curves than the corresponding standard was obtained for hybrid laser welded eccentric fillet joints

## Acknowledgements

The authors are grateful to VINNOVA – The Swedish Innovation Agency (project HYBRIGHT, no. 2005-02895, project LOST, no. 2006-00563) for funding the research.

## References

- [1] A. Fatemi, L. Yang, Cumulative fatigue damage and life prediction theories: a survey of the state of the art for homogeneous materials, *Int. J. Fatigue* 20 (1998) 9-34.
- [2] X. Y. Li, H. G. Zhu, X. T. Tian, A study of fatigue crack growth and crack closure in mechanical heterogeneous welded joints, *Eng. Fract. Mech.* 55 (1996) 689-697.
- [3] C. Buirette, G. Deqallaix, J.Y. Dauphin, J. Menigault, Microstructural effects on short fatigue crack initiation and propagation in high strength steel butt welded joints, *Welding in the World* 41 (1998) 37-48.
- [4] B. Christopher, G. Gregory, P. John, Fatigue crack initiation and growth in A517 submerged arc welds under variable amplitude loading, *Int. J. Fatigue* 22 (2000) 799-808.
- [5] X.Y. Li, X.T. Tian, H.G. Zhu, Fatigue crack growth and crack closure of simulated over matched welded joints, *ACTA Metallurgica Sinica (English Letters)* 13 (2000) 117-122.
- [6] J.H. Kim, Y.J. Oh, I.S. Hwang, D.J. Kim, J.T. Kim, Fracture behavior of heat-affected zone in low alloy steels, *J. of Nuclear Mater.* 299 (2001) 132-139.
- [7] U. Brandt, F.V. Lawrence, C.M. Sonsino, Fatigue crack initiation and growth in AlMg4.5Mn butt weldments, *Fatigue & Frac. of Eng. Mat. & Struct.* 24 (2001) 117-126.
- [8] I.T. Kin, K. Yamada, S. Kainuma, Fatigue behavior of butt welded joints containing inclined lack of-penetration, *Struct. Eng./Earthquake Eng.* 18 (2001) 53-62.
- [9] M.M. Saiama, Fatigue crack growth behavior of titanium alloy Ti-6Al-4V and weldment, *J. Offshore Mechanics and Arctic Eng.* 123 (2001) 141-146.
- [10] H.Q. Zhang, Y.H. Zhang, L.H. Li, X.S. Ma, Influence of weld mismatching on fatigue crack growth behavior of electron beam welded joints, *Mater. Sci. & Eng.* 334 (2002) 141-146.
- [11] Y. Naiquan, M. Torgeir, Fatigue and static behavior of aluminium box-stiffener lap joints, *Int. J. Fatigue* 24 (2002) 581-589.
- [12] V. Caccese, P.A. Blomquist, K.A. Berube, S.R. Webber, N.J. Orozco, Effect of weld geometric profile on fatigue life of cruciform welds made by laser/GMAW processes, *Marine Structures* 19 (2006) 1-22.

- [13] C.H. Lee, K.H. Chang, G.C. Jang, C.Y. Lee, Effect of weld geometry on the fatigue life of non-load carrying fillet welded cruciform joints, *Eng. Fail. Anal.* 16 (2009) 849-855.
- [14] T.N. Nguyen, M.A. Wahab, A theoretical study of the effect of weld geometry parameters on fatigue crack propagation life, *Eng. Fract. Mechanics* 51 (1995) 1-8.
- [15] M. Wouters, J. Powell, A. Kaplan, The influence of joint gap on the strength of hybrid Nd:yttrium aluminum-garnet laser-metal inert gas welds, *J. of Laser App.* 18 (2006) 181-184.
- [16] G. Rihar, M. Uran, Lack of fusion-characterisation of indications, *Welding in the World* 50 (2006) 35-39.
- [17] P.J. Singh, D.R.G. Achar, B. Guha, H. Nordberg, Influence of weld geometry and process on fatigue crack growth characteristics of AISI 304L cruciform joints containing lack of penetration defects, *Science and Technology of Welding and Joining* 7 (2002) 302-312.
- [18] J.L. Otegui, H.W. Kerr, D.J. Burns, U.H. Mohaupt, Fatigue crack initiation from defects at weld toes in Steel, *Int. J. Press. V. Pip.* 38 (1989) 385-417.
- [19] P.C. Paris, Fracture mechanics and fatigue: a historical perspective. *Fatig. Fract. Eng. Mater. Struct.* 21 (1998) 535-540.
- [20] D.J. Allen, G. Degnan, An Investigation of Fusion Quality in Conventional MIG, Synergic Pulsed MIG, Flux-Cored arc and Manual Metal Arc Welding, in *Proceedings of the 2nd European Conference on Joining Technology, Eurojoin 2*, Florence, 1994.
- [21] N. Yamauchi, Y. Inaba, T. Taka, Formation Mechanisms of lack of fusion in MAG welding, *International Institute of Welding, IIW Doc.* 212-529-82, 1982.
- [22] J. Tusek, T. Blatnik, Ultrasonic detection of lack of fusion in spot welds, *Insight* 44 (2002) 684 - 688.
- [23] Y. Yao, M. Wouters, J. Powell, K. Nilsson, A. Kaplan, Influence of joint geometry and fit-up gaps on hybrid laser-metal active gas (MAG) welding, *J. of Laser App.* 18 (2006) 283-288.
- [24] M. M. Alam, Z. Barsoum, P. Jonsén, A. F. H. Kaplan, H. Å. Häggblad, The influence of surface geometry and topography on the fatigue cracking behaviour of laser hybrid welded eccentric fillet joints, *Applied Surface Science* (2009, in press).
- [25] A. Hobbacher, Fatigue design of welded joints and components, *IIW document XIII-2151-07 XV-1254-07*.
- [26] T. Gurney, Cumulative damage of welded joints, Woodhead publishing limited, 2006
- [27] D.Radaj, C.M.Sonsino, W. Fricke, Fatigue assessment of welded joints by local approaches, Woodhead publishing, second ed. Abington, Cambridge, 2006.
- [28] Y. Verreman, B. Nie, Short crack growth and coalescence along the toe of a manual fillet weld, *Fatigue Fract. Eng. Mat. Struct.* 14 (1991) 337-349.
- [29] T. Mori, M. Ichimiya, Fatigue crack initiation point in load carrying fillet-welded cruciform joints, *Welding International* 13 (1999) 786-794.
- [30] E. Peeker, E. Niemi, Fatigue crack propagation model based on a local strain approach, *J. of Con. Steel Research*, 49(1999) 139-155.

- [31] V. Balasubramanian, B. Guha, Analysing the influences of weld size on fatigue life predication of FCAW cruciform joints by strain energy concept. *Int. J. of Press. V. Pip.* 76 (1999) 759-768.
- [32] M.M.K. Lee, Strength, stress and fracture analysis of offshore tubular joints using finite elements, *J. of Con. Steel Research*, 51 (1999) 265-286.
- [33] T. Nykänen, V. Lihavainen, Geometric dependency of fatigue strength in a transverse load carrying cruciform joint with partially penetrating V-welds, *IIW Doc. XIII-1838- 00*, 2000.
- [34] R. Bell, O. Vosikovsky, D.J. Burns, U.H. Mohaupt, A fracture mechanics model for life prediction of welded plate joints, *Proc. 3rd Int. ESCS Offshore conf. On Steel in Marine Structures (SIMS'87)*, Delft, The Netherlands, ed. C. Noordhoek and J. De Back (1987) 901-910.
- [35] T.J. Smith, S.J. Hurworth, The effect of geometry changes upon the predicted fatigue strength of welded joints, *Report of The Welding Institute*, No. 224, UK, 1984.
- [36] X.Y. Li, T. Partanen, T. Nykänen, T. Björk, Finite element analysis of the effect of weld geometry and load condition on fatigue strength of lap joint, *Int. J. for Pressure V. Pip.* 78 (2001) 591-597.
- [37] X.Y. Li, T. Partanen, T. Nykänen, T. Björk, Evaluation of fatigue strength of angle joint with fully penetration, *Proceedings of the 7th International Symposium of Japan Welding Society in the Theme "Today and Tomorrow in Science and Technology of welding and Joining"*, Kobe, Japan, 2(2001) 1225-1230.
- [38] X.Y. Li, T. Nykänen, T. Björk, G. Marquis, Fracture Mechanics Analysis of Partial Penetrated Butt Welds, *Design and Analysis of Welded High Strength Steel Structures*, Editor J. Samuelsson, Fatigue 2002, Held in Stockholm, Sweden (2002) 139- 149.
- [39] H. Alizadeh, S. Simandjuntak, D. Smith, M. Pavier, Prediction of fatigue crack growth rates using crack closure finite element analysis, *Int. J. Fatig.* 29 (2007) 1711–1715
- [40] X. Zhang, A.S.L. Chan, G.A.O. Davies, Numerical simulation of fatigue crack growth under complex loading sequences. *Eng. Fract. Mech.* 42 (1992) 305–321.
- [41] S. Simandjuntak, H. Alizadeh, D.J. Smith, M.J. Pavier, Three dimensional finite element prediction of crack closure and fatigue crack growth rate for a corner crack. *Int. J. Fatig.* 28 (2006) 335–345
- [42] L. Llopart, B. Kurz, C. Wellhausen, M. Anglada, K. Drechsler, K. Wolf, Investigation of fatigue crack growth and crack turning on integral stiffened structures under mode I loading. *Eng. Fract. Mech.* 73 (2006) 2139–2152
- [43] Alegre, J.M., Gutierrez-Solana, F., Aragon, A.: A finite element simulation methodology of the fatigue behavior of punched and drilled plate components. *Eng. Fail. Anal.* 11 (2004) 737 - 750.
- [44] Shih CF, de Lorenzi HG, German MD. Crack extension modeling with singular quadratic isoparametric elements. *Int J Fract.* 12 (1976) 647–651.

- [45] B.D. Fehl, K. Z. Truman, An evaluation of fracture mechanics quarter-point displacement techniques used for computing stress intensity factors, *Eng. Strut.* 21 (1999) 406-415.
- [46] I.S. Raju, Calculation of strain-energy release rates with higher order and singular finite elements. *Eng. Fract. Mech.* 28 (1987) 251-274.
- [47] E.F. Rybicki, M.F. Kanninen, A finite element calculation of stress-intensity factors by a modified crack closure integral, *Eng. Fract. Mech.* 9 (1977) 931-938.
- [48] G.P. Nikishkov, S.N. Atluri, Calculation of fracture mechanics parameters for an arbitrary three-dimensional crack by the equivalent domain integral method. *Int. J. Numer. Meth. Eng.* 24 (1987) 1801-1821.
- [49] Anderson, T.L.: *Fracture Mechanics, Fundamentals and Applications*, 2nd ed, p. 704. CRC Press, Boca Raton (1994)
- [50] FRANC2D. Version 3.2 <http://www.cfg.cornell.edu>
- [51] M. A. Abdalnaser, A. A. Kamal, Finite element simulation of stress intensity factors in elastic-plastic crack growth, *Journal of Zhejiang University SCIENCE A* 7 (2006) 1336 – 1342.
- [52] F. Erdogan, G.C. Sih, On the crack extension in plates under plane loading and transverse shear, *ASME Journal of Basic Engineering* 85 (1963) 519-527.
- [53] M.A. Hussain, S.U. Pu, J. Underwood, Strain energy release rate for a crack under combined mode I and II. *ASTM STP.* 560 (1974) 2-28.
- [54] G.C. Sih, Strain-energy-density factor applied to mixed mode crack problems, *Int. J. Fract. Mech.* 10(1974) 305-321.
- [55] T.N. Bittencourt, P.A. Wawrzynek, A.R. Ingraffea, J.L. Sousa, Quasi-automatic simulation of crack propagation for 2D LEFM problems, *Eng. Fract. Mech.* 55 (1996) 321-334.
- [56] A. Ural, G. Heber, P.A. Wawrzynek, A.R. Ingraffea, D.G. Lewicki, J.B.C. Neto, Three dimensional parallel finite element simulation of fatigue crack growth in a spiral bevel pinion gear. *Eng. Fract. Mech.* 72 (2005) 1148-1170.
- [57] C.A. Rogers, G.J. Hancock, Fracture toughness of G550 sheet steels subjected to tension, *J. Constr. Steel Res.* 57 (2001) 71-89.
- [58] M. Fulland, M. Sander, G. Kullmer, H.A. Richard, Analysis of fatigue crack propagation in the frame of a hydraulic press, *Eng. Fract. Mech.* 75 (2008) 892-900.
- [59] ANSYS guide, ANSYS release 11. Houston: Swanson Analysis Systems.

## **Paper IV**

### **GENERALISED FATIGUE STRESS ANALYSIS OF DIFFERENT LASER WELD GEOMETRIES**

M. M. Alam, J. Karlsson, A. F. H. Kaplan

Mechanics of Materials, 2009 (submitted)



## **Generalising fatigue stress analysis of different laser weld geometries**

**Authors: M. M. Alam<sup>\*</sup>, J. Karlsson, A. F. H. Kaplan**

### **Affiliation:**

Luleå University of Technology, Dept. of Applied Physics and Mechanical Engineering,  
SE-971 87 Luleå, Sweden  
Email: minhaj.alam@ltu.se, jan.karlsson@ltu.se, alexander.kaplan@ltu.se

\*Corresponding author: minhaj.alam@ltu.se  
Phone: +46(0)920 493917  
Fax: +46(0)920 49 22 28

### **Abstract**

Two dimensional elastic-plastic finite element analyses is carried out on laser welded box beam in order to study the impact of geometrical aspect of weld toe and root on the fatigue performance. Different weld geometry was studied by changing the position of laser beam inclination angle, the beam position and the focal plane position. Metallurgical analysis was carried out to observe the weld defect and the plastic replica method was used in order to measure the toe and root geometry. Critical geometrical aspects were classified and then studied by FE-analysis with respect to their impact on the fatigue behaviour. Stress comparison of full 15 mm and partial 6 mm weld penetration of the beam was done by varying the toe and root geometry to identify the critical details. Generalization of the knowledge by new methods; bifurcation flow chart (BFC) was an important aspect, particularly to apply the findings for other joints.

Keywords: stress analysis, laser welding, finite element analysis, root shape, joint type

### **1. Introduction**

Welding often has a strong impact on the product value, but the quality of a weld for avoiding failure is a complex issue that requires improved understanding. The weld quality is directly influenced by the process parameters; therefore, welding can be considered as a multi-input multi-output process. A common problem faced is the control of the process input parameters to obtain an acceptable welded joint with the required weld geometry and weld quality and with minimal detrimental residual stresses and distortion. It can be divided into research of the influence of the parameters on the process and on the resulting weld quality and into research on the weld under mechanical load from which the quality standard can be derived and specified. This paper focuses on the latter, but also links to the former. While research is commonly conducted case-specific, it is often difficult to interpret and use the

results for other applications, both quantitatively and qualitatively. Although the here presented study is also case-based, it tries to develop methods and approaches for generalising the findings and the explanations behind.

During laser welding, applied here, the beam is focused onto the substrate material where its high power density enables to drill a vapour capillary where the beam energy is absorbed over depth, thus typically creating a deep, narrow weld [1]. Laser welding has progressively attracted the attention of engineers during last decades for its many advantages over more traditional technologies, but suffers from difficulties in controlling the process quality, as it is a complex and not fully understood process, including also the quality standard specifications [2-3]. The laser welded joint geometry is mainly dependent on the parameters welding speed, laser power, focal plane position shielding gas type/flow and the joint gap [4]. Variation of the main process parameters (power, speed) has a strong effect on the bead profiles (width, penetration depth, melted area) [5-6]. The relationships among the focal point position, laser power, welding speed and the responses of tensile strength, impact strength and joint operating cost were also established [7]. A comparative study was carried out on the influence of different shielding gas systems on the laser welding process of aluminium alloys [8]. A systematic study on variation of the root geometry by the effect of laser beam angle, focal point position and focal depth was carried out by Karlsson et al, which is a base for the present study [9].

The particular technique of hybrid laser-arc welding, simultaneously operated, combines the advantages of laser and arc welding, producing deep penetration welds comparable with laser welds, yet at the same time due to the robust wire addition having an improved tolerance to joint fit-up when compared with laser welding [10]. From a fundamental analysis of hybrid welds it was shown that sharp root edges lower the impact strength, thus a gap with a rounded root is even favourable to a zero-gap situation [11]. Other works about the effects of the interaction of welding speed and wire feed rate on penetration are examined in [12-13].

Fatigue life is a combination of crack initiation and propagation stages [14] (followed by the fast failure stage). It usually depends on the weld geometry, e.g. toe radii, root radii, weld angle and defects e.g. lack of penetration, cold laps, etc. [15-18]. Finite Element Analysis (FEA) for predicting the fatigue life was e.g. done by Nykanen et al [19] who investigated the effect of weld size and joint dimension ratio on fatigue strength by 2D linear elastic fracture mechanics analysis. Remes [20] carried out elastic-plastic FE simulation to predict fatigue crack initiation on different weld joint geometries. A series of crack initiation and propagation analysis is carried out by measuring the weld geometry and assuming initial weld defects with the help of FE stress analysis in [21-25].

Laser welding and hybrid laser welding both create improved weld geometries either on the top or root, increasing the mechanical strength compared to tradition arc welding [26-28]. A comprehensive literature survey on stress analysis for laser and hybrid laser welded can be found in [29]. The geometrical aspects for stress raisers



obtained by hybrid laser welding [30-31] have shown that the mechanical strength increases when avoiding surface ripples, confirming the IIW-recommendations [32] and being a base for the present study.

The aim of the present study is to provide improved stress analysis methods in form of guidelines, accompanying the FEA, in order to facilitate joint design and to judge weld geometry details. In particular, the systematic documentation and generalisation of findings such as the transition from one geometrical category to another was studied. Various shape cases were therefore investigated by applying several methods. The locations and values of maximum stress are studied as the key property for judging certain geometries with respect to their fatigue cracking behaviour.

## **2 Methodology**

### **2.1 Methodological approach**

For a high strength steel beamer four similar joint types A, B, C, D with the same load situation, see Fig. 1, were studied and compared, also to an additional different joint geometry E published earlier [28].

The beamer that can have a length of several meters consists of four identical laser welds at the four corners. The different joints offer different advantages. The full penetration for Joint A provides a compact geometry, but is over dimensioned. Joint B provides a suitable throat depth but still a notch-free root, and in a modified version C with filler wire also the top geometry can be shaped, also enhancing the throat depth. Joint D maintains an outer rectangular shape, but a welding depth same as the side plate thickness leads to a notch-character root. In service the beamer experiences a complex load that is in the present study described by a simplified force at the upper left corner, reducing the problem to the cross section where two corners experience widening of the 90°-angle, the other two an angle compression, which gives much insight into the basic load behaviour.

Joint E bears geometrical similarities in dimension, shape and load, although resulting from laser hybrid welding of stainless steel and to be compared upside down. The manifold complementary findings from this study [28] are very useful for adding understanding to the present study that particularly tries to transfer knowledge between different publications.

From the weld surface geometries resulting from experiments for joint type A, five representative root geometries of different categories were selected. In addition, several hypothetical root dimensions describing the transition from one category to the other were defined. For Joints B, C, D, that were not welded yet, roots are assumed. Joint B and C uses the same roots as A, while for the different type D a sharp root is compared with a rounded shape. The top of Case E is compared to the roots A-D, as its load is inverted, for comparing the essential tensile stress location. Linear FE-analysis

of the stress field for those geometries under bending load (arranged such that the root is critical, not the top) was carried out. The resulting stress field was analysed, in particular the peak stress values and their locations were compared.

Basic criteria governing the maximum stress were then formulated. The method of illustrating the geometrical stress behaviour and a new flow chart method were applied for qualitative comparison of the different situation, for stating weld design guidelines and for generalising the results, but also for interpreting the quantitative comparison between the different cases.

Eventually, the derived guidelines and results on the weld shape were combined with a recently developed flow chart and guideline on the welding process, thus enabling a holistic analysis on which weld shape to aim at and how to correspondingly choose the welding parameters. Maximum stress is here directly correlated to the location of fatigue crack initiation and to fatigue life, therefore the strategy is to enhance fatigue life by lowering the peak stress.

Beside the findings for the here studied application, an important result of the research is to provide new methods for improved and transferable stress analysis and weld design.

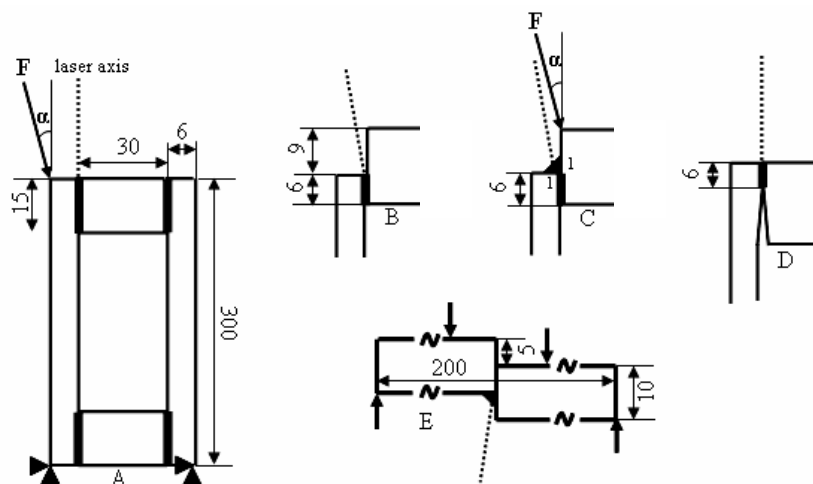


**Fig. 1:** Cross section with force  $F$  and the laser beam arrangement of four joint types A, B, C, D of the structural beamer studied and of a comparable Joint E published earlier

## 2.2 Welding set-up

The beamer (Joints A, B, C, D) consists of high strength steel Domex 700 (6 mm side plates) and Weldox 960 (15 mm horizontal plates). An Ytterbium Fiber Laser (YLR 15000, IPG Laser AG) with a maximum power of 15 kW (wavelength 1070 nm) and a beam parameters product of 10.4 mm·mrad, delivered through a 200  $\mu$ m fiber core,

was used for the experiments. For the hybrid laser welded joint E, where the laser was combined with a MIG-welding source (ESAB ARISTO), structural stainless steel SS1433 was used. The edges are laser cut (or milled for Joint E), providing zero gap. The filler wire had a diameter of 1.2 mm. During the hybrid laser welding process the laser beam was travelling 2 mm in front of the MIG torch. The chemical composition and mechanical properties for the materials applied are summarized in Tables 1 and 2. A deeper study of the material behaviour, particularly the hardness transition is prepared for publication in a parallel manuscript for Joint A, for Joint E see 1[16]. The parameters concerning the experimental welding set up are shown in Table 3 (Joint B,C,D: planned parameters).

**Table 1:** Chemical composition [%] of the materials used for the sheets and for the filler wire

Joint / Material	C	Si	Mn	Cr	Ni	P	S	N	Al
A-D: Domex 700(6mm thick)	0.12	0.10	2.10	-	-	0.025	0.010	-0.015	
A-D: Weldom 960(15mm thick)	0.20	0.50	1.60	0.70	1.5	0.02	0.010	0.0	0.018
E: S142333 (sheets, 10 mm)	0.05	1.0	2.0	19.0	11.0	0.045	0.030	-	-
E: Avesta 253MA (filler wire)	0.07	1.6	0.6	21.0	10.0	-	-	0.15	-

**Table 2:** Mechanical properties of the materials used

Joint / Material	$R_{p0.2}$ (N/mm <sup>2</sup> )	$R_m$ (N/mm <sup>2</sup> )	$A_5$ (%)	Hardness (HB)
	min	min	max	
A-D: Domex 700 (6mm)	700	750	12	270
A-D: Weldom 960 (15mm)	960	980	12	320
E: SS142333 (sheets)	210	490 – 690	45	200
E: Avesta 253MA (wire)	440	680	38	210

**Table 3:** Laser and hybrid laser welding parameters

Parameter	Laser welding		Hybrid laser
	Joint A	Joint B,C,D	Joint E
Laser beam power	15 kW	5 kW	3.25 kW
Welding speed	2.5 m/min	5 m/min	1.05 m/min
Laser beam angle, $\alpha$	10 °	10 °	10 °
Shielding gas type	Ar	Ar	Ar
Shielding gas flow	20 l/min	20 l/min	20 l/min
Focal length	500 mm	500 mm	300 mm
Rayleigh length	± 8 mm	± 8 mm	± 4 mm
MIG current (constant) -	-	-	328 A
MIG voltage (resulting) -	-	-	27 V
MIG pulse time -	-	-	2.4 ms
MIG pulse frequency -	-	-	90 Hz
Wire stick out length	-	-	16 mm
Wire feed rate -	-	-	4.2 m/min

### 2.3 Numerical stress analysis

In order to calculate the stress fields in the weld root, stress analysis was carried out with the FEM using the ANSYS 11 software. An elastic-plastic 2D-model was applied, with the assumption of triangle plane strain and 30 000 elements of 6-nodes quadrilateral type were used, with mesh refinement around the root regions for joint types A-D. Since these joint types are laser welded, homogeneous material properties are assumed. The element size near the root region was 0.03 mm and 1 mm in the base metal. A unit load of 1 kN was applied for joint types A-D which was 10° tilted from the horizontal plate, see Fig. 1. The quantitative real load situation was not essential here, as the load situation studied is a simplified approach, representative for opening of the corner, which happens in practice. The aim was to judge for this opening tendency (and closing at the opposite corner) different geometries. In the FE model the materials were considered isotropic with Young's modulus  $E = 210$  GPa and a Poisson ratio of 0.3. The weld material was assumed to have the same elastic properties as the base metal.

### 2.4 The illustrative analysis method

A key task of the present study is to describe the obtained findings by methods that are highly suitable for transfer to other applications. Beside the flow chart method, described in the next section, illustration of the essential criteria and phenomena will be carried out. Stress formation of welded products is a highly geometry-dependent mechanism and the geometrical contributions quickly become complex (like also e.g. fluid flows), even for a very local study, as of the weld root here. Therefore an illustrative description of the conditions is essential, particularly the trends if a certain dimension changes, as successfully done in earlier publications [28]. Although the different geometrical contributions have a combined impact that can hardly be isolated (despite the detailed stress fields computed by FEA), it is tried to identify and illustrate the different key contributions. The judgment of specific geometry contributions became clearer by carrying out sensitivity studies of certain dimensions (e.g. the throat depth or the surface curvature).

### 2.5 Flow charts as standardised documentation methods

The authors recently started developing a method [33] for more systematic and standardised documentation of findings, called the Bifurcation Flow Chart, BFC. The BFC-method was originally developed for the welding process, i.e. the dependency of the resulting weld quality on the process parameters and process physics. The basic structure of the BFC, see Fig. 2(a) for the welding process, starts with the parameters, followed by the process mechanisms, with a criterion in between that determines the bifurcation whether perturbed (or changed) parameters  $A'$  lead to a (defined, e.g. standards) welding defect compared to the branch of good weld quality for parameters  $A$ . The method turned out to be powerful already for several applications [33]. In particular, the BFCs from the findings of up to six different cases with the same defect risk were combined, thus generalising the findings and facilitating analysis.

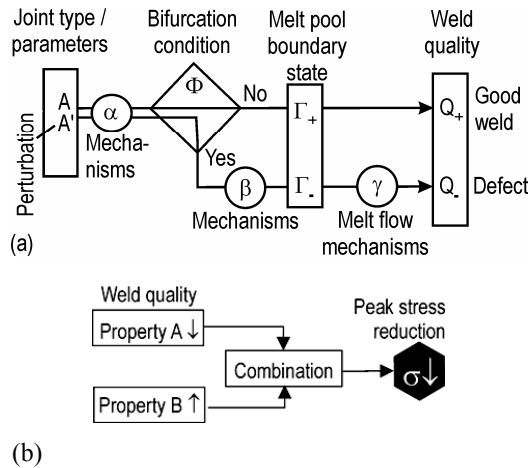


**Fig. 2:** Basic structure of (a) the Bifurcation Flow Chart, (b) the Tuning Flow Chart

Due to its general nature (Input-Process-Good vs. Bad Output), the BFC-method is applicable to systems of many kinds. For documenting the experimental findings from Joint A, beside the BFC a Matrix Flow Chart, MFC, was developed, to be shown in the next section, as it could well describe the trend for the weld result for manifold parameter variations, thus having different advantages. While these methods have been used for the welding process, in the present study we for the first time apply them to develop a flow chart for stress analysis (i.e. the output from the process is instead the input here). However, the goal of such study has a different nature. For the welding process a bifurcation describes the digital response whether a certain defined quality defect occurs or not. For stress analysis the goal is to reduce the maximum stress as much as possible by suitable weld (and material) shaping. Therefore we here needed to develop a different flow chart, the Tuning Flow Chart, TFC, that instead illustrates and formulates the measures that lower the peak stress by tuning certain properties. Its basic structure is shown in Fig. 2(b). The change of a certain property A, e.g. the lowering of surface roughness, was found to lower the peak stress, perhaps in combination (of additional or multiplicative nature) with other property trends. Again, although here developed for stress reduction, this method is suitable for many systems. Critical for the accomplishment of these flow charts is its appropriate formulation and the reduction to the essential phenomena.

Eventually, the developed TFC, that explains which weld shape properties to aim at for lowering the stress, will be used in combination with the MFC that in turn derives (for the desired weld properties) which process parameters need to be chosen. Such chart combination is here carried out for the first time.

### 3 Results and discussion

#### 3.1 Experimental welding results

Typical weld cross sections obtained are shown in Fig. 3(a) for Joint B and in Fig. 3(b) for Joint E, the latter after fatigue testing, thus with a propagated crack. A systematic survey on a series of experimental weld cross section (Joint A) for variation of different parameters (speed  $v$ , beam angle  $\theta$ , lateral beam positioning  $y$ , focal plane position  $z_0$ ) is shown in Fig. 4. As can be seen, the weld geometry, in particular the top and root shape varies significantly. For the here studied load situation (angular momentum opening the joint corner) the weld top is expected to be under compressive stress and thus not critical to initiate fatigue cracking, in contrast to the root. Therefore five characteristic root shapes were selected for detailed study, numbered  $i-v$  in Fig. 4. A publication on a comprehensive study of all shown weld cross sections and corresponding classification of the shapes (accompanied by high speed images of the weld pool and by hardness evaluation) is under parallel development.

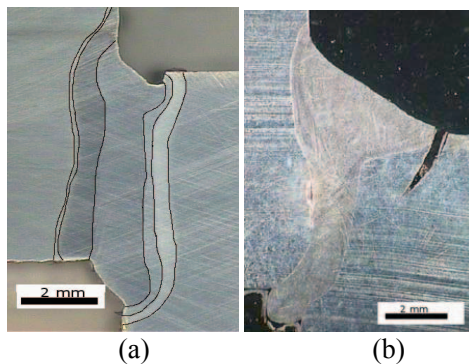


**Fig.3:** Typical laser weld cross section for (a) Joint A (after laser welding) and (b) Joint D (upside down, after laser hybrid welding and fatigue testing)

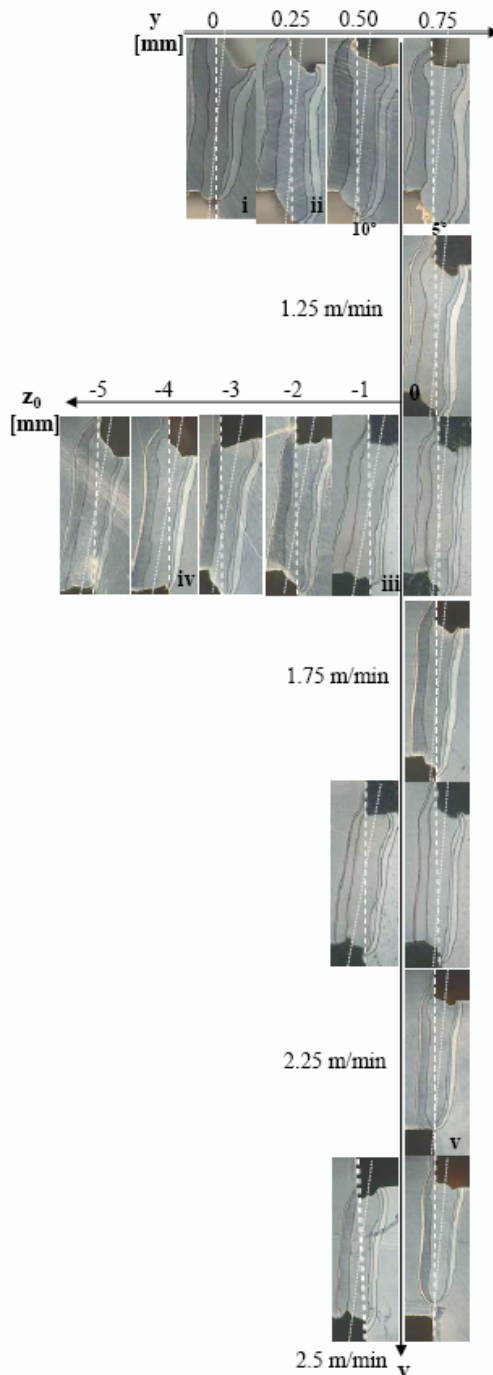


**Fig.4:** Laser weld cross sections as a function of parameters for joint type A; the five selected roots are assigned *i...v*

The dependency of the root categories on the welding parameters is formulated by an MFC in Fig. 5. The connected lines correspond to optimisation guidelines according to the below presented findings when comparing the root categories, as will be discussed later. Important is the graphical formulation of the findings in a manner suitable for later extension. The Cases B-D were not welded yet, as the present study aims at supporting the expectations, planning and preparation. The experimental results for Case E are published and described in detail in [28]-[31].

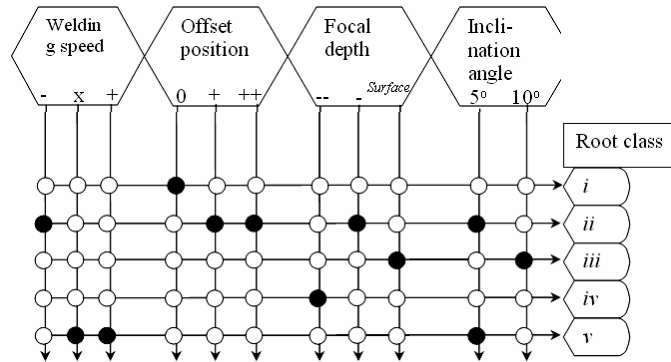


**Fig. 5:** MFC for the welding process of joint A, i.e. the parameters leading to root classes *i-v*

### 3.2 Stress simulation results

#### 3.2.1 Basic FEA results

Figure 6 shows the FE-simulated stress field for the complete beamer cross section, here for Joint C, root type *i* (Fig. 6(a): von Mises stress, only positive values, Fig. 6(b)-(d): 1<sup>st</sup> principal stress). The top dislocation (about 4 mm) by deformation can be seen, too. Most of the beamer cross section remains at low stress. The upper left and right corner roots are magnified in Fig. 6(c), (d). While the upper right and lower left corner experience compressive stress, in most cases of low magnitude, significant tensile stress raising takes place at the upper left and lower right corner roots. Due to the comparatively thick horizontal plates and their stiffness the outside corners hardly show increased stress for the present load conditions. Due to these trends, in the following only the roots of the upper left corner as the most critical location for initiating fatigue cracking will be studied in detail (well representing the lower right corner, too).



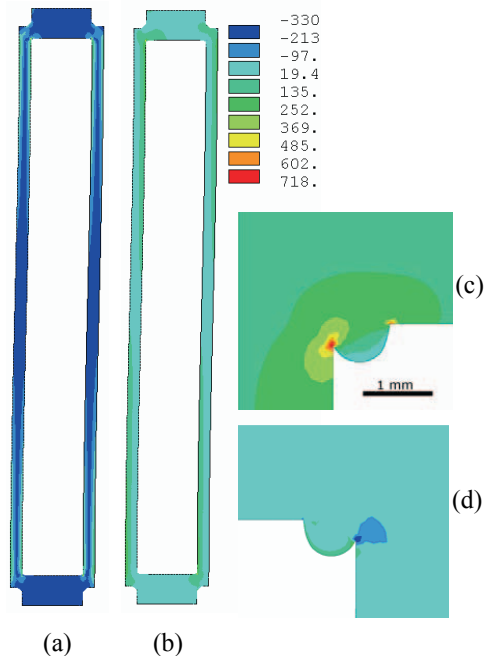


**Fig. 6:** Calculated stress field across the beamer (Joint C, root *i*): (a) von Mises stress, (b) 1<sup>st</sup> principal stress; magnification (1<sup>st</sup> principal stress, in MPa) of (c) the left upper root and (d) the right upper root

### 3.2.2 FEA results for the different cases

The stress field was computed by FEA for the five selected experimental roots for the three joint types A, B and C (similar to B), for two roots for the joint type D, see the root stress fields in Fig. 7(a)-(c), and for different radii and roughness for the joint type E [28], e.g. Fig. 7(d) (left: smooth weld top surface, right: rough lower toe surface), moreover for several hypothetical roots describing transitions between the different root types.

Although a stress peak in the corners can be anticipated, the detailed analysis is in some cases non-trivial, particularly the comparison between the cases. From detailed quantitative analyses of the computed stress fields it was partially possible to identify and separate the responsible dimensions and mechanisms. It should be emphasized that the location of maximum stress is a combination of the shortest anchors and the smallest curvatures. In particular, slight offsets from the original joint corner (being root case v) modify the anchor length, which can have a significant impact in either direction.

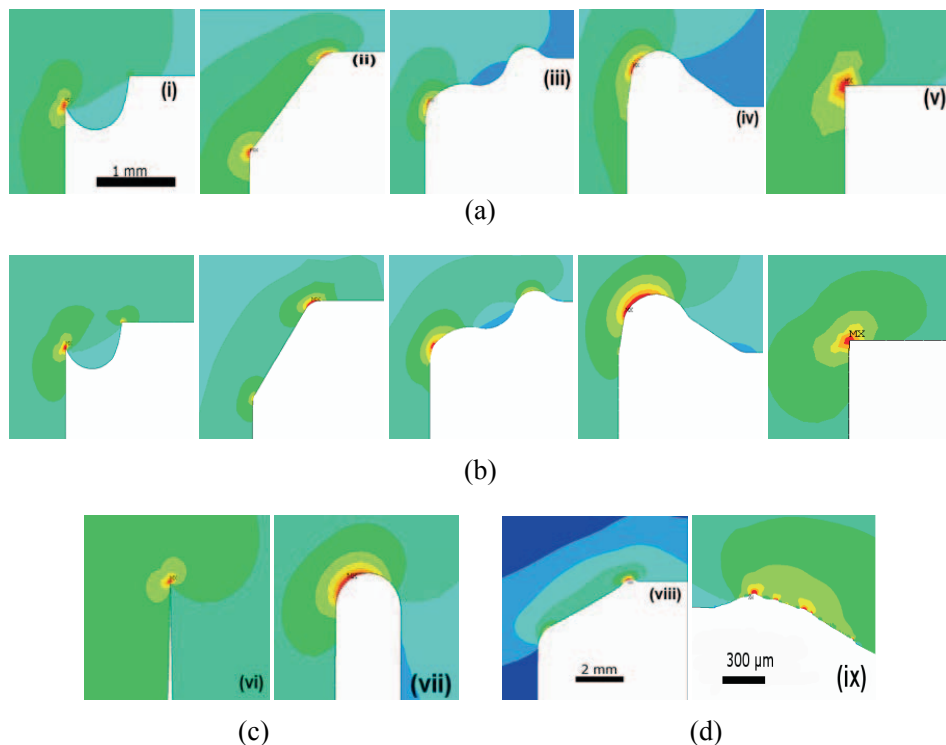


**Fig.7:** Calculated stress field at the upper left corner root: (a) Case A, roots *i-v*, (b) Case B, roots *i-v*, (c) Case D, roots *vi,vii*, (d) Case E, top *viii,ix*

The root types *i,ii,iii* have two geometrical peak points and it is not always obvious which causes the higher stress. Figure 8(a) shows the stress distribution along the horizontal and vertical anchor paths for root *iii* for Joints A and B. Far from the peak location there is no indicator on which of the two joints leads to the higher stress, i.e. the lower impact from the 15 mm anchor is not obvious. Only about 1-2 mm close to the peak Joint B increases stronger. The stress across the five weld root surfaces is plotted in Fig. 8(b) for Joint A and in Fig. 8(c) for Joint B. As can be seen, sharp corners lead to sharp stress changes while rounded shapes have a smoother, but not necessarily lower stress distribution.

Several phenomena should be highlighted. For Root *iii* the maximum stress is located at the left lower corner for Joint A but at the right upper corner for Joint B, as can be explained by the short secondary anchor for the latter (for the here applied dimensions, not in general). The importance of the opening angle has to be considered, being of significance for Roots *i* and *iv*. Thus not only confinement (anchor length) but also local expansion can increase the stress values, as the material flow requires stress to be redirected. From Case E, studied extensively earlier, [28] important findings are that beside the toe radius and angle also the surface roughness (its local curvatures) contributes significantly while Lack of Fusion as a severely appearing defect hardly (10% lowered fatigue life) had an impact when experiencing compressed conditions.

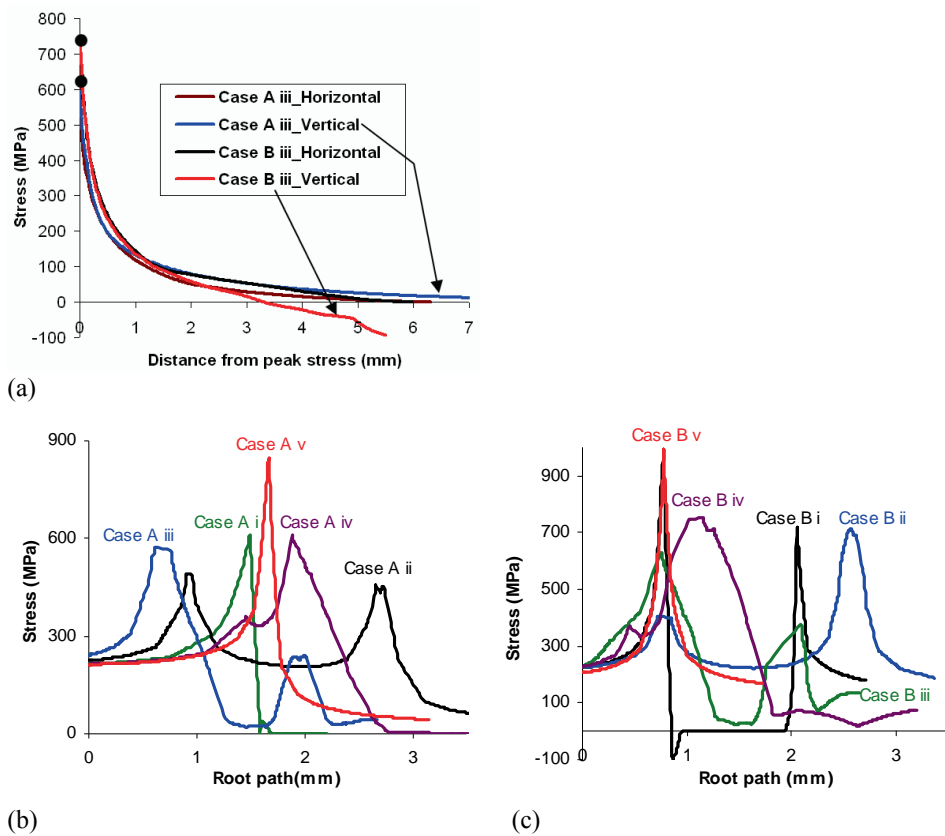


**Fig. 8:** Stress distribution: (a) along the horizontal and vertical anchors for different cases; across the root shape (starting from the left sheet below the root) for the five roots for (b) Joint A and (c) Joint B

From the simulations several determining criteria  $K$  can be derived that can be applied as qualitative and quantitative guidelines for judging joint geometries and root shapes, either in a separated or combined manner. The shortest throat thickness or the primary anchor length  $S_1$  can be combined with the secondary anchor length  $S_2$  as follows:

$$K_s = \frac{1}{S_1} + \frac{1}{S_2} \quad (1)$$

The radius describing the curvature of the root surface (here: only cross section-plane) at a certain location results from the following equation

$$R(\xi) = - \left[ 1 + \left( \frac{\partial \zeta}{\partial \xi} \right)^2 \right]^{3/2} \left( \frac{\partial \zeta}{\partial \xi} \right)^{-1} \quad (2)$$

where  $\xi$  is the coordinate along the (cross section) root path while  $\zeta$  is the coordinate normal to the surface and  $R$  is the resulting radius describing the curvature. The

minimum radius is the key criterion applied for the equations, except where a shorter anchor length  $S$  takes over. Beside the global curvature, for significant surface roughness profiles the same equation can be applied, resulting in a local value  $r$ , competing with  $R$ , as can be formulated as follows:

$$K_R = \frac{1}{R} + \frac{1}{r} \quad (3)$$

The opening angle  $\beta$ , identified as an important contribution, too, is here defined by the locations where the curvature changes sign or transfers to a straight line.

$$K_\beta = \frac{1}{\beta} \quad (4)$$

A combination of the above stress raisers is:

$$K_{tot} = K_{s\beta} K_S K_R = \frac{1}{\beta} \left( \frac{1}{S_1} + \frac{1}{S_2} \right) \left( \frac{1}{R} + \frac{1}{r} \right) \quad (5)$$

The above formulations basically describe the trends experienced from the FE-simulations, both in a qualitative and to some extent in a quantitative manner, although of course not precisely, only indicative. Further modelling could introduce a weighting potency for each contribution, e.g. a potency  $p$  for the curvature:

$$K_{Rp} = R^{-p} \quad (6)$$

For Joint A, the dimensions of the roots studied, including beside the experimental shapes also the hypothetical shapes for describing their transitions, are listed in Tab. 4 along with the above derived stress raising factors.

Tab. 4: Maximum stress computed, main dimensions and derived stress raiser indicators (normalized to root  $i$ ) for Joint A for the five experimental root types  $i-v$  and for hypothetical transition root shapes with similar dimensions

Root	$\sigma_{\max}$ MPa	$S_1$ mm	$S_2$ mm	$R$ mm	$\beta$ °	$K_S$ 1	$K_R$ 1	$K_\beta$ 1	$K_{tot}$ 1	$\sigma_{\max}$ 1	$K_{R0.3}$ 1
$i$	819	5.83	15.3	0.05	30	1.000	1.000	1.000	1.000	1.000	
$ii$	492	5.83	16.6	0.25	150	0.978	0.200	0.200	0.039	0.601	
$iii$	573	5.87	15.4	0.45	90	0.993	0.111	0.333	0.037	0.700	
$iv$	579	5.93	14.5	0.44	45	1.002	0.114	0.667	0.076	0.707	
$v$	840	5.83	15.0	0.05	90	1.006	1.000	0.333	0.335	1.026	
$ii$	525	5.87	15.5	0.33	91	0.992	0.152	0.330	0.050	0.641	
$ii$	510	5.86	15.5	0.33	104	0.993	0.152	0.288	0.043	0.623	
$ii$	501	5.86	15.5	0.33	114	0.993	0.152	0.263	0.040	0.612	
$v$	840	5.84	15.1	0.05	90	1.006	1.000	0.333	0.335	1.026	1.00
$v$	833	5.86	15.3	0.1	90	1.006	0.500	0.333	0.168	1.017	0.81
$v$	680	5.90	15.7	0.25	90	1.006	0.200	0.333	0.067	0.830	0.62
$v$	391	6.12	15.8	1	90	1.006	0.050	0.333	0.017	0.477	0.41

Although the above criteria  $K$  widely indicate the trends, the quantitative prediction of the maximum stress (the ratio between any two peak values) is unsatisfactory, due to the strongly non-linear mechanisms and interactions. For example even for the less complex root shape  $v$ , the influence of the corner radius cannot be described

sufficiently. In the last column the best fitting potency, 0.3 was applied to Eq. (6), providing better relations but still overestimating small radii.

The stress peak values obtained from FEA are inserted in the scale in Fig. 9 for the different joint cases and roots, including the hypothetical transition cases studied.

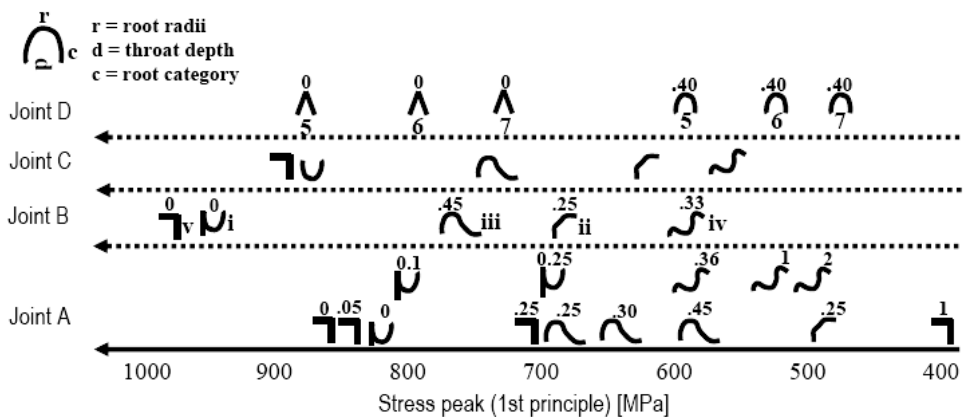


**Fig. 9:** 1<sup>st</sup> principle peak stress values (root of the upper corners) for the different cases

Widely the trends, i.e. the change of the stress peak when comparing one geometry to another, follow the above formulated criteria and can thus be explained. For the sharp corner Root *i* too low values result, probably due to meshing difficulties, but the asymptotic trend of reduced curvature towards a corner confirms the expected trend.

### 3.3 Generalised formulation of the trends

Plotting of the computed results quantitatively describes the studied cases. While this is the traditional way of publishing, a main difficulty is to make the results applicable for other situations, thus to generalise the findings. Therefore, the present study tries several partially new approaches to describe the findings in a manner qualitatively and quantitatively suitable for transfer to different cases. The above expressions (1)-(8) are one approach for describing the conditions.

The main mechanisms contributing as stress raisers (for the here studied shapes), governed by the anchor lengths, surface radii and opening angles (including roughness) are illustrated in Fig. 10.

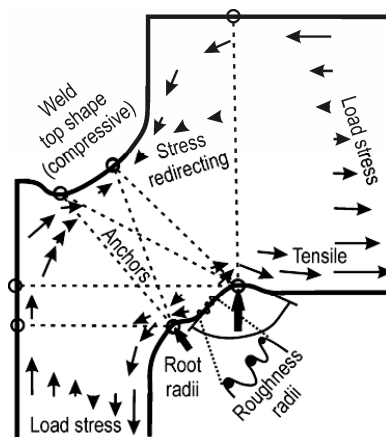


**Fig. 10:** Illustration of the geometry-dependent trends of the stress flow (angular momentum load) governed by the joint anchors and by the surface curvature

The impact of different anchors is illustrated in Fig. 11(a), showing that the secondary anchor has an important influence. Two hypothetical joint types are added to illustrate that the approach/guidelines can be transferred in a more general manner.

The curvature and opening angle of the root is illustrated in Fig. 11(b), in particular the shapes describing the transition from one root to another. Essential is the surface curvature and the opening angle, however for the corresponding anchor lengths, particularly for more complex root shapes like *i* and *iii*, with two maxima.

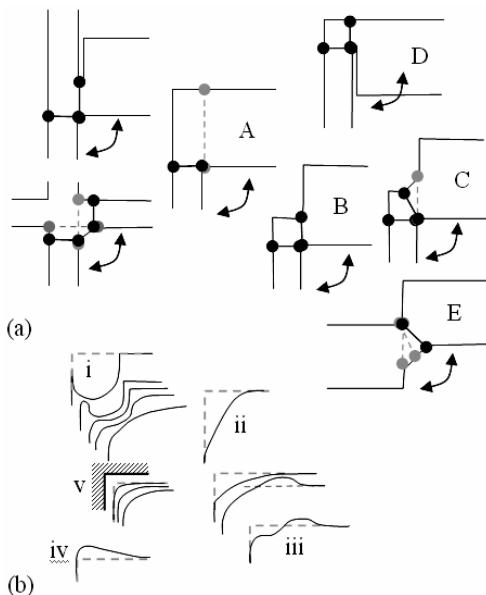


**Fig. 11:** Transitions (a) from one joint geometry to another, (b) from one root geometry to another

Another formulation recently developed is the BFC. While the BFC well describes digital situations, i.e. acceptable vs. unacceptable weld quality, the present study aims at a continuous scale, namely lowering the stress peak as much as possible. Therefore we here present a similar, but new scheme for the first time, namely the Tuning Flow Chart, TFC, where the peak stress is aimed to be tuned down as much as possible, by suitable process and design measures. The TFC documenting the findings of the present study is shown in Fig. 12. It describes how different geometrical properties can lower the peak stress. These methods aim at extension by findings from other research in order to gradually accomplish a comprehensive picture of the essential mechanisms for a wide range of conditions, to be applicable for a wide range of situations. One example applied here are the findings from a different case and publication, Case E [28].

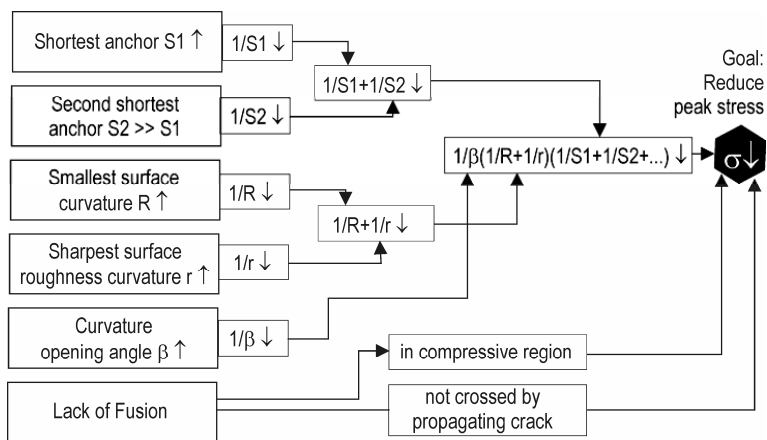


**Fig. 12:** Tuning Flow Chart (TFC) of the combined processes welding-load; tuning recommendation for reducing the maximum stress

For the present study, the optimum conditions with respect to long fatigue life, i.e. low peak stress are Joint A, however, overdimensioned (avoiding a significant secondary anchor), combined with root *ii* (well defined, controllable shape) or root *iv* (lower stress, but less controllable shape). These roots offer smooth transitions (small angle, large radius) and additional anchor lengthening. For proper dimensioning, Joint B is recommended (rather than Joint C that requires filler wire), while Joint D would require measures to avoid zero gap.

#### 4. Conclusions

From the numerical study of the stress field of four laser welding joint geometries and manifold similar surface geometries the following conclusions can be drawn:

- (i) The combination of throat depths (anchors), local surface curvature (including roughness and sharp corners) and its opening angle determines the peak stress value and its location, as was discussed for a series of joint types and root shapes studied
- (ii) Basic relations, derived from inverting the above key geometrical properties, widely explained the qualitative trends, but only to a limited extent the quantitative relations when comparing the stress peaks of different cases; the interacting origins are difficult to separate, even in the simulated stress field data, except when conducting sensitivity studies
- (iii) Little surface radii, small opening angles or sharp corners (e.g. at the root or by surface ripples) can attract the maximum stress to a different location than the minimum throat depth location; small radii, the avoidance of sharp corners, of ripples or of small opening angles are highly efficient design guidelines for lowering the stress
- (iv) Illustration of the main geometrical aspects and of the stress distribution is a suitable tool for qualitative stress analysis of different joint and surface geometries, particularly for the transition between similar kinds; a modified flow chart method was developed for formulating and documenting the findings, suitable for extension

#### Acknowledgements

The authors are grateful for funding by VINNOVA – The Swedish Innovation Agency (projects LOST, no. 2006-00563 and HYBRIGHT, no. 2005-02895) and by the K&A Wallenberg Foundation (Fibre Laser, project no. KAW 2007-0119). The contributions from the Swedish industrial and academic partners involved are highly appreciated.

#### References

- [1] Duley, W.W, Laser welding, Newyork Wiley 1999 ISBN 0.471-24679-4
- [2] Costa, A.P., Quintino, L., Greitmann, M., 2003. Laser beam welding hard metals to steel. *Journal of Materials Processing Technology* 141 (2), 163–173.
- [3] A. Klimpel, A. Lisiecki, Laser welding of butt joints of austenitic stainless steel AISI, *J. of Achievements in Materials and Manufacturing Engineering*, 25 (2007) 63-66



- [4] Cicala, E., Duffet, G., Andrzejewski, H., Grevey, D., Ignat, S., 2005. Hot cracking in Al–Mg–Si alloy laser welding operating parameters and their effects. *Materials Science and Engineering A* 395 (1–2), 1–9.
- [5] Ancona, A., Sibillano, T., Tricarico, L., Spina, R., Lugarà, P.M., Basile, G., Schiavone, S., 2005. Comparison of two different nozzles for laser beam welding of AA5083 aluminium alloy. *Journal of Materials Processing Technology*, 971–977.
- [6] Curcio, F., Daurelio, G., Minutolo, F.M.C., Caiazzo, F., 2006. On the welding of different materials by diode laser. *Journal of Materials Processing Technology* 175 (1–3), 83–89.
- [7] Benyounis, K.Y., Olabi, A.G., Hashmi, M.S.J., 2008. Multi-response optimization of CO<sub>2</sub> laser-welding process of austenitic stainless steel, *Optics & Laser Technology* 40 (1), 76–87.
- [8] Sibillano, T., Ancona, A., Berardi, V., Schingaro, E., Basile, G., Lugarà, M., 2006. A study of the shielding gas influence on the laser beam welding of AA5083 aluminium alloys by in-process spectroscopic investigation. *Optics and Lasers in Engineering* 44 (10), 1039–1051.
- [9] Karlsson, J., Kaplan A., Fibre laser welding for lightweight design, *ICALEO 28 Conference*, Orlando, Florida, USA, 2009 1548–1557.
- [10] Y. Yao, M. Wouters, J. Powell, K. Nilsson, A. Kaplan, Influence of joint geometry and fit-up gaps on hybrid laser-metal active gas (MAG) welding, *J. Laser Appl.* 18(2006) 283–288.
- [11] M. Wouters, Hybrid laser-MIG welding- An investigation of geometrical considerations, Lic. Thesis, Luleå University of Technology, 2005.
- [12] Correia, D.V., Gonc<sub>\_</sub>alves, C.V., Simões da Cunha, S., Ferraresi, V.A., 2005. Comparison between genetic algorithms and response surface methodology in GMAW welding optimization. *Journal of Materials Processing Technology* 160 (1), 70–76.
- [13] Yi, X., Shan, P., Hu, S., Luo, Z., 2002. A numerical model of wire melting rate in CO<sub>2</sub> gas-shielded welding. *Materials & Design* 23 (5), 501–504.
- [14] Z. Xiulin, L. Baotong, C. Tianxie, L. Xiaoyan, L. Chao, Fatigue tests and life prediction of 16 Mn steel butt welds without crack-like defect, *Int. J. of Fracture*, 68(1994) 275–85.
- [15] C. H. Lee, K. H. Chang, G. C. Jang, C. Y. Lee, Effect of weld geometry on the fatigue life of non-load-carrying fillet welded cruciform joints, *Engineering Failure Analysis* 16 (2009) 849–855

- [16] Z. Barsoum, Residual Stress Analysis and fatigue assessment of welded steel structures, Doctoral dissertation, Department of Aeronautical and Vehicle Engineering, Royal Institute of Technology, Stockholm, 2007.
- [17] C.Y. Hou, Fatigue analysis of welded joints with the aid of real three-dimensional weld toe geometry, *Int. J. Fatig.* 29(2007) 772-785.
- [18] J. L. Otegui, H. W. Kerr, D. J. Burns, U. H. Mohaupt, Fatigue crack initiation from defects at weld toes in Steel, *Int. J. Press Vessels Piping.* 38(1989) 385-417
- [19] T. Nykanen, X. Li, T. Bjork, G. Marquis, A parametric fracture mechanics study of welded joints with toe cracks and lack of penetration, *Engineering Fracture Mechanics* 72 (2005) 1580–1609
- [20] H. Remes, Strain-based approach to fatigue strength assessment of laser-welded joints, Doctoral dissertation, Department of Mechanical Engineering, Ship Laboratory, Helsinki University of Technology, Helsinki, 2007.
- [21] S. Kainuma, T. Mori, A study on fatigue crack initiation point of load-carrying fillet welded cruciform joints, *Int. J. Fatig.* 20(2008) 1669-1677.
- [22] F.P. Brennan, P. Peleties, A.K. Hellier, Predicting weld toe stress concentration factors for T and skewed T-joint plate connections, *Int. J. Fatig.* 22(2000) 573-584.
- [23] H.L.J. Pang, Analysis of weld toe profiles and weld toe cracks, *Int. J. Fatig.* 15(1993) 31-36.
- [24] H.L.J. Pang, Analysis of weld toe radius effects on fatigue weld toe cracks, *International J. Press. Vessels Piping.* 58(1994) 171–177.
- [25] J.A.M. Ferreira, C.A.M. Branco, Influence of the radius of curvature at the weld toe in the fatigue strength of fillet weld joints, *Int. J. Fatig.* 11(1989) 29–36.
- [26] V. Caccese, P.A. Blomquist, K.A. Berube, S.R. Webber, N.J. Orozco, Effect of weld geometric profile on fatigue life of cruciform welds made by laser/GMAW processes, *Mar. Struct.* 19 (2006) 1-22.
- [27] M. Ring, W. Dahl, Fatigue properties of laser-beam weldments on the high strength Steels, *Steel Research.* 65(1994) 505-510.
- [28] M. M. Alam, Z. Barsoum, Z., P. Jonsén, H. A. Häggblad, A. Kaplan, A, The influence of surface geometry and topography on the fatigue cracking behaviour of laser hybrid welded eccentric fillet joints, *Applied Surface Science* (in press), 2009.
- [29] M. M. Alam, Z. Barsoum, Z., P. Jonsén, H. A. Häggblad, A. Kaplan, (2009) Fatigue behaviour study of laser hybrid welded eccentric fillet joints – Part II: State-

of-the-art of fracture mechanics and fatigue analysis of welded joints, in Proceedings of NOLAMP 12 Conference, Copenhagen, Denmark.

[30] M. M. Alam, Z. Barsoum, Z., P. Jonsén, H. A. Häggblad, A. Kaplan, The effects of surface topography and lack of fusion on the fatigue strength of laser hybrid welds, in Proceedings of ICALEO 28 Conference, Orlando, Florida, USA, 2009 38-46

[31] M. M. Alam, Z. Barsoum, Z., P. Jonsén, H. A. Häggblad, A. Kaplan, Geometrical aspects of the fatigue behaviour of laser hybrid fillet welds, in Proceedings of Fatigue Design Conference, Senlis, Paris, France, 2009.

[32] A. Hobbacher, Fatigue design of welded joints and components, IIW document XIII 2151-07 / XV-1254-07.

[33] Kaplan, A. F. H, P. Norman and G. Wiklund, The bifurcation flow chart as a method for a generalised theory, applied to spatter defects during laser welding, Proc. 12th NOLAMP, August 24-26, 2009, Copenhagen (DK), FORCE Technology (2009)